Downloaded from orbit.dtu.dk on: Dec 18, 2017

Technical University of Denmark

Exhaust Recirculation Control for Reduction of NOx from Large Two-Stroke Diesel Engines

Nielsen, Kræn Vodder; Blanke, Mogens; Vejlgaard-Laursen, Morten; Eriksson, Lars

Publication date:
2016

Document Version
Publisher's PDF, also known as Version of record

Link back to DTU Orbit

Citation (APA):
Nielsen, K. V., Blanke, M., Vejlgaard-Laursen, M., & Eriksson, L. (2016). Exhaust Recirculation Control for Reduction of NOx from Large Two-Stroke Diesel Engines. Technical University of Denmark, Department of Electrical Engineering.

DTU Library
Technical Information Center of Denmark

General rights
Copyright and moral rights for the publications made accessible in the public portal are retained by the authors and/or other copyright owners and it is a condition of accessing publications that users recognise and abide by the legal requirements associated with these rights.

- Users may download and print one copy of any publication from the public portal for the purpose of private study or research.
- You may not further distribute the material or use it for any profit-making activity or commercial gain
- You may freely distribute the URL identifying the publication in the public portal

If you believe that this document breaches copyright please contact us providing details, and we will remove access to the work immediately and investigate your claim.

Technical University of Denmark

Kræn Vodder Nielsen

Exhaust Recirculation Control for Reduction of NO_x from Large Two-Stroke Diesel Engines

PhD Thesis, November 2016

DTU Electrical Engineering
Department of Electrical Engineering

MAN Diesel & Turbo

Exhaust Recirculation Control for Reduction of NO_x from Large Two-Stroke Diesel Engines

Kræn Vodder Nielsen

Technical University of Denmark
Kgs. Lyngby, Denmark, 2016

Technical University of Denmark
Automation and Control (AUT)
Elektrovej Building 326
DK-2800, Kgs. Lyngby
Denmark
Phone: (+45) 45 25 35 76
Email: info@elektro.dtu.dk
www.elektro.dtu.dk

Summary

Increased awareness of the detrimental effects on climate, ecosystems and human health have led to numerous restrictions of the emissions from internal combustion engines. Recently the International Maritime Organization has introduced the Tier III standard, which includes a significantly stricter restriction on NO_x emissions from large two-stroke diesel engines on vessels operating in certain NO_x Emission Control Areas.

Exhaust Gas Recirculation (EGR) is one of the three technologies on the market that are able to reduce the NO_x emission adequately for Tier III operation. EGR is well known from the automotive industry, but have only recently been introduced commercially to large two-stroke diesel engines. Recirculation of exhaust gas to the cylinders lowers the oxygen availability and increases the heat capacity during combustion, which in turn leads to less formation of NO_x. Experience shows, that while large two-stroke engines with EGR perform well in steady state, fast engine load transients cause smoke formation due to the decreased oxygen availability.

The aim of this thesis is to design a control system that enables the large two-stroke engines with EGR to meet the emission limits of the Tier III standard, while still maintaining maneuverability performance without smoke formation. The design methods acknowledge that engine specific parameter tuning is a scarce resource in the industry and controller complexity is kept to a minimum.

An existing dynamic model of the engine and EGR system is adapted and used for high-fidelity simulation. By isolating the gas composition part of the model and removing non-essential dynamics, a novel nonlinear reduced model of scavenge oxygen fraction is developed. Based on the reduced model, a novel nonlinear joint state and parameter observer for the scavenge oxygen fraction is designed. This observer compensates for a significant delay in the oxygen sensor, and observer errors are proven to converge exponentially. By inverting part of the reduced model and using the parameter observer, a novel scavenge oxygen controller based on nonlinear adaptive feed forward is developed. The controller error is proven to converge exponentially. This controller requires only one tuning parameter in addition to a number of physical parameters of the engine system. It exploits the availability of fuel and EGR flow estimates and the turbocharger speed to provide fast adjustment of EGR flow. In addition to the scavenge oxygen controller, a novel fuel index limiter based on oxygen/fuel-ratio is introduced and investigated. The limiter ensures that the maximal fuel flow set by the engine speed governor does not exceed the amount that can be completely burned, by considering the oxygen contents of the scavenge gas.

The reduced model, observer, controller and limiter designs are validated by simulation of the high-fidelity engine model, and by closed loop experiments on an engine at test bed and on a vessel operating at sea. Significant performance improvements promised by the simulations are verified in the experiments. Scavenge oxygen control during transients is improved, when compared to the reference controller. Formation of visible smoke is completely avoided, while acceleration performance is maintained.

The contributions of this project enable the EGR technology on large two-stroke diesel engines to reduce NO_x emissions by a factor of four without compromising vessel maneuverability. Project partner MAN Diesel & Turbo has applied for a patent covering the EGR controller design in Japan, China and South Korea. The controllers developed in this project are planned to be included as standard in commercially

available EGR controller software by 2017.

The thesis consists of a summary of the methods developed and validations performed during the project. The results are disseminated in a number of papers submitted to research journals and a conference.

Resumé

Øget fokus på udstødningsprodukters skadelige påvirkninger af klima, økosystemer og folkesundheden har ført til en lang række restriktioner på emissioner fra forbrændingsmotorer. International Maritime Organization (IMO) har for nylig indført Tier III standarden, der specificerer betydeligt strengere restriktioner på NO_x emissioner fra store to-takts dieselmotorer på nye skibe, der opererer i såkaldte NO_x Emission Control Areas.

Recirkulering af udstødningsgas (EGR) er en af de tre teknologier på markedet, der er i stand til at reducere NO_x emissionen tilstrækkeligt til at opfylde Tier III kravet. EGR er velkendt i automobilindustrien, men er først for nylig blevet indført kommercielt til store to-takts dieselmotorer. Recirkulering af udstødningsgas sænker tilgængeligheden af ilt og øger varmekapaciteten under forbrændingen, hvilket formindsker dannelsen af NO_x. Erfaringer viser at selvom de store motorer med EGR kører godt under stabile forhold, kan hurtige ændringer af motorlasten medføre transient røgdannelse på grund af lavere tilgængelighed af ilt under lastændringen.

Denne afhandling omhandler udviklingen af et kontrol-system, der gør store to-takts dieselmotorer med EGR i stand til at leve op til Tier III standarden og samtidigt være stand til at manøvrere uden røgdannelse. Designet tager hensyn til at både kompleksiteten af kontrol-systemet og nødvendigheden af fintuning af parametre til den enkelte motor skal begrænses.

I projektet tilpasses en eksisterende dynamisk model af motoren og EGR systemet og denne bruges som simuleringsmodel. En ny ulineær reduceret model af ilt-niveauet i skylleluften udvikles ved at isolere den del af modellen, der beskriver gassernes sammensætning og ved at fjerne ikke-essentiel dynamik. En ny ulineær kombineret tilstands- og parameter-estimator udvikles på basis af den reducerede model af iltniveauet i skylleluften. Denne estimator er i stand til at kompensere for en forsinkelse i målingen af iltniveauet og det bevises at estimations-fejlen konvergerer eksponentielt. En ny regulator af iltniveauet i skylleluften designes ved at invertere en del af den reducerede model og bruge parameter-estimatoren. Regulatoren er baseret på adaptiv fremkobling og det bevises at reguleringsfejlen konvergerer eksponentielt. Regulatoren har kun én tuningsparameter og derudover et antal parametre, der beskriver fysiske størrelser i motoren. Regulatoren benytter let tilgængelige målinger eller estimater af brændstof-tilførsel, recirkuleret flow og hastigheden af turboladeren til hurtigt at kunne justere det recirkulerede flow efter omstændighederne. Udover ilt-regulatoren udvikles en ny begrænser til motorens hastighedsregulator. Begrænseren sørger for at den maksimale brændstof-indsprøjtning ikke overskrider den mængde, der højst kan blive komplet forbrændt, ved at tage hensyn til indholdet af ilt i skylleluften.

Den reducerede ilt-model, tilstands-estimatoren, ilt-regulatoren og begrænseren valideres alle ved simulering af den komplette model og under lukket-sløjfe eksperimenter på en testmotor og på et skib. Simuleringen viser betydelige forbedringer af præstationsevnen og forbedringerne verificeres under eksperimenterne. Reguleringen af iltniveauet er væsentligt bedre med den nye regulator end med referencesystemet. Røgdannelse undgås og accelerationsevnen er bevaret i forhold til det oprindelige system.

Resultaterne af dette projekt gør EGR teknologien i stand til at reducere NO_x emissionerne fra store to-takts diesel motorer med 75% uden at gå på kompromis med manøvredygtigheden. Projekt-partneren MAN Diesel & Turbo har ansøgt om et patent, der dækker EGR regulatoren i Japan, Kina og Sydkorea.

Det er planlagt at implementere regulatorsystemet, der blev udviklet under projektet, som standard i kommerciel EGR software fra 2017.

Denne afhandling består af et resume af de udviklede metoder og resultaterne fra eksperimenter, der blev udført under projektet. Disse resultater er beskrevet i detaljer i en række artikler, der er indsendt til videnskabelige tidsskrifter og en konference.

Preface

This project was carried out as a collaboration between academia and industry, as part of the Industrial Ph.D. program funded by the Danish Agency for Science, Technology and Innovation, grant number 1355-00071B. The university partners were the Automation and Control Group, Department of Electrical Engineering, Technical University of Denmark and Vehicular Systems, Department of Electrical Engineering, Linköping University, Sweden. The industrial partner was MAN Diesel & Turbo (MDT), Copenhagen, Denmark.

The thesis was prepared in partial fulfillment of the requirements for acquiring the Ph.D. degree in engineering. The aim is design and validation of control of exhaust gas recirculation in large diesel engines. Such a control system must avoid smoke formation during engine loading transients, apply to a wide range of engines and should require only a minimum of tuning.

The thesis consists of a summary report and a collection of research papers written during the period 2013-2016, which were published or submitted for publication.

Kongens Lyngby, November 2016
Kræn Vodder Nielsen

Acknowledgments

I would like to thank main supervisor Professor Mogens Blanke for good collaboration and for sharing from his extensive experience with research in control system design. Professor Lars Eriksson has also been a valuable resource for teaching me about engine modeling and control and for his advise on how to present engine research. I highly recommend his course on modeling and simulation of engines and drivelines for anyone interested in engine research.

I also thank the original company supervisor Morten Vejlgaard-Laursen for giving me the opportunity to participate in this project and for our endless discussions on two-stroke engines and how to design control systems that can be operated and maintained by normal human beings. Substitute company supervisor Casper Hededal Svendsen has also been a valuable part of the project since the beginning. He has provided insights on the reference EGR controller, design and implementation of the new EGR controller and participated in sea-trials.

I am grateful to my colleagues at MAN Diesel & Turbo for the support they have given me throughout the project. My group LDC3 deserves special acknowledgment for cheering on through the project, even though my ideas might seem rather "abstract" at times. The LEO8 group deserves acknowledgment for helping out on sea-trials. I thank the DRC test engine crew and the crew of Maersk Cardiff for supporting my acceleration experiments and Maersk Line for providing us with test opportunities on board Maersk Cardiff.

I would like to thank my colleagues at the Automation & Control Group at DTU-Elektro for good collaboration during my studies. I likewise thank the Vehicular Systems group at Linköping University for supporting me during my stay in Sweden.

Finally I would like to thank my family and friends for always listening to my interesting stories about engine research.

This work was partially funded by the Danish Agency for Science, Technology and Innovation, grant number 1355-00071B.

Table of Contents

List of Abbreviations

AFF Adaptive Feedforward Controller.

CBV Cylinder Bypass Valve.

COM Control-Oriented Model.

COV Cut-Out Valve.

DLF Dynamic Limiter Function.

DRC Diesel Research Center.

EEDI Energy Efficiency Design Index.

EGB Exhaust Gas Bypass.

EGR Exhaust Gas Recirculation.

HFO Heavy Fuel Oil.

HHI Hyundai Heavy Industries.

IMC Internal Model Control.

IMO International Maritime Organization.

LLO Limiter Loop Oscillations.

MCR Maximum Continuous Rating.

MDO Marine Diesel Oil.

MDT MAN Diesel & Turbo.

MVEM Mean-Value Engine Model.

NECA NO_x Emission Control Area.

NO_x Nitrogen Oxides.

PI Proportional-Integral.

PID Proportional-Integral-Derivative.

QFT Quantitative Feedback Theory.

SCR Selective Catalytiic Reduction.

SECA SO_x Emissiovnn Control Area.

SFOC Specific Fuelk Oil Consumption.

SISO Single-Input, Single-Output.

TC Turbocharger.

VGT Variable Geometry Turbine.

WMC Water Mist Catcher.

List of Symbols

Symbol	Unit	Description
A	m^2	Area.
c_p	$J/(mol \cdot K)$	Specific heat for constant pressure.
d	-	Known disturbances.
g	-	Input nonlinearity.
h	-	g(θ,d,u) inverted w.r.t. u.
J	$kg \cdot m^2$	Moment of inertia.
k	-	Constant.
K	-	Constant vector.
m	kg	Mass.
M	kg/mol	Molar mass.
n	mol	Amount of moles.
N	-	Amount of cylinders.
$\dot{n}$	mol/s	Molar flow.
O	%	Molar oxygen fraction.
p	Pa	Pressure.
P	W	Power.
r	-	Setpoint.
R	$J/(mol \cdot K)$	Universal gas constant.
T	K	Temperature.
u	-	Actuated input.
U	-	Input vector.
V	m^3	Volume.
x	-	State variable.
X	-	Molar gas fraction vector.
y	-	Ratio of H to C atoms in fuel.
$y(t)$	-	Sensor output at time t.
Y	%	Fuel index.
Y_{LA}	%	Fuel index limiter based on air/fuel-ratio.
Y_{LO}	%	Fuel index limiter based on oxygen/fuel-ratio.
Y_{LOM}	%	Fuel index limiter based on oxygen/fuel-ratio and model.
Y_{LOS}	%	Fuel index limiter based on oxygen/fuel-ratio and sensor.
Z	-	Molar gas fraction vector.
α	%	Valve opening angle relative to fully open.
γ	-	Ratio of specific heats or minimum sensitivity of g(θ,d,u) w.r.t. θ.
Γ	-	Combustion reaction constant vector.
Δp	Pa	Pressure difference.
Δt	s	Time delay.
η	-	Thermal efficiency.
θ	-	Time-varying parameter.

λ	$1/s$	Eigenvalue.
λ_A	-	Air/fuel-ratio.
λ_O	-	Oxygen/fuel-ratio.
λ_{LA}	-	Air/fuel-ratio limit.
λ_{LO}	-	Oxygen/fuel-ratio limit.
μ	-	Maximum sensitivity of g(θ,d,h($\hat{\theta}$,d,r)) w.r.t. $\hat{\theta}$.
Π	-	Pressure ratio.
ρ	-	Maximum sensitivity of g(θ,d,u) w.r.t. θ.
τ	s	Oxygen mixing time constant.
ϕ	-	Constant.
Φ	-	Flow coefficient.
ψ	-	Auxiliary state.
Ψ	-	Head coefficient.
ω	rad/s	Rotational speed.

Chapter 1

Introduction

1.1 Background

1.1.1 Emission regulation

Increased awareness of the detrimental effects from emissions from internal combustion engines to essential ecosystems has lead to numerous emission restrictions. Common restrictions refer to emission of CO_2 (or fuel efficiency), particulate matter, SO_x and NO_x. The internal combustion engine constitutes one of the major sources of NO_x caused by humans. So-called thermal NO_x is formed during combustion of fuel, when the temperature of combustion is high. NO_x reacts in the troposphere to form ozone (O_3). This is not to be confused with stratospheric ozone, which protects the earth from ionizing radiation. Tropospheric ozone is the primary constituent of smog. NO_x emissions also lead to nutrient enrichment problems in bodies of water and form acid rain which severely affect certain ecosystems[1, 2].

NO_x emissions from automotive engines have been restricted for many decades and the maritime sector has also begun introducing emission legislation. United Nations agency IMO have specified NO_x emission limits, commonly referred to as the Tier I, II and III standards, which are increasingly strict. The IMO Tier III standard restricts the emission of nitrogen oxides (NO_x) from ships entering a NO_x Emission Control Area (NECA). Ships built after 1st of January 2016 are subject to the restrictions. For large two-stroke cross-head diesel engines with a rated speed below 130 RPM the Tier III standard specifies a NO_x emission limit of 3.4 g/kWh inside the NECAs. This constitutes a reduction by a factor of four, compared to the Tier II standard. So far the US and Canadian coast, Puerto Rico and the Virgin Islands are NECAs. The North Sea and the Baltic Sea will become NECAs from 2021 [3].

1.1.2 The Marine Two-Stroke Crosshead Diesel Engine

The majority of modern large container ships and oil tankers use a two-stroke cross-head diesel engine as prime mover. This design choice is made for a number of reasons: the thermal efficiency of this engine type is high; low quality fuel such as heavy fuel oil can be used; the reversible slow-speed engine can be connected directly to the propeller shaft, avoiding the need of a gearbox and the simplicity of the configuration increases reliability [4]. The engines come up to sizes of 14 metres high, 30 metres long and at a weight of 2300 tons. The power output range from 1500 kW to 100 MW, with maximum engine speeds from 60 to 250 RPM and 4 to 14 cylinders. Heavy Fuel Oil (HFO) or Marine Diesel Oil (MDO) is commonly used as fuel, but gas fuel engines also exist. Scavenge air is supplied by one or several turbochargers, assisted by auxiliary blowers at low engine loads [5]. Figure 1.1 shows an example of such an engine during shoptest, where the engine is tested before being installed in a vessel.

Emissions from large marine two-stroke diesel engines have been gradually restricted by the International Maritime Organization. Apart from the Tier I-III standards for NO_x emission the IMO has also

Figure 1.1: MAN Diesel & Turbo 6S80ME engine built by HHI. The engine is being tested before installation on the vessel Maersk Cardiff. The size of the engine can be inferred by comparing to the personnel at the base.

specified and restricted the Energy Efficiency Design Index (EEDI) for reduction of CO_2 and introduced SO_x Emissiovnn Control Area (SECA) for reduction of SO_x. Three approaches to reduction of NO_x emission from two-stroke cross-head diesel engines dominate the market: EGR, Selective Catalytiic Reduction (SCR) and use of alternative fuels (gas and dual-fuel engines). EGR and SCR exist in both high-pressure and low-pressure versions, depending on whether the system is placed before or after the turbocharger [6, 7, 8, 9, 10]. All three methods have their specific advantages and disadvantages and since the Tier III regulation have only applied since January 2016 it is still not certain which of the approaches will be preferred. This project concerns the high-pressure EGR system developed by MAN Diesel & Turbo.

1.1.3 Exhaust Gas Recirculation

Thermal NO_x is formed during combustion where high temperatures lead to reactions between nitrogen and oxygen from the scavenging air. These reactions are described by the Zeldovich mechanism [11]. Recirculation of exhaust gas to the scavenging air changes the gas composition and thus the combustion conditions. Increased heat capacity and decreased oxygen availability leads to lower peak combustion temperatures and less formation of thermal NO_x. EGR is a well established NO_x reduction technology within the automotive industry. Several different EGR approaches exist. Exhaust gas can be recirculated before or after the turbocharger with or without cooling of the flow. On four-stroke engines the exhaust pressure is higher than the inlet pressure, so the amount of recirculated flow is controlled by adjusting a valve in the EGR string [12].

EGR for large two-stroke engines has only recently become commercially available, enabled by the Tier III standard. While several EGR projects are under development among different engine designers [6, 7, 9, 10], this project deals specifically with the high-pressure EGR system developed by MAN Diesel & Turbo. A diagram of the airflow of this system is shown in Figure 1.2. Burned gas from the exhaust receiver is cooled in the EGR string and pressurized by the EGR blower before being recirculated to the scavenge receiver. The need for the EGR blower is special for two-stroke engines as the pressure is highest on the scavenging side, opposite to four-stroke engines where a control valve is sufficient.

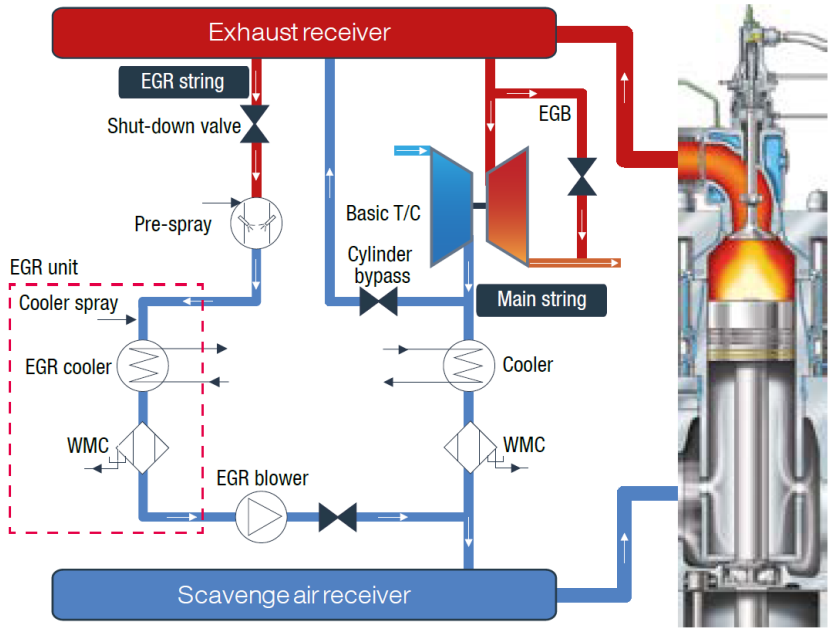

Figure 1.2: Overview of gas flows in the high-pressure EGR system developed by MDT. The recirculated exhaust gas is cooled and cleaned with water (sprays) in the EGR Unit before being pressurized by the EGR blower. A Water Mist Catcher (WMC) captures water droplets after the cooler. The diagram also shows a Cylinder Bypass Valve (CBV) and an Exhaust Gas Bypass (EGB) used for optimally matching the turbocharger (T/C) for various load conditions.

The Tier III compliant MDT high-pressure EGR system was first installed in the 4T50ME-X test engine in the Diesel Research Centre in Copenhagen in 2009. Service experience was attained when the system was retrofitted on board the small container feeder Alexander Maersk. The third system was developed for a 6S80ME-C9.2 EGR engine built by Hyundai Heavy Industries (Figure 1.1) and installed on the 4500 TEU container vessel Maersk Cardiff in 2013 [13]. Since then the system has been installed on at least 3 additional vessels and many more are expected.

1.1.4 Reference EGR Controller

The thermal NO_x formation in the engine has been shown to correlate well with the partial pressure of oxygen in the scavenge receiver [13]. This relationship is used for establishing the correct amount of recirculated flow. At a number of engine load points, the optimal scavenge oxygen fraction is decided by calculation or experiment. Figure 1.3 shows an example of such operating points. The oxygen fractions are then linearly interpolated in engine load, and the result is used as a setpoint for the EGR controller.

A ZrO_2 type sensor measures the partial pressure of oxygen in the scavenge receiver. Such sensors are designed for engine exhaust conditions with high temperatures, close to ambient pressures, low humidity and O_2-fraction below 10%. As the conditions of the scavenge receiver violates all these specifications a

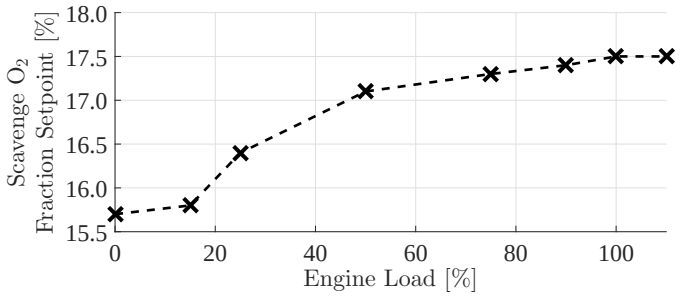

Figure 1.3: Example of load dependent scavenge oxygen fraction setpoint.

gas extraction system has been developed in order to treat the gas before measurement. The EGR flow rate is adjusted by varying the EGR blower speed. In order to avoid blower surging the blower has a minimum speed. If the minimum speed is reached the flow can be reduced further by adjusting the opening angle of the EGR Cut-Out Valve (COV) placed after the EGR blower. Fixed-gain Proportional-Integral (PI) feedback control has been implemented to handle this control task. Figure 1.4 shows a simplified overview of the engine system and the existing PI EGR controller that is used as reference for controller validation in this thesis.

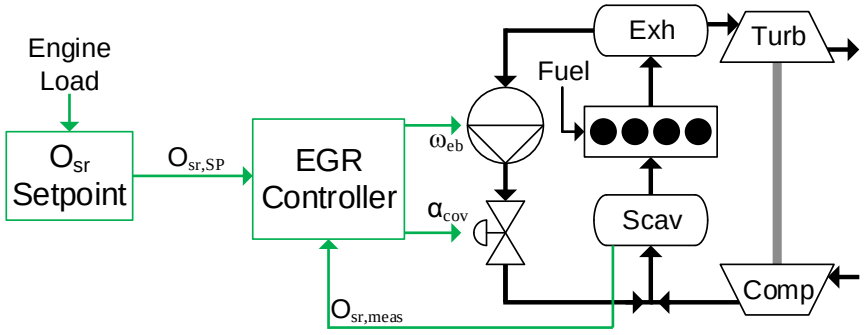

Figure 1.4: The PI EGR controller compares a measurement of the scavenge oxygen fraction to a load dependent setpoint and adjusts EGR blower speed and COV opening angle accordingly.

The PI EGR controller performs adequately in steady state conditions and is able to keep the oxygen fraction error within the required margin. As the Tier III standard applies to steady state conditions only, the system is fully compliant. However, the EGR controller struggles during engine load transients. Measurement data from an acceleration maneuver on Maersk Cardiff is shown in Figure 1.5. The engine RPM setpoint was increased at 50 seconds, causing the governor to order injection of more fuel and thus increasing the engine load. During the next 100 seconds the turbocharger speed slowly increased, until it reached its steady state value. In this interval the flow of fresh air from the compressor was relatively low, compared to the amount of fuel injection. Therefore the EGR rate needed to be low, to avoid oxygen deprivation. Unfortunately, the gas extraction system caused a severe delay of the scavenge oxygen measurement, so the EGR PI controller was not able to react immediately to the decreasing oxygen fraction. It did react to the small increase in setpoint, but this was not sufficient. The sensor delay also caused the feasible gains of the control loop to be limited, which further slowed down the reaction. The measured scavenge oxygen fraction dropped significantly (peaked below 13%) for about a minute.

Such an extremely low scavenge oxygen fraction led to an incomplete combustion and thus formation of black smoke. Figure 1.6 shows a photo of the exhaust outlet on Maersk Cardiff during the incident. Black smoke was emitted for more than 45 seconds. Besides being damaging to the engine such smoke formation

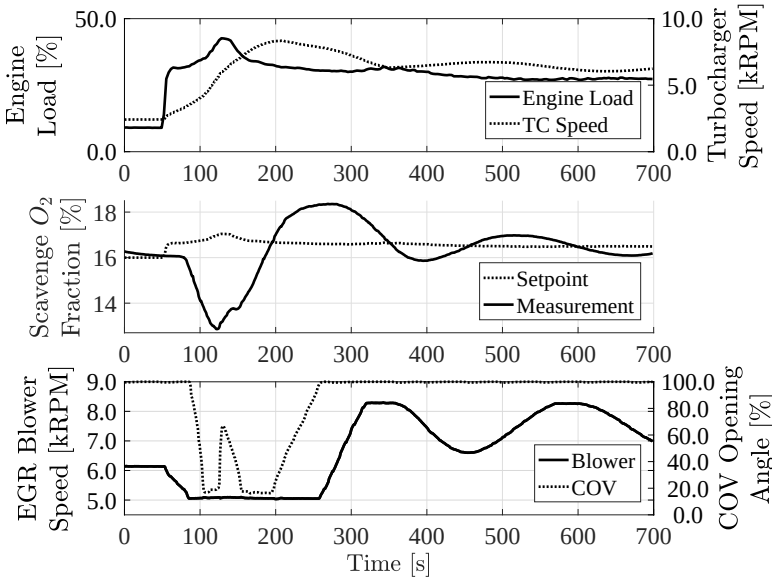

Figure 1.5: Measurement data from a large engine load transient on the vessel Maersk Cardiff. The reference EGR controller struggles to keep the scavenge oxygen fraction near its setpoint.

is restricted by authorities. Slowing down the possible engine loading would decrease the problem but maneuverability is essential in the NECAs, which cover ports and coastal areas.

Figure 1.6: Exhaust smoke on the vessel Maersk Cardiff during a large engine load transient. The reference EGR control system was used. Thick black smoke was emitted for 45 seconds.

1.2 State of the Art

Engine Processes

Internal combustion engines have made a profound impact on today's society and the subject is common in literature. Heywood [11] gave an extensive treatment of the fundamental principles of internal combustion engines, including thermodynamics, combustion physics, fluid flow, heat transfer, emissions and much more. The book has become somewhat of a classic and an impressive part of today's literature on engines still refer to it. More recent texts with focus on engine modeling and control include Guzzella and Onder [14] and Eriksson and Nielsen [12]. While these are mostly focused on four-stroke automotive engines, many of the concepts apply to two-stroke engines as well.

Four-Strokes and EGR

Modeling and control of EGR on automotive four-stroke engines is considered to be a related area of research. In this area the interactions between the EGR valve, Variable Geometry Turbine (VGT) and the nonlinearity of the system makes for an interesting control problem with a wide variety of proposed solutions [15, 16, 17, 18, 19, 20, 21]. Slow sensor dynamics have led to research into observers, feed-forward and other methods of compensation for engines with and without EGR [22, 23, 24]. Observer designs have also been proposed for cost reduction or to estimate engine variables that are difficult to measure[25, 26, 27]. While many concepts are shared between EGR systems for the automotive four-strokes and large marine two-strokes, the two areas of control design differ considerably due to differences in two- and four-stroke scavenging, system time constants, engine test availability, sensor availability and general maturity of the field.

Large Two-Strokes without EGR

The large two-stroke crosshead diesel engine receives less attention in literature than the automotive four-strokes. The topic of governor (engine speed controller) design has attracted some research effort into dynamic modeling of the large engines. A number of classic texts lay the foundation: Woodward and Latorre [28] discussed methods of modeling diesel engines for simulation of propulsion transients; Blanke and Andersen [29] showed that the turbocharger inertia has a significant impact on the engine speed dynamics; a Mean-Value Engine Model (MVEM) of a two-stroke diesel engine without filling and emptying dynamics was developed by Hendricks [30]. Winterbone and Jai-In [31] discussed how the introduction of electronic governors allowed for more advanced controller designs. An example was a multi-variable control system of diesel engine with VGT that improves transient fuel economy and smoke formation. Banning et al. [32] presented how the combination of H_∞ control and non-linear techniques could be used for fuel efficiency optimization. The increasingly strict emission constraints inspired Stefanopoulou and Smith [33] to further investigate the use of VGT as an extra degree-of-freedom to mitigate the trade-off between optimizing the engine for steady state and avoiding emissions during transients. Coordination of injected fuel and VGT area was proposed for control of the air/fuel-ratio. A multiple-input multiple-output controller developed but not experimentally verified. Further treatment of governor design was given by Xiros [4] that investigated the use of Proportional-Integral-Derivative (PID) and linear-state-feedback methods for disturbance rejection and robustness. The design was based on a state-space model from physical, thermodynamic engine description and mapping using neural nets.

The necessity of filling-and-emptying dynamics in mean-value models of a marine two-stroke was investigated by Theotokatos [34]. It was found that a model with simplified dynamics (quasi-steady) could represent engine speed response but only after increasing the turbocharger inertia parameter to indirectly include the dynamics of the scavenge and exhaust receivers. Models with filling-and-emptying dynamics was deemed more appropriate for prediction of engine dynamics and for more advanced control system design studies. The quasi-steady model was used by Xiros and Theotokatos [35] to map torque-response with neural nets, create a neural state-space model and suggest a supervisory speed control structure. The full model from [34] was used by Guan et al. [36] for investigation of engine performance and auxiliary blowers at low load. Guan et al. [37] extended the model by replacing the cylinder block with a zero-dimensional model and used it for investigation of turbocharger cut-out and auxiliary blower activation in low load conditions. Theotokatos and Tzelepis [38] used the full model from [34] to map the performance and emission parameters of a ship and showed how the result could be used for minimizing fuel consumption of a typical ship.

The last part of this project concerns the development of fuel index limiters. This rather specialized topic has not been found in literature except for brief mention of scavenge pressure limiters by Xiros [4]

and in the technical paper by MAN Diesel & Turbo [39], which introduced the Dynamic Limiter Function (DLF) as part of MDT's suite of control tools.

Large Two-Strokes with EGR

The application of exhaust gas recirculation on a two-stroke cross-head diesel was published by MAN Diesel & Turbo in a number of technical reports [13, 40, 41, 42] which mainly reported about mechanical and chemical challenges, and little on control. A mean-value engine model of the DRC test engine with EGR was published by Hansen et al. [43] along with a black-box nonlinear model identification approach. Hansen et al. [44] also published a companion paper that investigated scavenge oxygen control on the basis of the MVEM. Classical feed-forward and feedback designs were compared to Quantitative Feedback Theory (QFT) designs applied to a linearized version of the MVEM. The work only considered Single-Input, Single-Output (SISO) control. Dead time of the primary sensor (scavenge gas extraction system and oxygen fraction measurement) was shown to be the main limitation of control performance. Further work on modeling the Diesel Research Center (DRC) test engine was published by Alegret et al. [45]. Fuel injection timing, exhaust valve timing and the cylinder bypass valve was included in the model. A Seiliger cycle was used for calculation of temperature of gas flow from cylinders and an elaborate scheme for parameter identification was presented. The operating region of the model only included the upper half of the engine load range since auxiliary blowers were not included and available maps of turbine, compressor and EGR blower performance were limited in range. Efforts to extrapolate to low load conditions where presented by Llamas and Eriksson in [46] and [47] as part of the Hercules II project [48].

1.3 Objectives

The present thesis is a result of a research project financed by MAN Diesel & Turbo in collaboration with the Danish Agency for Science, Technology and Innovation within the Industrial Ph.D. program. MAN Diesel & Turbo contributed with experience with large two-stroke diesel engines and EGR systems along with facilities for model validation and closed loop engine experiments. Collaboration with the Technical University of Denmark brought expertise on nonlinear, robust and fault-tolerant control systems to the project and Linköping University provided state-of-the-art knowledge on modeling and control of combustion engines.

Taking offspring in results from previous projects, where a high-fidelity simulation model of the control objective was designed, this project focused on the design of high performance nonlinear EGR controllers of low complexity, in order to minimize tuning and maintenance.

The main objectives of the project were to

- Analyze and generalize the process dynamics of the scavenge oxygen fraction of a large two-stroke diesel engine with exhaust gas recirculation.
- Employ appropriate methods to obtain high performance robust control of the EGR system, generic over the entire engine range. The controller should minimize scavenge oxygen error, avoid smoke formation and maintain engine acceleration capability.
- Obtain a generic controller design, where known or easily obtainable physical parameters can be used for controller parameters, and where remaining tuning is obtained by adaptive or self-tuning techniques with guaranteed robustness.
- Validate the performance of the controller design with closed loop engine experiments on a vessel operating at sea.

1.4 Thesis Outline

The thesis is written as a collection of articles. The first part describes the main research results and the appended articles describe the research in detail. Chapter 2 presents the main contributions of the project. The dynamic models that make the foundation of the subsequent control design are described in Chapter 3. A novel observer design based on these models are presented in Chapter 4. The newly developed adaptive feedforward control concept used for scavenge oxygen control is presented in Chapter 5. Development and validation of fuel index limiters for engines with EGR is treated in Chapter 6. Chapter 7 summarizes the results of the project and presents perspectives and possible future research within the field. Appendices A to E contain journal and conference articles written as part of the project.

Chapter 2

Summary of Main Contributions

Journal Articles

The main contributions of the project have been disseminated in four journal articles. At the time of thesis submission, one paper has been published, while three papers have been submitted. These are included as papers A, B, C and D:

(A) K. V. Nielsen, M. Blanke, L. Eriksson, and M. Vejlgaard-Laursen. "Control-Oriented Model of Molar Scavenge Oxygen Fraction for Exhaust Recirculation in Large Diesel Engines". *Journal of Dynamic Systems, Measurement and Control - ASME* 139.2 (2017). DOI: 10.1115/1.4034750.

This paper presents a low complexity dynamic model of the molar scavenge oxygen fraction, that is designed for direct use in an observer. The starting point is a mean-value, filling and emptying model of the engine air flow and gas compositions, adapted from another project. The gas composition part is isolated and reduced using nonlinear model reduction techniques to capture only the dynamics that are essential for control design. The resulting model is validated against the full model and against data from both an engine at a test bed, and from a vessel operating at sea. The model is shown to be able to replicate the scavenge oxygen behavior well over the load and blower speed range relevant for EGR.

(B) K. V. Nielsen, M. Blanke, and L. Eriksson. "Adaptive Observer for Nonlinear Parameterised Hammerstein System with Sensor Delay - a Technology for Ship Emissions Reduction". *Transactions on Control Systems Technology* (2016). Submitted.

This paper formulated the simplified scavenge oxygen model as a generic first order Hammerstein system with a time-varying parameter and sensor delay. A joint state and parameter observer is suggested for this model type and exponential error convergence is proven. The observer is applied to the scavenge oxygen model and tested against simulation of the MVEM and against data from engine tests. The observer is shown to avoid the sensor delay and provide a prediction of the scavenge oxygen fraction 10-25 seconds ahead of the measurement.

(C) K. V. Nielsen, M. Blanke, L. Eriksson, and M. Vejlgaard-Laursen. "Adaptive Feedforward Control of Exhaust Recirculation in Large Diesel Engines". *Control Engineering Practice* (2016). In review.

An Adaptive Feedforward Controller (AFF) is proposed in this work for a first order Hammerstein system with sensor delay and known disturbances. When applied to the task of controlling the scavenge oxygen fraction the AFF controller significantly outperforms the reference PI controller. The improvement is both in terms of controller error and smoke formation during load transients and in terms of control error at almost steady load conditions.

(D) K. V. Nielsen, M. Blanke, L. Eriksson, and M. Vejlgaard-Laursen. “Diesel Engine Control System to meet Strict Emission Requirements while Maintaining Full Ship Manoeuvring Capability”. *Applied Energy* (2016). Submitted.

In this paper a fuel index limiter based on air/fuel-ratio is extended in order to apply to engines with EGR. The result is a fuel index limiter based on oxygen/fuel-ratio. Two extension methods of different complexity are suggested. The first method is scaling of the original limiter value, based on the scavenge oxygen sensor. The second method uses the COM to solve the potentially problematic coupling between fuel index and scavenge oxygen fraction during accelerations. The suggested limiters are validated by simulation and by closed loop engine tests on a vessel. Smoke formation is shown to be eliminated by use of the new limiters without compromising the engine acceleration ability.

Conference Articles

An early version of the proposed scavenge oxygen controller was presented at a conference. The resulting conference paper is included here as Paper E.

(E) K. V. Nielsen, M. Blanke, and M. Vejlgaard-Laursen. “Nonlinear Adaptive Control of Exhaust Gas Recirculation for Large Diesel Engines”. *IFAC-PapersOnLine* 48.16 (2015). 10th IFAC Conference on Manoeuvring and Control of Marine Craft, MCMC 2015 Copenhagen, 24-26 August 2015, pp. 254 –260. DOI: 10.1016/j.ifacol.2015.10.289.

This conference article presents a nonlinear adaptive EGR controller along with analytical proof of exponential stability. The control design and proofs are based on a control-oriented model of the scavenge oxygen mass fraction. The closed loop system is proven to converge exponentially to the best achievable state in spite of actuator saturation. The controller is validated by simulation of the control-oriented model.

Patents

As a result of the project MAN Diesel & Turbo has applied for a patent titled "A Large Turbocharged Two-Stroke Self-Igniting Internal Combustion Engine with an EGR Control System" in China (Application number 2016103083895), Japan (2016-084946) and South Korea (10-2016-0055137) with the inventors Nielsen, K. V. and Svendsen, C. H. The patent covers the concept published in Paper C. At the time of thesis submission the patent status was "Intension to grant."

Chapter 3

EGR System Modeling

This chapter describes the dynamic models used for control design in the present project. The main results were published in a journal article included as Paper A. A dynamic model of engine speed was added in the journal article included as Paper D to support fuel index limiter development.

Dynamic models are essential to the control design and validation in this project. A mean-value engine model is adapted from existing literature and slightly altered to provide for a high-fidelity simulation model. The MVEM also serves as a basis for development of a novel control-oriented model, that aims to capture only the dynamics and nonlinearities, that are essential for the design of a scavenge oxygen fraction controller.

3.1 Mean-Value Engine Model

Mean-value modeling is a common method of modeling combustion engine dynamics for simulation and controller design from a gas flow perspective. A mean-value model neglects the discrete cycles of the cylinder strokes in a reciprocating engine and approximates a continuous mean flow through the cylinders, which is spread out over a cycle. For simulation of an engine with EGR, it is common to couple the mean-value concept with filling-and-emptying dynamics of the scavenge and exhaust receiver. Such a model was presented in [45] and that model is used as a basis for the simulation model in the present project.

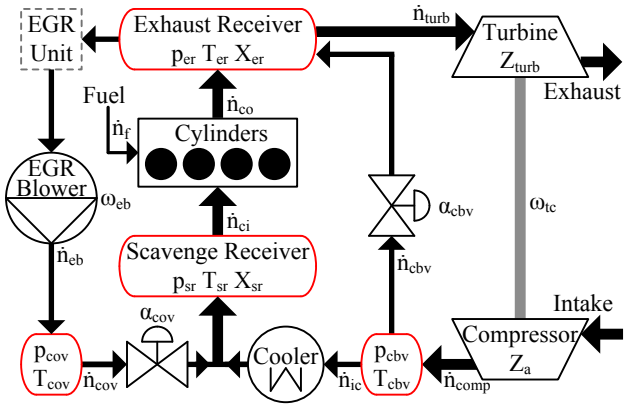

Figure 3.1: Overview of components included in the MVEM. Crankshaft-propeller system is not shown.

An overview of the components included in the MVEM is shown in Figure 3.1. The crankshaft-propeller system is not shown. Volume components with filling-and-emptying dynamics (gas reservoirs) are drawn

as red cylinders. The pressure in such a volume component i is modeled with an isothermal model

$$\dot{p}_i = \frac{RT_i}{V_i}\left(\dot{n}_{in} - \dot{n}_{out}\right) \tag{3.1}$$

The flows between the volume components (and intake/exhaust) are modeled using flow component models. Compressor, turbine, scavenge cooler, cylinders, EGR blower and a number of valves are flow components in the MVEM. Standard models of such components exist in literature, where the mass flow is calculated from pressure on both sides, upstream temperature and typically an additional variable ε such as valve opening or blower speed. In this project the models are converted to molar rather than mass flow, so the generic formulation is

$$\dot{n}_i = f(p_{in}, p_{out}, T_{in}, \varepsilon) \tag{3.2}$$

The mean-value assumption of the cylinder flow (which gives the MVEM its name) is modeled with such a function. Note that $\dot{n}_i$ denotes a molar flow, so (3.2) represents a static relation and is not a dynamic equation of a system state. The scavenge and EGR coolers are assumed to keep a constant temperature T_{sr} in the scavenge receiver. The temperature in the exhaust receiver equals the output temperature of the cylinders, which in turn is calculated with a modified Seiliger cycle [45].

Turbocharger speed dynamics depend on the power delivered from the exhaust gas to the turbine P_{turb} and the power delivered from the compressor to the inlet air P_{comp}

$$\dot{\omega}_{tc} = \frac{P_{turb} - P_{comp}}{J_{tc}\omega_{tc}} \tag{3.3}$$

These powers are found using standard thermodynamic considerations and compressor and turbine maps. A simple model of engine (crankshaft) speed ω_c is attained by calculating the power delivered by the combustion P_{ind}, power consumed by friction P_{fric} and power consumed by the propeller P_{prop}

$$\dot{\omega}_c = \frac{P_{ind} - P_{fric} - P_{prop}}{J_c\omega_c} = \frac{k_{hc}M_f k_f Y \omega_c \eta - k_{fric}\omega_c - k_{prop}\omega_c^3}{J_c\omega_c} \tag{3.4}$$

Variation of ship speed is too slow to affect the EGR system dynamics and is not included in the model. The composition of gas species in a volume component is described by a vector of molar fractions of O_2, CO_2 and H_2O

$$X_i = \frac{\begin{bmatrix} n_{i,O_2} & n_{i,CO_2} & n_{i,H_2O} \end{bmatrix}^T}{n_{i,total}} \tag{3.5}$$

where $n_{i,total}$ is the total amount of moles in the volume, found with pressure, temperature and the ideal gas law. The sum of the fractions is less than one and the remaining gas in a volume is assumed to be N_2. Gas mixing in the scavenge and exhaust receivers are modeled as ideal with the following dynamics

$$\dot{X}_i = \frac{RT_i}{p_i V_i}\sum_{input=j}\dot{n}_j\left(X_j - X_i\right) \tag{3.6}$$

Combustion of fuel alters the composition of the gas flowing through the cylinders. A lean combustion with the following reaction is assumed

$$CH_y + \left(1 + \frac{y}{4}\right)O_2 \rightarrow CO_2 + \frac{y}{2}H_2O \tag{3.7}$$

The fuel is described as virtual molecules CH_y, where y specifies the average ratio of hydrogen atoms to carbon atoms among the species in the fuel. The oxygen fraction vector of the flow exiting the cylinders is calculated as

$$X_{co} = \frac{\dot{n}_{ci}X_{sr} + \dot{n}_f\Gamma}{\dot{n}_{co}} \quad , \quad \Gamma = \begin{bmatrix} -1 - \frac{y}{4} \\ 1 \\ \frac{y}{2} \end{bmatrix} \tag{3.8}$$

In total the MVEM contains 4 pressure states, 2 rotational speed states and 6 gas composition states (2 vectors of each 3 molar fractions). Thus the state vector is

$$x = \begin{bmatrix} p_{sr} & p_{er} & p_{cbv} & p_{cov} & \omega_{tc} & \omega_c & X_{sr} & X_{er} \end{bmatrix}^T \tag{3.9}$$

and the dynamic model can be expressed in state space form as

$$\dot{x} = f(x,u), \quad u = \begin{bmatrix} Y & \omega_{eb} & \alpha_{cov} & \alpha_{cbv} \end{bmatrix}^T \tag{3.10}$$

where the inputs are fuel index Y, EGR blower speed ω_{eb}, cut-out valve opening angle α_{cov} and Cylinder Bypass Valve (CBV) opening angle α_{cbv}.

Whereas quite complex models of gas flow structures can be built using volume and flow components, it can be challenging to determine the parameters of the flow components. In this project the parameters of the MVEM model were obtained from [45] where an elaborate estimation scheme was presented. The model in [45] was based on mass flows so some conversion was necessary in order to base the model on molar flows. This conversion is a technicality that does not affect the validity of the model and no further validation has been pursued.

The operating region of the MVEM only includes the upper half of the engine load range. This limitation stems from the lack of turbine, compressor and EGR blower maps that cover the conditions experienced at low engine loads. Another issue is the auxiliary blower, used for maintaining sufficient scavenge pressure at low load. The auxiliary blower is not included in the MVEM. Extension of the MVEM to regions of low engine load has not been pursued in this project. Another project, stemming from [45] has however made progress in meeting this challenge [46, 47].

Fast engine load transients (which make the EGR controller struggle) mainly occur in the lower half of the engine load range. It is therefore unfortunate that the MVEM is not able to simulate this region. Nevertheless, closed loop simulations of the MVEM and PI EGR controller, experiencing fast transients at higher loads, do replicate the control issues which we seek to solve. Therefore the MVEM is deemed valid for initial controller validation in this project. The question, of whether a given controller also performs at lower loads, is answered by testing on real engines.

3.2 Control-Oriented Scavenge Oxygen Model

Whereas the MVEM is intended as a first principle physical model of the engine speed, pressures and gas compositions, the purpose of the Control-Oriented Model (COM) is to capture only the dynamics and nonlinearities that are essential for control of the scavenge oxygen fraction, in a model that is as simple as possible. The reason for developing a low complexity model is to express the essential system dynamics as clearly as possible for the control designer and to decrease the amount of parameter tuning, if the model is used in an observer.

3.2.1 Model Reduction

The development of the COM takes its offspring in the MVEM. The gas composition states have a negligible effect on the pressure and speed states. Therefore the MVEM can be expressed as a cascade of two subsystems, where the state vector of Subsystem 1 is

$$x_1 = \begin{bmatrix} p_{sr} & p_{er} & p_{cbv} & p_{cov} & \omega_{tc} & \omega_c \end{bmatrix}^T \tag{3.11}$$

As Subsystem 1 is not affected by Subsystem 2 the dynamic equation is

$$\dot{x}_1 = f_1(x_1,u_1), \quad u_1 = \begin{bmatrix} Y & \omega_{eb} & \alpha_{cov} & \alpha_{cbv} \end{bmatrix}^T \tag{3.12}$$

Subsystem 2 has the gas composition vectors as states

$$x_2 = \begin{bmatrix} X_{sr} & X_{er} \end{bmatrix}^T \tag{3.13}$$

and the states of Subsystem 1 is considered as part of the input vector in the dynamic equation

$$\dot{x}_2 = f_1(x_2, u_2), \quad u_2 = \begin{bmatrix} x_1 & Y & \omega_{eb} & \alpha_{cov} & \alpha_{cbv} \end{bmatrix}^T \tag{3.14}$$

As a matter of fact, the individual species do not affect the other species in the composition model. It is therefore possible to divide Subsystem 2 into isolated models for each species. As gas mixing in two receivers are included, such a model is of order 2. Paper A shows how to reduce these second order models to first order Hammerstein models, by removing nonessential dynamics. The one describing scavenge oxygen fraction is used for control design. By defining $O_{sr} = \frac{n_{sr,O_2}}{n_{sr,total}}$ the control-oriented scavenge oxygen model (COM) is

$$\tau \dot{O}_{sr} = -O_{sr} + O_a - \frac{(1 + \frac{y}{4}(O_a + 1))\dot{n}_f \dot{n}_{egr}}{\left(\dot{n}_{ic} + \frac{y}{4}\dot{n}_f\right)(\dot{n}_{ic} + \dot{n}_{egr})} \tag{3.15}$$

The COM has only 3 parameters: O_a is the molar fraction of oxygen in ambient air ($\approx$21%), y specifies the average ratio of hydrogen atoms to carbon atoms in the fuel ($\approx$1.8) and τ is the overall mixing time constant. Simulation of the MVEM shows τ to be within the range 11-13 seconds throughout the operating range. Scavenge pressure (and thus amount of moles in the receivers) increases with load, but so do gas flows and therefore the mixing dynamics are close to constant. The inputs of the COM are three molar flows: fuel flow, EGR flow and scavenge cooler flow. These can be enterpreted as the influence from Subsystem 1 to Subsystem 2.

3.2.2 Flow Estimation

Fuel flow and EGR flow can both be estimated from signals that are available to the EGR controller. Fuel flow is proportional to the product of fuel index and engine speed and the constant of proportionality depends on the engine size. EGR blower data, provided by the blower manufacturer, is sufficient for estimation of EGR flow from pressure signals and blower speed. The intercooler flow is more challenging to estimate but a decent approximation can be made from the turbocharger speed

$$\dot{n}_{ic} = \theta \cdot \beta(\omega_{tc}), \quad \beta(\omega_{tc}) = (1-\phi)\frac{\omega_{tc}}{1000 rad/s} + \phi\left(\frac{\omega_{tc}}{1000 rad/s}\right)^2 \tag{3.16}$$

This model is rather rough and only works when the CBV opening angle α_{CBV} is fixed. Varying α_{CBV} changes θ. Simulations of the MVEM shows that (3.16) captures the main behavior of the scavenge cooler flow during transients but the steady state result is not exact.

Estimation of $\dot{n}_f$, $\dot{n}_{egr}$ and $\dot{n}_{ic}$ and simulation of the COM leads to a dynamic estimate of the scavenge oxygen level that can be validated against simulation and experiment data. Figure 3.2 shows an overview of the calculation.

3.2.3 Validation

The COM was validated by comparison to data from simulation of the MVEM and against measurement data from experiments on the DRC test engine and the vessel Maersk Cardiff. The COM was able to replicate the dynamic behavior of the scavenge oxygen fraction in engine load transients, even in the low load region of the engines, which was not covered by the MVEM. In order to compare to the experiment data, the oxygen sensor dynamics were mimicked by increasing the mixing time constant of the COM and adding a time delay of 10-20 seconds. An example of performance during loading transients on the test engine is seen in Figure 3.3.

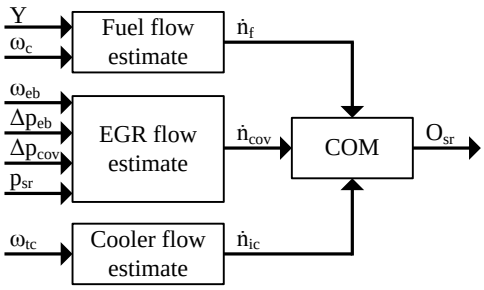

Figure 3.2: Engine signals are used for estimation of three molar flows which are inputs to control-oriented model of scavenge oxygen fraction.

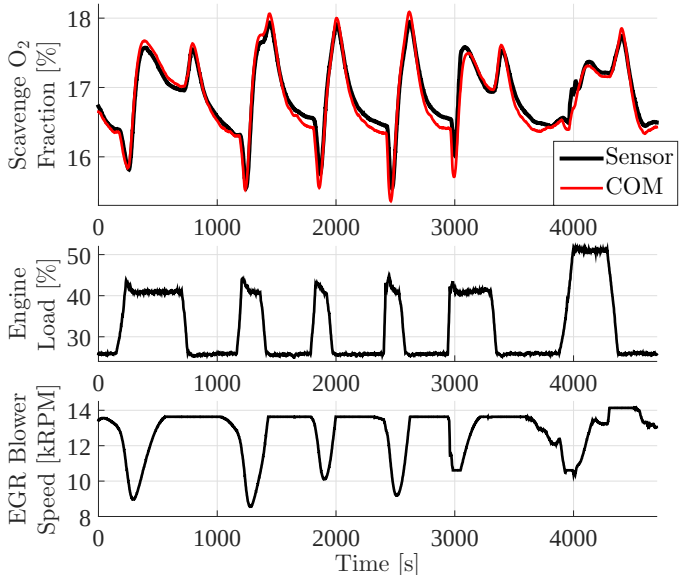

Figure 3.3: Comparison of O_{sr} measured on test engine and estimated by COM during a series of engine RPM setpoint changes.

3.3 Conclusions

A simulation model of the engine with exhaust gas recirculation was developed by adapting an existing mean-value engine model. The MVEM includes filling-and-emptying dynamics and gas mixing in the scavenge and exhaust receivers and turbocharger inertia. Engine speed dynamics were added to support fuel index limiter development.

The MVEM served as an offspring for the development of a simpler control-oriented model of scavenge oxygen fraction, that only included the dynamics and nonlinearities essential for scavenge oxygen control design. The COM is a first order Hammerstein model. Fuel, EGR and scavenge cooler flows are input to the COM. The scavenge cooler flow was difficult to estimate but a simple correlation to turbocharger speed provided a rough approximation. Validation of the COM against the MVEM and engine experiments showed good ability to replicate scavenge oxygen behavior during engine load transients, over the load range. The scavenge oxygen sensor dynamics were included in the COM by increasing the time constant and adding a time delay.

Chapter 4

Joint State and Parameter Observer

This chapter describes the novel state and parameter observer that was used as part of the control design in the present project. The observer and proof of exponential observer error convergence were published in the journal publication included as Paper B.

4.1 Generic Observer

The significant time delay and first order filter dynamics of the scavenge oxygen sensor decrease the possible gain of the EGR control loop. An immediate suggestion is therefore to implement a state observer for the scavenge oxygen fraction. The simplicity of the COM makes it an excellent basis for observer design. The COM's weakness is the difficulty of accurately estimating the scavenge cooler flow. Equation (3.16) provides an approximation but the parameter θ varies within a small interval which is not known a priori. In this section the COM and the cooler flow model are combined and the observer problem is stated as an issue of online joint parameter and state estimation.

By inserting the scavenge cooler flow approximation in the COM, and assuming that the fuel and EGR flows are known, the system can be expressed as a first order Hammerstein model on the following form

$$\tau \dot{x}(t) = g(\theta(t), u(t)) - x(t) \tag{4.1a}$$

$$y(t) = x(t - \Delta t) \tag{4.1b}$$

$$\bar{\theta} - \kappa \leq \theta(t) \leq \bar{\theta} + \kappa \tag{4.1c}$$

where $x(t)$ is the plant state, $u(t)$ is the input, $\theta(t)$ is a time-varying parameter, $g()$ is the input nonlinearity, τ is the system time constant and Δt is the delay of the sensor. The constants $\bar{\theta}$ and κ describe the interval to which $\theta(t)$ belongs. A joint state and parameter observer has been developed for this model class. The novel joint state and parameter observer is

$$\dot{\hat{x}}(t) = \frac{1}{\tau}\left(g(\hat{\theta}(t), u(t)) - \hat{x}(t)\right) \tag{4.2a}$$

$$\hat{\theta}(t) = \left(\tau y(t) + \int y(t) - g(\hat{\theta}(t), u(t - \Delta t))\,\mathrm{dt}\right) \cdot k \tag{4.2b}$$

where $\hat{x}$ is the state estimate, $\hat{\theta}$ is the parameter estimate and $k > 0$ is the observer gain. The parameter observer is independent of the state observer, so it can be employed separately. The known input u is delayed in the parameter observer in order to synchronize with the delayed measurement y. The state observer is simply a simulation of the dynamic equation of the system, using the non-delayed input and

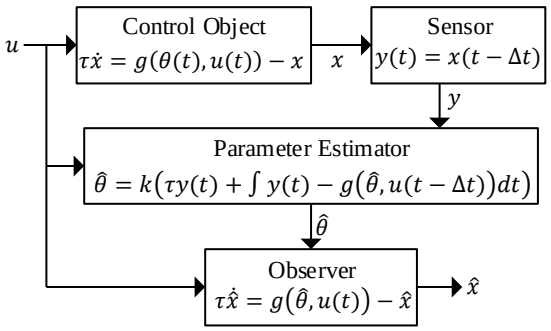

Figure 4.1: Overview of the signal paths of the joint parameter and state observer. The parameter estimator uses the inputs and the sensor signal, whereas the observer only uses inputs and estimated parameter.

the latest parameter estimate. The inherent stability of the plant and the exponential convergence of the parameter leads to exponential convergence of the state error. A weakness of the observer is that the parameter estimator has a direct gain from the measurement which makes it vulnerable to sensor noise.

The observer only applies to models of the class specified in Equation 4.1. A further requirement is that the input nonlinearity $g(\theta,u)$ must have limited sensitivity to θ. If g is continuously differential in θ the requirement is satisfied if

$$\gamma \leq \left| \frac{\partial g(\theta,u)}{\partial \theta} \right| \leq \rho \tag{4.3}$$

with $\gamma > 0$. If g has negative instead of positive sensitivity to θ the observer can still be applied, but the sign of the observer gain k must be switched. It was proven in Paper B that the parameter estimate converges at least exponentially to the interval to which θ belongs ($[\bar{\theta} - \kappa; \bar{\theta} + \kappa]$). The bound of the estimated parameter is

$$|\hat{\theta}(t) - \bar{\theta}| \leq \kappa + \left(|\hat{\theta}(0) - \bar{\theta}| - \kappa\right) e^{-k\gamma t} \tag{4.4}$$

The minimum convergence rate depends on the sensitivity limit from (4.3) and the observer gain. With $\tilde{x} = \hat{x} - x$, the exponentially converging bounds of the state observer error are

$$\tilde{x}(t) \geq -2\rho\kappa + (\tilde{x}(0) + 2\rho\kappa)\, e^{-\frac{t}{\tau}} - \eta \left(e^{-k\gamma t} - e^{-\frac{t}{\tau}}\right) \tag{4.5a}$$

$$\tilde{x}(t) \leq 2\rho\kappa + (\tilde{x}(0) - 2\rho\kappa)\, e^{-\frac{t}{\tau}} + \eta \left(e^{-k\gamma t} - e^{-\frac{t}{\tau}}\right) \tag{4.5b}$$

where

$$\eta = \frac{\rho\left(\left|\hat{\theta}(0) - \bar{\theta}\right| - \kappa\right)}{1 - k\gamma\tau} \tag{4.6}$$

Thus the state error converges to an interval $\pm 2\rho\kappa$. The minimum convergence rate of the state error convergence depends on parameter sensitivity limits, observer gain and system time constant.

4.2 Scavenge Oxygen Observer

Application of the joint state and parameter estimator as a scavenge oxygen fraction observer is easily achievable by using the COM. System inputs, state and measurement are defined as

$$x = O_{sr}, \quad y = O_{sr,meas}, \quad u = \begin{bmatrix} \dot{m}_f & \dot{m}_{egr} & \omega_{tc} \end{bmatrix}^T \tag{4.7}$$

The input nonlinearity is defined as

$$g(\theta,u) = O_a - \frac{(1 + \frac{\gamma}{4}(O_a + 1))\dot{m}_f \dot{m}_{egr}}{(\theta\beta(\omega_{tc}) + \frac{\gamma}{4}\dot{m}_f)(\theta\beta(\omega_{tc}) + \dot{m}_{egr})} \tag{4.8}$$

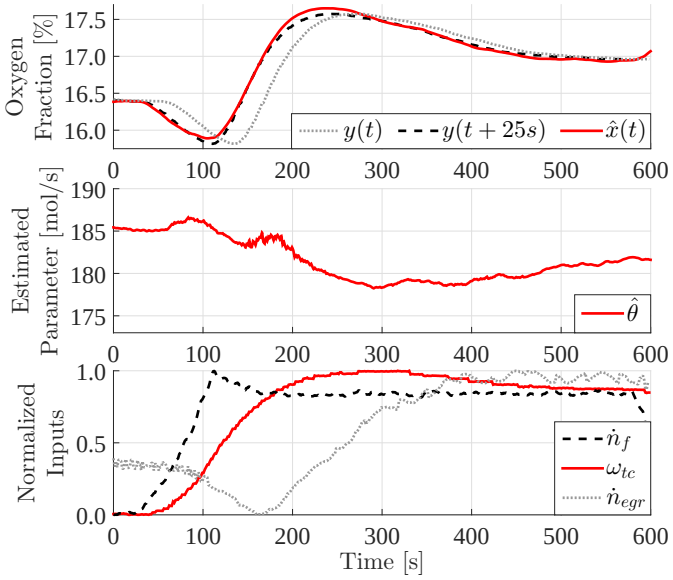

Figure 4.2: Results from application of the joint state and parameter observer to an engine load ramp performed on an engine test bed.

It is more problematic to determine the limits of the sensitivity of g with respect to θ. Equation (4.8) is nonlinear in both θ and in the three inputs which are dynamically coupled by the engine dynamics. Conservative limits can be found by assuming that the inputs are independent and specifying possible intervals for each. This is sufficient to prove exponential convergence but the limits to the convergence rate is slower than what can be expected by the closed loop system. The conditions for slow convergence are only present at short intervals during engine deceleration, which is not a critical scenario for the EGR controller as plenty of oxygen is available for combustion in this scenario.

The convergence proofs show that $\hat{\theta}$ will converge to within the interval that $\theta(t)$ belongs to. At steady state $\theta(t)$ is constant, so $\hat{\theta}$ will converge to the true value. When applying the parameter observer to an MVEM simulation the estimate will track the variations of θ. Thus the scavenge oxygen observer includes a scavenge cooler flow sub-estimator, which also converges exponentially (4.9). The TC-speed signal provides for a coarse model and the oxygen feedback compensates for the inaccuracies of the model.

$$\hat{n}_{ic} = \hat{\theta} \cdot \beta(\omega_{tc}) \tag{4.9}$$

Figure 4.2 shows the result of applying the observer to data from the test engine. The scenario is an engine load ramp, during which a PI EGR controller sets the EGR blower speed. The scavenge oxygen measurement fluctuates significantly during the experiment and the observer is able to provide a good estimate of the oxygen fraction without the time delay, effectively predicting the measurement.

$\hat{\theta}$ also fluctuates during the experiment. This artifact is caused by the discrepancies between the COM and actual dynamics of the system. The reduction of second order mixing dynamics to first order and the assumption of fixed sensor delay are not exact and this disturbs the observer. Nevertheless these issues are small enough that the oxygen estimate is not deteriorated.

Figure 4.3 shows the result of a similar experiment on the vessel, that lead to even larger fluctuations of both the oxygen fraction and of the parameter estimate. Again the observer efficiently predicts the measurement.

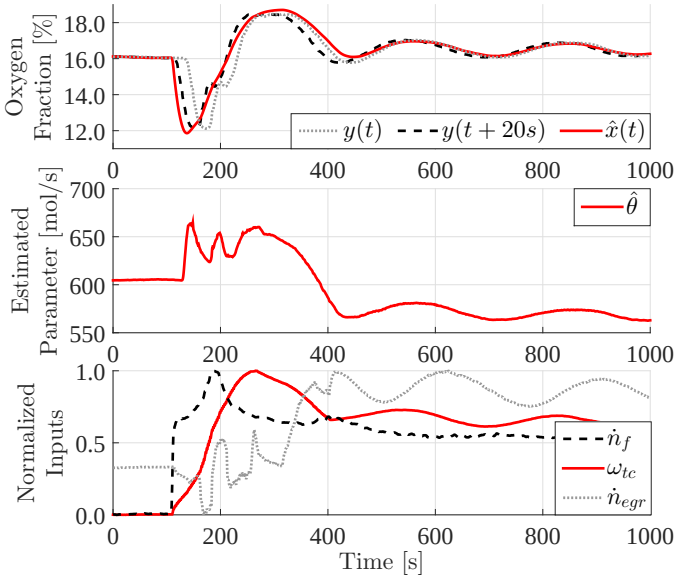

Figure 4.3: Results from application of the joint state and parameter observer to an engine speed setpoint step performed on a vessel operating at sea.

4.3 Conclusions

The observer compensates for the weakness of the COM by estimating the time-varying parameter in the scavenge cooler flow submodel. The resulting observer is simple enough for implementation as part of the EGR controller and only one parameter requires tuning. The output predicts the oxygen sensor measurement 10-25 seconds in advance which makes the observer a possibly valuable contribution to the EGR control loop.

Chapter 5

Adaptive Feedforward Control

Paper C describes the controller, presents a proof of error convergence and shows validation results. This chapter presents highlights from Paper C.

The adaptive feedforward concept is first introduced for a generic first order Hammerstein system with sensor delay. The concept is then applied to scavenge oxygen control of the EGR system. Control performance is compared to that of the PI controller in closed loop simulation with the MVEM and experiments on the test engine and on a vessel in different scenarios.

5.1 Adaptive Feedforward Concept

Chapter 3 showed that the scavenge oxygen fraction of the EGR system can be modeled as a first order Hammerstein model with input that are available to the EGR controller. This model was used in Chapter 4 to design a joint oxygen and parameter observer. In this chapter this generic model is reused now with the objective being control of the scavenge oxygen fraction rather than estimation. The generic control object is again the exhaust gas system, where the inputs are now divided into controlled inputs u and known disturbances d.

$$\tau\dot{x}(t) = g(\theta(t), d(t), u(t)) - x(t) \tag{5.1a}$$

$$y(t) = x(t - \Delta t) \tag{5.1b}$$

$$\bar{\theta} - \kappa \leq \theta(t) \leq \bar{\theta} + \kappa \tag{5.1c}$$

where $\bar{\theta}$ and $\kappa > 0$ describes the bound of $\theta(t)$. An additional requirement is that the input nonlinearity g must be invertible with respect to the controlled input u. If the inverted nonlinearity is designated h this can be expressed as

$$r = g(\theta, d, h(\theta, d, r)) \tag{5.2}$$

This inversion is used in directly in the control law

$$u = h(\hat{\theta}, d(t), r) \tag{5.3}$$

where r is the setpoint for the plant state. The parameter estimator from Chapter 4 provides an estimate of the unknown parameter.

$$\hat{\theta} = -k\left(\tau y(t) + \int y(t) - g(\hat{\theta}(t), d(t - \Delta t), u(t - \Delta t))\,\mathrm{dt}\right) \tag{5.4}$$

where $k > 0$. Notice that the division of controlled input and known disturbances does not affect the parameter estimator. A block diagram of the AFF controller structure is shown in Figure 5.1.

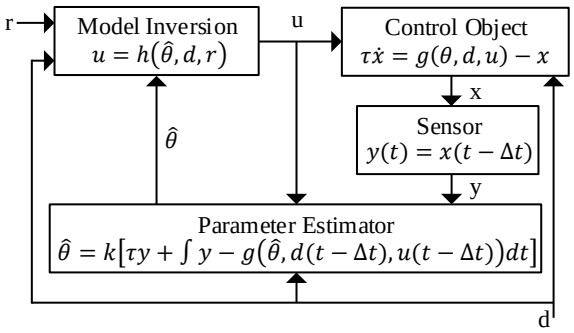

Figure 5.1: Structure of the adaptive feedforward control system.

The controller error $\tilde{x} = x - r$ was proven in Paper C to remain within two bounds that converge exponentially to a small interval around zero. The proof assumes exponential convergence of the parameter estimate (proven in Paper B) and the following sensitivity requirement must be fulfilled

$$\left| \frac{\partial g(\theta, d, h(\hat{\theta}, d, r))}{\partial \hat{\theta}} \right| \leq \mu \tag{5.5}$$

With these assumptions it is shown in Paper C that

$$\tilde{x}(t) \geq -2\mu\kappa + (\tilde{x}(0) + 2\mu\kappa) e^{-\frac{t}{\tau}} - \eta \left(e^{-k\gamma t} - e^{-\frac{t}{\tau}} \right) \tag{5.6a}$$

$$\tilde{x}(t) \leq 2\mu\kappa + (\tilde{x}(0) - 2\mu\kappa) e^{-\frac{t}{\tau}} + \eta \left(e^{-k\gamma t} - e^{-\frac{t}{\tau}} \right) \tag{5.6b}$$

where

$$\eta = \frac{\mu \left(\left| \hat{\theta}(0) - \bar{\theta} \right| - \kappa \right)}{1 - k\gamma\tau} \tag{5.7}$$

When $\theta(t)$ is constant, $\kappa = 0$ and the control error converges to zero.

The intention of the adaptive feedforward controller is to take advantage of the known model and disturbances, in order to react fast to changes of the latter. The adaptation part ensures convergence of control error and thus compensate for model inaccuracy, which is otherwise one of the weaknesses of direct system inversion for control. An additional advantage is that the AFF concept has only one tuning parameter, which is the observer gain. The additional parameters are part of the plant model and thus resemble physical properties of the system behavior.

5.2 Adaptive Feedforward EGR Control

The adaptive feedforward concept is developed for scavenge oxygen control in the EGR system. Plant state, known disturbances and controlled input is defined as

$$x = O_{sr} \quad , \quad d = \begin{bmatrix} \dot{n}_f & \omega_{tc} \end{bmatrix}^T \quad , \quad u = \dot{n}_{egr} \tag{5.8}$$

It is noted that EGR blower speed and COV opening are the actual controlled inputs whereas EGR flow control is an abstraction. This issue is handled by implementing an inner flow control loop. The input nonlinearity is the same as for the control-oriented scavenge oxygen model (3.15), with the scavenge cooler flow approximated by (3.16) and inserted

$$g(\theta, d, u) = O_a - \frac{(1 + \frac{y}{4}(O_a + 1))\dot{n}_f \dot{n}_{egr}}{(\theta\beta(\omega_{tc}) + \frac{y}{4}\dot{n}_f)(\theta\beta(\omega_{tc}) + \dot{n}_{egr})} \tag{5.9}$$

The inversion of $g(\theta,d,u)$ with respect to u is

$$h(\theta,d,r)=\frac{\theta\beta(\omega_{tc})\cdot(O_a-r)}{r-\frac{\theta\beta(\omega_{tc})\cdot O_a-\dot{n}_f\cdot\left(1+\frac{y}{4}\right)}{\theta\beta(\omega_{tc})+\frac{y}{4}\cdot\dot{n}_f}} \tag{5.10}$$

As some oxygen ratios are not reachable by the system, the inversion result is not always physically meaningful. Such cases are compensated by defining the control law as

$$u=\begin{cases} h(\hat{\theta},d,r) & \text{if } h(\hat{\theta},d,r)\in[0;u_{max}[\\ u_{max} & \text{otherwise} \end{cases} \tag{5.11}$$

Thus, when the inversion result is not within the range of possible EGR flows, the controller chooses the maximum EGR flow. In Paper C it was shown that this control law leads to convergence to the best possible flow setpoint in case of actuator saturation. The reason for this is, that the inversion only returns negative or undefined values when the oxygen setpoint is lower than what is reachable. In these cases the maximum EGR flow is the best choice.

5.3 Experiments

The AFF convergence proof assumes system dynamics defined by the COM, that the EGR flow is perfectly controlled and that the oxygen setpoint is constant. With these assumptions the AFF has perfect compensation of known disturbances. On the real engines these assumptions are not entirely accurate. In order to test the robustness and performance of the AFF it was first simulated with the MVEM. These simulations showed that the AFF controller outperformed the reference PI EGR controller significantly during engine load transients.

The AFF EGR controller was then implemented as an option in a test version of the MDT EGR controller software in order to facilitate closed loop experiments. A series of engine load ramps was performed on the DRC test engine, switching between the PI and the AFF controller between the ramps. Figure 5.2 compares the results of two such ramps. As was expected from the MVEM simulations, the AFF outperformed the PI controller significantly. Both with respect to controller error and (as an intended side effect) with respect to smoke formation. The latter was measured with an opacimeter mounted in the chimney of the test facility. When using the PI controller, the opacity opacity shortly from 4 to 16% whereas it peaked at only 8% with the AFF. The normal aim in the test facility is to keep the opacity below 12%.

After the successful application of AFF at the engine test bed, a similar but larger series of experiments where carried out on the vessel Maersk Cardiff, during operation in the South China Sea. Here the transient scenario was an engine speed setpoint step from 35 to 50 RPM. Figure 5.3 shows a direct comparison of the PI and AFF controllers. Again the AFF significantly outperformed the PI controller. Using the PI controller caused the oxygen ratio to drop below 13% and the opacimeter to saturate. Note that the opacimeter measurement from the vessel should not be directly compared to the one on the engine test bed. The AFF controller was able to avoid the large oxygen fraction decrease and make the opacimeter peak at 90%.

Beside the opacimeter the smoke formation on the vessel was also visually validated by video recordings of the exhaust outlet. Stills from these recordings are compared in Figure 5.4. Smoke formation was severe with the PI controller and a visible smoke tail (cloud) was formed. With the AFF controller the smoke was much lighter and dispersed quickly, close to the outlet.

The AFF controller reacts fast to load changes. This is valuable during fast transients, but makes the control system more vulnerable to noise. Figure 5.5 shows an example of this in practice. The data was recorded on the vessel Maersk Cardiff. The scenario is a constant engine RPM setpoint. The load oscillates slightly. The PI and the AFF controller is compared to a fixed EGR blower speed. The AFF is able to keep a smaller control error but it comes at the cost of running the EGR blower harder (more and faster speed

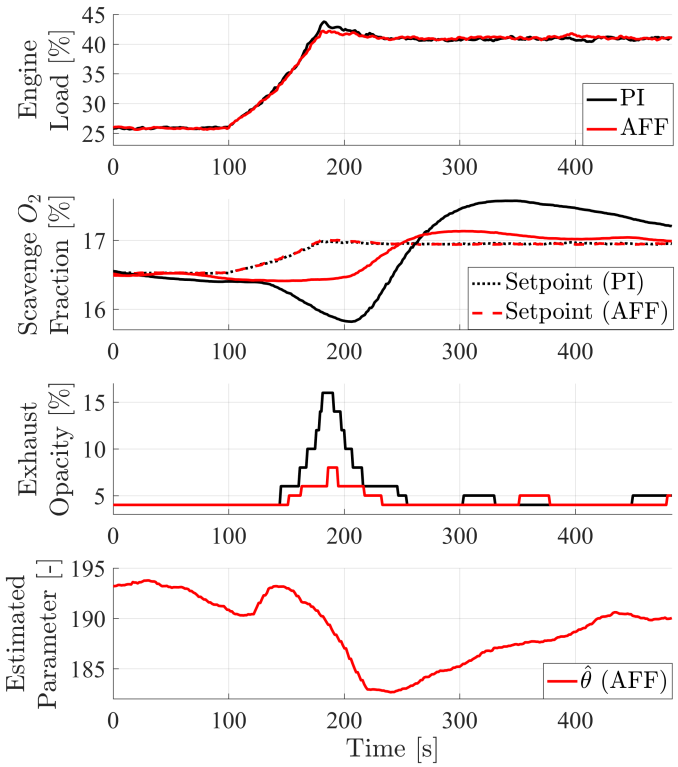

Figure 5.2: Comparison of similar engine load ramps with PI and AFF EGR controller, respectively, at engine test bed. A significant difference in scavenge oxygen fraction and exhaust opacity is observed, showing superior performance of the AFF over the reference controller.

changes). When compared to a fixed blower speed, the AFF reduces the fluctuation of oxygen fraction, whereas the PI controller amplifies the oscillations.

One question that remains regards the robustness of the AFF controller toward the CBV opening. This input is not part of the scavenge cooler flow model and thus it is not directly compensated by the AFF controller, unlike the fuel flow and Turbocharger (TC) speed. Instead it is up to the parameter estimator to adapt to the consequences of changing the CBV opening. This has not been tested on an engine but the scenario was simulated with the MVEM. Figure 5.6 shows a comparison of how the PI and the AFF compensates for the CBV. As none of the controllers have direct compensation of the CBV the responses start out equally. However, the AFF compensates converges back to the setpoint faster than the PI. Therefore the CBV is not considered to be a show stopper for the AFF EGR controller.

5.4 Conclusions

A novel scheme of adaptive feedforward control of a first order Hammerstein system with sensor delay was introduced. The controller is based on a nonlinear parameter estimator and inversion of the input nonlinearity. Exponentially converging error bounds were found analytically.

The adaptive feedforward concept was applied to scavenge oxygen control in the EGR system and validated by simulation of the MVEM and by experiments on test engine and vessel. AFF significantly outperformed the reference PI controller in terms of scavenge oxygen error during transients and at a steady engine speed setpoint. Smoke formation was reduced during loading transients. An experiment on the vessel with constant engine RPM setpoint showed that the AFF EGR controller is harder on the EGR blowers but keeps a smaller control error the the PI controller. Simulation with the MVEM showed the AFF

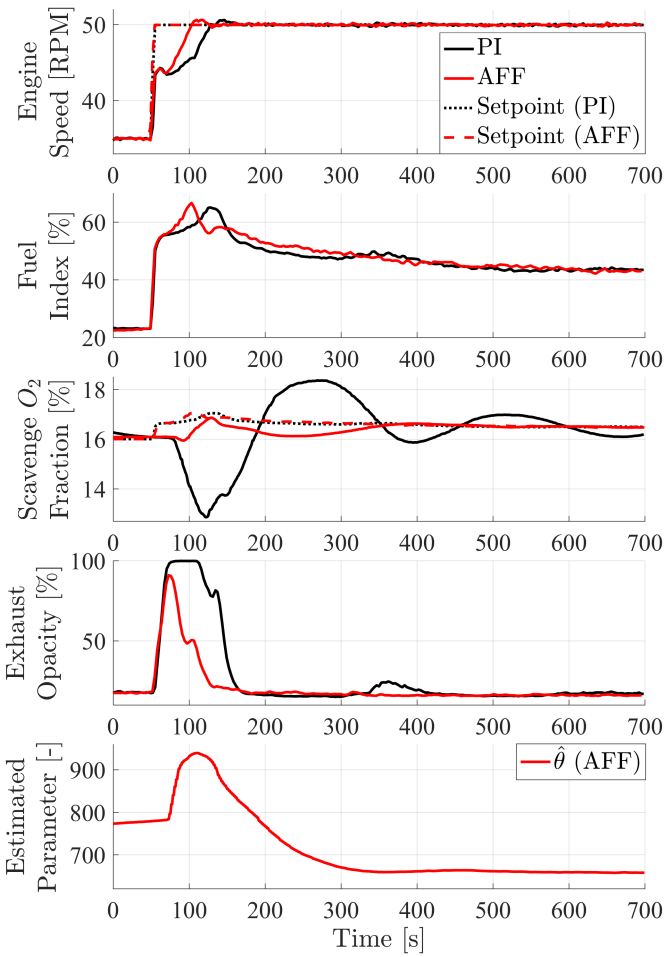

Figure 5.3: Comparison of similar engine RPM setpoint step-responses with PI and AFF EGR controller, respectively, on the vessel Maersk Cardiff. A significant difference in scavenge oxygen fraction and exhaust opacity is observed, showing superior performance of the AFF over the reference controller.

to be robust against changes of the CBV opening.

(a) PI EGR controller. 45 seconds of black smoke.

(b) AFF EGR controller. 20 seconds of light smoke.

Figure 5.4: These photos compare the smoke from the exhaust outlet of the vessel Maersk Cardiff during large engine load transients.

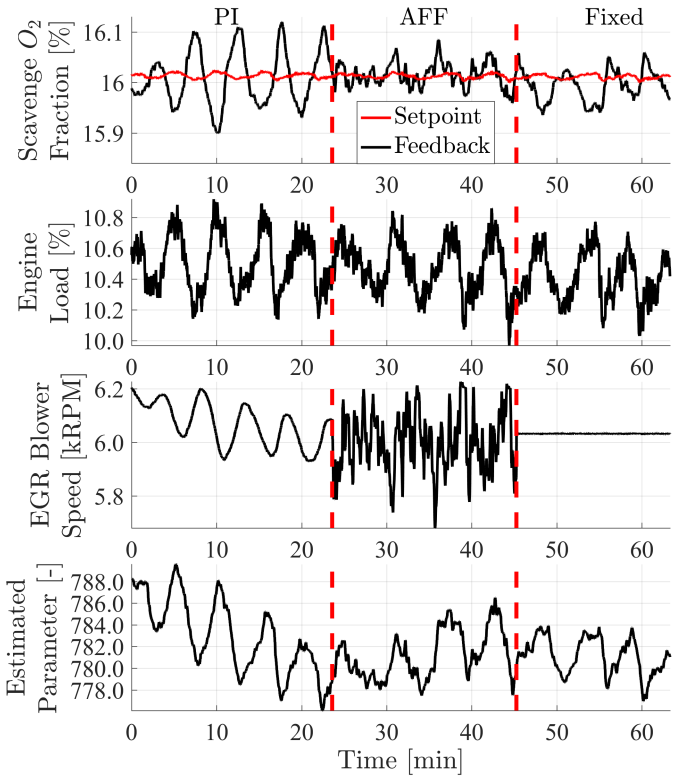

Figure 5.5: Comparison of existing PI controller, nonlinear controller and fixed EGR blower speed at close to steady state conditions. A small load oscillation is propagated to the scavenge oxygen level.

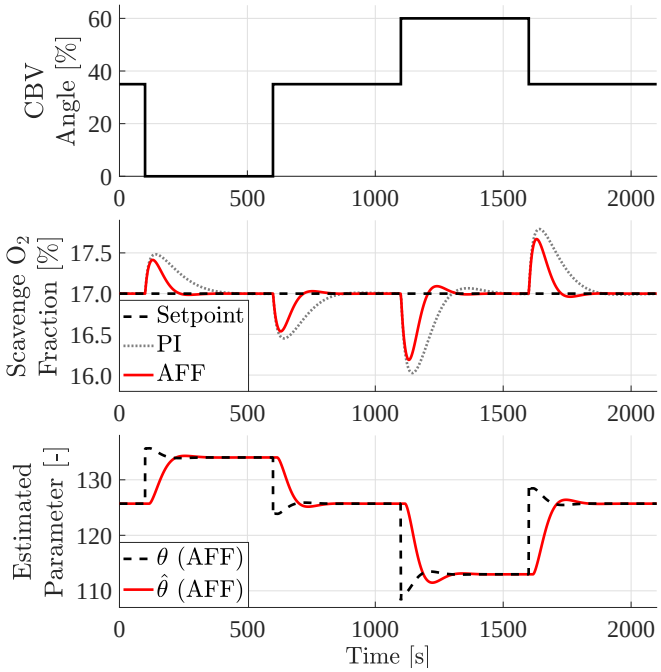

Figure 5.6: Comparison of CBV opening steps with PI and AFF EGR controller, respectively, simulated with the MVEM. The AFF controller is faster than the PI.

Chapter 6

Fuel Index Limiters

This chapter describes two fuel index limiters which are based on oxygen/fuel-ratio. The limiters and validation results appear in Paper D, submitted to a journal. This chapter provides an introduction to fuel index limiters and motivation for their use, followed by a description of a fuel index limiter based on air/fuel-ratio. Taking offspring in the latter, two novel methods are presented for calculating a fuel index limiter for engines with EGR. These are validated in simulation and in experiments on a vessel.

6.1 Fuel Index Limiters

An electronic governor regulates the crankshaft speed of a two-stroke marine diesel engine by adjusting the amount of injected fuel. A so-called fuel index specifies the amount injected per cycle, relative to the amount injected at Maximum Continuous Rating (MCR). The feedback loop is optimized for near steady state operation so large steps of speed setpoint can lead to undesirable transient behavior. In order to avoid excessive shaft torque and also to avoid injecting more fuel than what can be burned, a number of artificial actuator saturations are implemented in the governor software. These are called fuel index limiters. Figure 6.1 shows how the limiters are placed in the feedback loop.

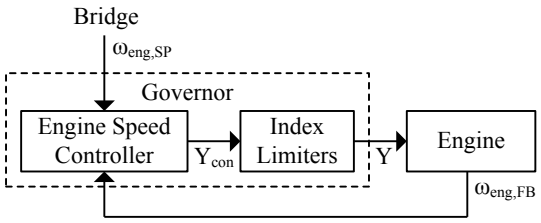

Figure 6.1: An engine speed setpoint is set by the bridge. The index limiters prevent the output from the engine speed controller from making the engine reach unwanted regions of operation (to limit e.g. smoke formation and shaft stress).

When maneuvering at low loads the oxygen content of the charge is the limiting factor. This is normally handled by a limiter based purely on scavenge pressure. As scavenge pressure is not the only factor that affects oxygen availability this limiter ends up being rather conservative and requires engine specific tuning.

6.2 Dynamic Limiter Function

Parallel to the development of NO_x emission reduction systems, the restrictions of Energy Efficiency Design Index (EEDI) and focus on fuel efficiency has led to downsizing and derating of engines. Smaller engines have less power surplus for acceleration and the need to exploit the engine optimally in transients

has also become essential. To meet this demand MDT has introduced a control technology update named Dynamic Limiter Function that optimizes certain parameters such as valve timing during accelerations [39]. The update also includes a fuel index limiter based on an estimate of trapped scavenge gas and a minimum air/fuel-ratio. The air/fuel-ratio λ_A is defined from trapped scavenge gas as

$$\lambda_A = \frac{m_{trap}}{m_f} = \frac{m_{trap}}{k_{fm} Y} \tag{6.1}$$

where m_{trap} is the mass of scavenge gas trapped in the cylinder and m_f is the mass of injected fuel. If a minimum air/fuel-ratio λ_{LA} is specified and the mass of trapped scavenge gas is known a fuel index limit Y_{LA} can be calculated as

$$Y_{LA} = \frac{m_{trap}}{k_{fm} \lambda_{LA}} \tag{6.2}$$

The Y_{LA} limiter has been proven superior to the conventional limiter which is based on scavenge pressure only. However, the limiter only applies to engines with atmospheric composition of air in the scavenge receiver.

6.3 Limiters based on Oxygen/Fuel-Ratio

The basic concept of an exhaust gas recirculation system is to lower the oxygen content of the scavenge gas. This violates the assumption of fresh air scavenging made in the calculation of Y_{LA}. Using this limiter on an engine with EGR leads to excessive injection of fuel during large accelerations and the fuel that is not burned exits the exhaust outlet as visible smoke. The fast AFF EGR controller reduces the issue compared to a PI EGR controller, but a physical limit to oxygen availability still exists due to the inertia of the turbocharger and scavenging system.

For an engine with EGR the oxygen/fuel-ratio is relevant instead of the air/fuel-ratio. The existing limiter calculates the trapped-gas/fuel-ratio and assumes that fresh air has been trapped. Paper D investigated two methods of converting the existing limiter value by considering the oxygen fraction of the trapped gas. The limiter conversion is

$$Y_{LO} = Y_{LA} \frac{O_{sr}}{O_a} \tag{6.3}$$

where Y_{LO} is a limiter based on oxygen/fuel-ratio, O_{sr} is the scavenge oxygen fraction and O_a is the oxygen fraction of ambient air. Two methods of implementing this conversion was developed and investigated. The first method (Y_{LOS}) was to base the extension on the scavenge oxygen sensor signal $O_{sr,meas}$

$$Y_{LOS} = Y_{LA} \cdot \frac{O_{sr,sens}}{O_a} \tag{6.4}$$

This method is easy to implement and parameterize, but two possible drawbacks have been identified. The slow dynamics of the oxygen sensor will lead to an inaccurate limit if the scavenge oxygen fraction changes during a transient. Furthermore, if the limiter is based on the instantaneous oxygen fraction an inferior EGR controller could cause oscillations in the fuel index as the fuel index and scavenge oxygen fraction is closely coupled. Such oscillations are referred to as Limiter Loop Oscillations (LLO) in this work.

A second method of extending the limiter has been developed, aimed at avoiding both LLO and the direct dependence on the oxygen sensor. The idea is to use the COM but neglect its first order dynamics. Only the input nonlinearity $g(\dot{n}_f, \dot{n}_{ic}, \dot{n}_{egr})$ of the COM is used in the limiter conversion, resulting in the following equation

$$Y_{LOM} = Y_{LA} \cdot \frac{g(k_f \cdot \omega_{eng} \cdot Y_{LOM}, \dot{n}_{ic}, \dot{n}_{egr})}{O_a} \tag{6.5}$$

where the relation $\dot{n}_f = k_f \cdot \omega_{eng} \cdot Y$ is used. Inserting and rearranging this leads to a second-order equation (6.6). This is solved online for its positive solution, which is used as a fuel index limiter (Y_{LOM}).

$$k_f \omega_c \left(\frac{y}{4} - \frac{1 + \frac{y}{4}(O_a + 1)}{O_a} \cdot \frac{\dot{n}_{egr}}{\dot{n}_{ic} + \dot{n}_{egr}} \right) Y_{LOM} - \frac{\dot{n}_{ic}}{Y_{LA}} Y_{LOM} - \frac{\frac{y}{4} k_f \omega_c}{Y_{LA}} Y_{LOM}^2 + \dot{n}_{ic} = 0 \tag{6.6}$$

The parameter estimate from Chapter 4 is used for estimation of the scavenge cooler flow $\dot{m}_{ic} = \hat{\theta} \cdot \beta(\omega_{tc})$. The Y_{LOM} limiter has the property that it sets a limit low enough, such that if the fuel index is suddenly increased up to the limit, the resulting scavenge oxygen drop will not lead to a decrease in the limit, thus avoiding the mechanism that can lead to oscillation. The Y_{LOM} limit is lower than Y_{LOS} at steady state, but increases more rapidly after a fuel index step, as it reacts instantaneously to changes in EGR flow and scavenge cooler flow. Such a rapid increase in fuel index leads to a rapid acceleration of the engine. Figure 6.2 shows how the governor, limiter and EGR control systems interact.

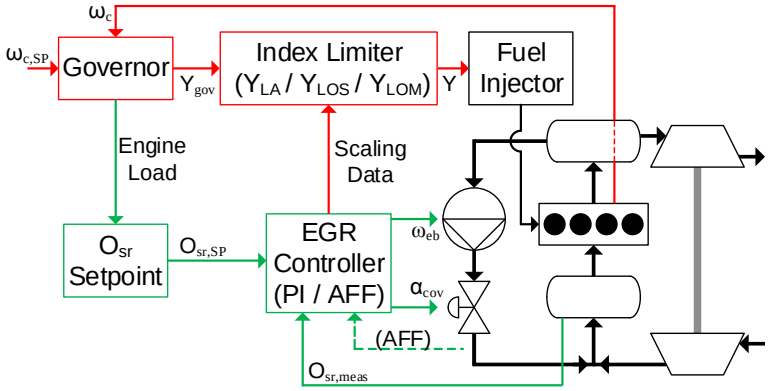

Figure 6.2: Overview of the governor (red) and EGR (green) control systems. The two systems control coupled variables of the same process and interacts through the engine load signal and data for scaling of the index limiter. The dashed green line refers to TC-speed, EGR flow and fuel flow data used by the AFF EGR controller.

6.4 Experiments

Simulation of transients with the normal MVEM showed that the limiters performed equally well when combined with the AFF EGR controller and showed no sign of LLO. When the system dynamics where slowed down in order to replicate low load conditions and a PI EGR controller was used, the sensor based extension led to a small fluctation but no severe oscillation. Y_{LOM} avoided LLO completely whenever it was applied.

The limiters were further validated as part of the experiment series described in Chapter 5. These tests gave similar results as the MVEM simulations. The combination of Y_{LOS} and a PI EGR controller caused a decrease in acceleration due to LLO. When combined with an AFF EGR controller both extended limiters performed well, with a small acceleration advantage by using Y_{LOM}. Smoke formation during the tests was measured by an opacimeter in the exhaust path and confirmed visually by video recordings of the exhaust outlet. Figure 6.3 shows a comparison of engine speed and opacity for several combinations of EGR control and limiter function. The combination of AFF EGR control with an extended limiter is clearly the best of the solutions with respect to exhaust opacity.

Figure 6.4 shows a series of stills from the video recordings of the exhaust outlet during accelerations. The photos 6.4(a) and 6.4(b) are repeats from Figure 5.5 showing the performance of the PI and AFF EGR controllers, respectively, without extending the limiter. Both of the extended limiters are able to reduce the visible smoke to a minimum, regardless of which EGR controller they are combined with.

6.5 Conclusions

It was shown how a fuel index limiter based on air/fuel-ratio can be converted to a fuel index limiter based on oxygen/fuel-ratio and thus apply to engines with exhaust gas recirculation. Two methods of

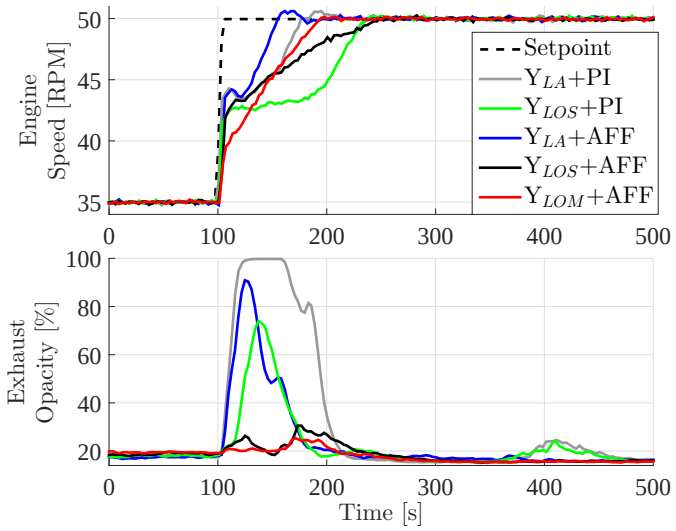

Figure 6.3: A comparison of engine speed and exhaust opacity for 5 similar engine speed setpoint steps carried on the vessel Maersk Cardiff with different combinations of limiters and EGR controllers. Acceleration performance slightly degrades when basing the limiter conversion on the oxygen sensor (Y_{LOS}).

implementing this conversion were proposed. Simulation and experiments showed that the first conversion method (Y_{LOS}) could lead to fuel index fluctuation when combined with a PI EGR controller. The second conversion method was designed to address this problem and did not cause fluctuations. Experiments on a vessel showed that both methods avoid smoke formation and fuel index fluctuation when combined with an AFF EGR controller. The second conversion method has a slightly better acceleration performance. Acceleration performance is not decreased significantly by applying this solution, when comparing to the non-extended limiter.

(a) Y_{LA}+PI. Thick black smoke is emitted for 45 seconds.

(b) Y_{LA}+AFF. The smoke level is reduced compared to the PI controller but still visible.

(c) Y_{LOS}+PI. Smoke formation is close to invisible.

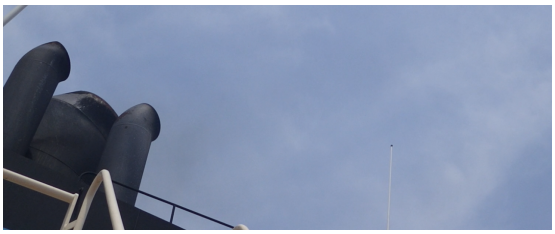

(d) Y_{LOS}+AFF. No visible smoke.

(e) Y_{LOM}+AFF. No visible smoke.

Figure 6.4: Exhaust smoke on a vessel with during accelerations from 35 to 50 RPM, with various combinations of fuel index limiters and EGR controllers.

Chapter 7

Conclusions

7.1 Conclusions

The project demonstrated a novel approach to scavenge oxygen control in a large two-stroke diesel engine with exhaust gas recirculation. Furthermore, two new fuel index limiters for these engines were proposed and investigated. Both separately and especially in combination, the suggested approaches significantly outperformed the reference methods in experiments on a vessel at sea.

The thesis showed how to derive a control-oriented model of the scavenge oxygen fraction from an existing first principle mean-value, filling and emptying model. The reduced model (COM) was validated in simulation and experiments and was found to replicate the essential dynamics for control design. A joint state and parameter observer was then developed, for a model class, to which the COM belongs. When applied to the COM, the observer was shown to be able to compensate for oxygen sensor delay and provide a real time estimate of the scavenge oxygen fraction plus an estimate of scavenge cooler flow. As a salient practical feature the observer included only one tuning parameter. Validation against simulation and experiment data showed good performance. The next contribution was the design of a novel adaptive feed-forward controller. It exploits the knowledge of known disturbances and compensates for model inaccuracies by parameter adaptation. The design was demonstrated be able to compensate for delays in measurement of the essential variable. When applied to scavenge oxygen fraction control the AFF controller was found to significantly outperform the reference PI controller, especially during engine loading transients. The final contribution of the project was to propose two methods for extending an existing fuel index limiter, in order to apply to engines with exhaust gas recirculation. It was also demonstrated from experiments that, when combining an extended fuel index limiter with the AFF EGR controller, smoke formation during vessel acceleration could be avoided without sacrificing maneuverability.

The project hence showed that an application specific control design, based on dynamic modeling of the EGR system, was able to solve the control challenges experienced in transients with generic PI control design. A sea trial with large vessel accelerations validated the superior performance in practice. The resulting controller was designed to be generic over a broad engine range and its low complexity should make it a realistic choice for application in final product software.

7.2 Perspectives

The superior performance offered by the proposed control design has convinced MAN Diesel & Turbo to incorporate it as standard in their EGR control software. The choice between the two limiter extensions is yet to be made. The acceleration advantage of Y_{LOM} must be held up against the complexity of Y_{LOS}. The first long term service tests of the new control system are planned to take place in 2017.

The fleet of ships with MDT EGR engines is expected to increase rapidly in the near future. A patent

that covers the AFF EGR controller has been applied so the control design developed in the project is likely to exist only on MDT engines. The competition between EGR, SCR and gas engines is yet to be settled. This project has solved one of the essential issues of the EGR technology, making it a feasible choice for commercial use.

7.3 Future Research

While the developments in this project has significantly improved the EGR controller, there are still areas of interest for future research. Part of the Hercules II project currently investigates how to expand the operating region of the MVEM to low loads [46, 47].

The inner EGR flow control loop was given only little attention in this project and required tuning. An adaptive or self-tuning solution would be optimal as the choice of EGR blower(s) and valves is up to the engine builder. Furthermore, larger engines might employ multiple parallel turbochargers. This configuration must be handled in the scavenge cooler flow model if the AFF EGR controller is applied to such an engine.

Another aspect, that has not been discussed in this thesis, is the scavenge oxygen setpoint. The current solution is load dependent, but only applies to the steady state case. During a transient the optimal scavenge oxygen fraction is most probably higher. Related to this, research into how EGR should behave at very low loads ($<10\%$) should also be under investigated along with engine speed reversal scenarios.

Paper A

Control-Oriented Model of Molar Scavenge Oxygen Fraction for Exhaust Recirculation in Large Diesel Engines

Kræn Vodder Nielsen[*1,2], Mogens Blanke[2,3], Lars Eriksson[4], Morten Vejlgaard-Laursen[1]

[1] MAN Diesel & Turbo, Teglholmsgade 41, 2450 København SV, Denmark [2]Department of Electrical Engineering, Automation and Control Group, Technical University of Denmark, Elektrovej Building 326, 2800, Kgs. Lyngby, Denmark

[3]AMOS CoE, Institute of Technical Cybernetics, Norwegian University of Science and Technology, 7491 Trondheim, Norway

[4]Vehicular Systems, Department of Electrical Engineering, Linköping University, 58183 Linköping, Sweden

Abstract:
EGR systems have been introduced to large marine engines in order to reduce Nitrogen Oxides (NO_x) formation. Adequate modelling for control design is one of the bottlenecks to design EGR control that also meets emission requirements during transient loading conditions. This paper therefore focus on deriving and validating a mean-value model of a large two-stroke crosshead diesel engines with EGR. The model introduces a number of amendments and extensions to previous, complex models and shows in theory and practice that a simplified nonlinear model captures all essential dynamics that is needed for EGR control. Our approach is to isolate and reduce the gas composition part of the more complex models using nonlinear model reduction techniques. The result is a COM of the oxygen fraction in the scavenge manifold with three molar flows being inputs to the COM, and it is shown how these flows are estimated from signals that are commonly available. The COM is validated by first comparing the output to a simulation of the full model, then by comparing with measurement series from two engines. The control oriented nonlinear model is shown to be able to replicate the behavior of the scavenge oxygen fraction well over the entire envelope of load and blower speed range that are relevant for EGR. The simplicity of the new model makes it suitable for observer and control design, which are essential steps to meet the emission requirements for marine diesel engines that take effect from 2016.

K. V. Nielsen, M. Blanke, L. Eriksson, and M. Vejlgaard-Laursen. "Control-Oriented Model of Molar Scavenge Oxygen Fraction for Exhaust Recirculation in Large Diesel Engines". *Journal of Dynamic Systems, Measurement and Control - ASME* 139.2 (2017). DOI: 10.1115/1.4034750

[*]Principal corresponding author. Tel.: +45 33851909; E-mail: kraenv.nielsen@man.eu

A.1 Introduction

Diesel engines have long been the preferred means of propulsion power production on ocean-going vessels for reasons of high fuel efficiency and reliability. Increased focus on environmental protection have introduced concern regarding the emissions of CO_2, SO_x and NO_x from the marine diesel engines. NO_x emissions are subject to restriction in the Tier III standard introduced by the International Maritime Organization [2]. These regulations apply to vessels built after 1st of January 2016 when operating in specified NO_x Emission Control Areas (NECA). Currently the North American coastal area is such an NECA and the North Sea and Baltic Sea are expected to become NECAs as well[54]. A reduction of 76% is required compared to the Tier II standard. Such reduction by a factor of four is difficult to obtain and models are needed that could be used for design of robust control and estimation schemes.

Formation of NO_x in a diesel engine occurs during the combustion process where high temperatures lead to reactions between nitrogen and oxygen, known as the Zeldovich mechanism [11]. Efforts to decrease the Specific Fuelk Oil Consumption (SFOC) have lead to increased peak combustion temperatures and thus NO_x. Therefore a trade-off between SFOC and NO_x formation must be made in a conventional diesel engine. The severity of emission reduction specified in the Tier III regulation however, makes it infeasible to simply shift this trade-off in favor of lower emissions. New approaches are necessary in order to meet the challenge. After-treatment systems such as SCR remove NO_x from the exhaust gas but consume supplied chemicals in the process. Several methods exist to add water to the combustion process by e.g. emulsion into the fuel or direct injection into the combustion chamber. This circumvents the SFOC/NO_x trade-off by changing the gas composition of the combustion. Addition of water increases the heat capacity and decreases the availability of oxygen, resulting in lower peak temperatures while maintaining acceptable SFOC.

Exhaust gas recirculation has a similar effect on heat capacity as water addition and decreases the oxygen fraction of the combustion mix more significantly. The latter affects flame formation and thus even lower peak temperatures occur. A trade-off with SFOC still exists when using EGR, but at much better terms. Choosing the right amount of recirculated gas flow is critical to obtain the best compromise. At excessively low scavenging oxygen levels the combustion is incomplete and visible smoke is produced. This effect is well known on turbocharged engines where turbo-lag limits the possible loading rates. Careful control of the exhaust gas recirculation is required if smoke is to be avoided when load increasing occurs, e.g. during manoeuvring.

Engine designer MAN Diesel & Turbo has introduced high pressure EGR technology to their large two-stroke diesel engines. A simplified sketch of the gas flows in such an engine is shown in Figure A.1. Gas from the exhaust receiver is cleaned and cooled in the EGR Unit before being pressurized by the EGR blower and mixed into the scavenge flow before the scavenge receiver. The flow rate of recirculated gas is controlled by varying blower speed ω_{eb} or cut-out valve opening α_{cov}.

The correct amount of recirculated flow is implicitly decided by calculating a number of operating points in which the NO_x emission is acceptable. These points are characterized by engine load and by the partial pressure of oxygen in the scavenge receiver (O_{sr}). Linear interpolation in load results in a scavenge oxygen set point for the EGR controller. An example is shown in Figure A.2. Engine load is a sufficient characteristic of the operating region as engine load and speed correlates due to the propeller curve.

The existing control strategy is fixed gain proportional-integral feedback control, which has been applied to several engine setups. During stationary running conditions the performance is adequate but it suffers in engine loading transients. In such a transient the fuel flow to the cylinders is adjusted by the governor. This affects the fraction of oxygen in the recirculated flow and thus O_{sr}. An opposite effect comes from the change in turbocharger speed and thus fresh air flow, but this response is slower. These disturbances are compensated by feedback control but the slow nature of the system and difficulties in

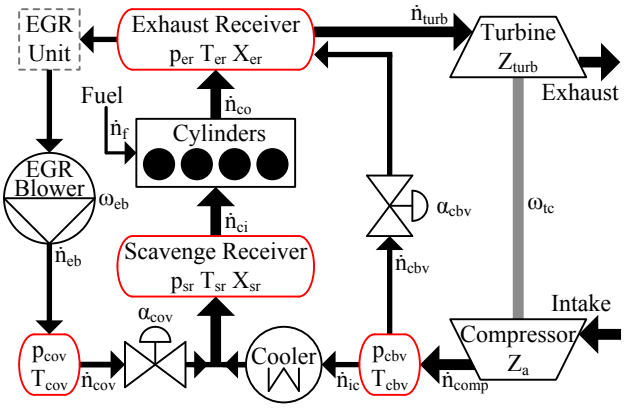

Figure A.1: Overview of main gas flows and components of the engine with exhaust gas recirculation and cylinder by-pass valve.

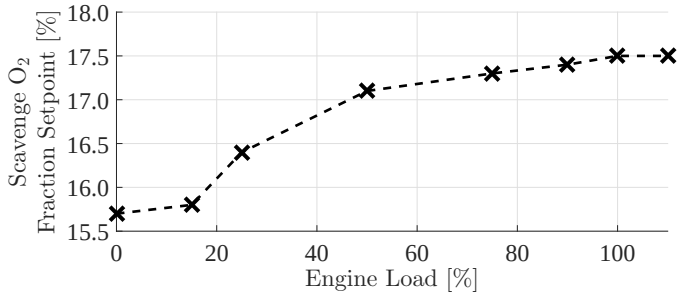

Figure A.2: An example of required scavenge oxygen fraction as a function of engine load. The linearly interpolated commissioning points are specific to the engine.

the measurement of O_{sr} limits the achievable performance[44]. As smoke formation must be avoided it is necessary to restrict the engine loading rate when running a fixed-gain EGR control. This is problematic considering that the Emission Control Areas cover ports and coastal areas where sufficient maneuvering capabilities are required.

In order to deal with these challenges a research effort was started that covers modeling and simulation of the airpath of large two-stroke crosshead engines with EGR, analysis of said models with respects to control properties and design of controllers based on the results. Where previous papers presented first principle simulation models, the present paper simplifies earlier models to arrive at a control-oriented model that only includes the most dominant effects of the gas composition system. This paper shows, through analytical considerations, how a low order nonlinear model can adequately describe the dominating effects. The efficacy of the model is validated by simulation, on a diesel engine at a test bed and at sea.

A.1.1 Literature

The popularity and wide-spread use of internal combustion engines have facilitated a large amount of research and published literature. An extensive treatment of engine processes and modeling was published by Heywood [11]. More recent material that also include more on control systems include Guzzella & Onder [14] and Eriksson & Nielsen [12]. Turbocharging issues were treated in works by Watson & Janota [55] and more recently by Dixon [56] among others.

The large two-stroke crosshead engines, which are treated in the present paper, are less common in literature. Most relevant is the governor (engine speed controller) design that had some popularity at the end of the last century [31, 32, 57, 58]. This incited the development of more accurate dynamic models of

the engine speed behavior as function of fuel pump index. Turbocharger dynamics turned out to be an important part of these models. A discussion of various model types are found in [28]. Examples of these are found in [29, 30]. Introduction of NO_x emission limits lead to the use of variable geometry turbines (VGT) as in [33]. Extensive treatment of marine diesel engine control was given in [4], that also discusses why it is challenging to provide an accurate model for such an engine. More recent investigations of large two-stroke marine diesel engine models are found in [34, 36, 37, 38, 59].

Due to the relative novelty and scarcity of EGR systems for large two-stroke crosshead engines only a few papers on its control properties have been found. All of them stem from the work published by Hansen et al in two papers about modeling [43] and control [44], respectively. The work on modeling was further developed by Alegret et al in [45] where the cylinder bypass valve (CBV) was introduced and estimation of model parameters was changed. A different approach to EGR control was published by the authors of the present paper in [53] based on a simple control oriented model and a nonlinear controller.

Literature on modeling and control of EGR systems is much more abundant for four-stroke automotive engines. Here the EGR system is usually accompanied by a variable-geometry turbine for faster response in transients. This naturally leads to a difficult optimisation problem with regards to control design as seen in [15, 18, 20, 21, 60, 61]. The mean value model of such a system published in [19] was the inspiration of the modeling work done by Hansen et al in [43]. The effect of fuel composition on intake oxygen fraction of an automotive engine with EGR was presented in [26] and an observer design that was able to estimate said fuel composition was presented in [27]. While the published literature on automotive engines serve as inspiration to the work on large two-strokes some significant differences do apply. The very limited engine test bed availability that makes extensive parameter mapping infeasible was discussed in [4]. Furthermore the time constants of e.g. turbo-lag and gas mixing is slower, the relationship between engine speed and torque is more predictable due to the propeller curve and the heavy fuel oil creates a hostile environment for the sensors.

A.1.2 Purpose

Mean value, filling and emptying models (MVEM) are an obvious choice for simulation of the EGR system when evaluating a controller design. It allows for modular model development with first principle modeling available for most component types. These models are accurate enough for simulation of essential control properties [19]. Parameter estimation can be challenging if the sensor setup and datasets are inadequate but it is possible [43, 45].

A simple model that only represents the most dominant behavior of the system is desirable for designing a simple and effective controller. It is not intuitively obvious how to design a controller from the MVEM models due to their complexity. SISO methods based on a linearized MVEM were investigated in [44] where it was difficult to achieve both performance and robustness. A simple control-oriented model was briefly presented in [53]. The main contribution of the present paper is a slightly different version of this model along with a direct derivation from the MVEM and validation by comparison to simulation results from the MVEM and a number of measurement series from two engines.

The starting point for this paper is an MVEM based on the work presented in [45]. A brief analysis of the model structure reveals that the gas composition part of the model can be isolated. It is then simplified by removing non-dominant dynamics. The result is a COM of the scavenge receiver oxygen fraction which is the essential parameter for the EGR controller. Three physical flows act as inputs to the model and it is shown how to approximate these from available sensor signals.

A.1.3 Outline of this Paper

A mean-value, filling and emptying model of the EGR system is introduced in Section A.2 along with a brief review of the model structure. Section A.3 presents an analytical approach to reduce the complexity of the gas composition model and how to estimate inputs to the simplified model from commonly available signals. Section A.4 compares the reduced model to simulations of the MVEM and measurement series from two engines, one running at a test bench, another during actual operation at sea.

A.2 Mean-Value Engine Model

This section presents a first principle model of the engine air path. As the model is a continuation of previous work some of the origins of the model is presented along with reasons for the changes and additions in the present version. The presentation of the model itself is divided into subsections of the main components of the engine air path. The oxygen sensor is discussed in a separate subsection. The last subsection reviews couplings between the states of the model.

The purpose of the MVEM is to model the behavior of the oxygen fraction in the scavenge receiver. The main inputs of the model is engine load, EGR blower speed and the opening angle of various valves in the engine airpath.

On the current engines the EGR system can only be started when the engine is running at steady state. During the EGR start-up procedure the blower speed and COV opening are defined by a fixed sequence of a few minutes. After this, the closed loop EGR controller is used. As the MVEM is intended for control design and closed loop EGR control only occurs with an up-and-running EGR system, the model is initialized as a running system as well.

A.2.1 Origin

The engine considered is the two-stroke crosshead diesel engine designated 4T50ME-X located in MDT's Diesel Research Center in Copenhagen. The most basic parameters of the engine is provided in Table A.1. The first effort to model scavenge receiver oxygen behavior when the EGR system is included was presented in [43]. This work was inspired by [34] and [19]. The result was a filling and emptying model with a mean value assumption for the flow through the cylinders. Identifiability of unknown parameters proved difficult due to system complexity, sensor setup and availability of suitable datasets.

Table A.1: Parameters of test engine

Number of cylinders	4	$[-]$
Bore	0.5	$[m]$
Stroke	2.2	$[m]$
Scavenge pressure at MCR	4.7	$[bar]$
Engine speed at MCR	123	$[RPM]$
Effective power at MCR	7.1	$[MW]$

Further work on this model was presented in [45]. The most notable changes were the addition of the cylinder bypass valve, advanced calculation of temperature of the flow from the cylinders and a new method of parameter estimation that included a larger number of datasets.

A.2.2 Changes and additions

The full model used in the present paper is based on [45]. Sections A.2.3-A.2.8 describe the main points of this model, including some changes that are listed and explained below:

1. Gas composition is modelled as a vector of molar fractions instead of oxygen mass fraction only.
2. Gas flows are modelled as molar flows instead of mass flow to support the gas composition model.
3. EGR string is split in separate flow components for EGR blower and cut-out valve with a volume in between.
4. Recirculation valve is removed.

As the oxygen level in the scavenge receiver is measured in molar fraction rather than mass fraction it is more convenient to model molar fraction directly instead of converting. To support this change the gas flows are modelled as molar flows rather than mass flow. The change in gas flow modelling allows for the use of the universal gas constant in the flow component models and thus simplifies the parameters of the model. Parameters of the flow components are based on the result of the estimation carried out in [45]. An overview of the engine air path and the flows included in the model is provided in Figure A.1. Models of the separate components are presented in the following sections.

A.2.3 Volumes

A filling and emptying model represents the amount of gas in a number of volumes between flow components as states. Some models also represent gas temperature in these volumes as state variables but in the present case these dynamics are neglected. This is referred to as an isothermal volume model [12]. As is common practice the amount of gas in a volume is expressed as a pressure state, by use of the ideal gas law.

Large volumes result in slower filling and emptying dynamics than smaller volumes as more gas flow is needed to change the pressure in the larger space. In a marine two-stroke engine the scavenge and exhaust receivers are the largest and thus most dominant in the frequency range of EGR control. They are, however, fast compared to the dynamics of engine and turbocharger RPM and [34] argues that they can be lumped together with the turbocharger speed dynamics for model simplification.

In the present model scavenge and exhaust receiver pressures are modeled with the following differential equations

$$\dot{p}_{sr} = \frac{RT_{sr}}{V_{sr}}(\dot{n}_{ic} + \dot{n}_{cov} - \dot{n}_{ci}) \tag{A.1}$$

$$\dot{p}_{er} = \frac{RT_{er}}{V_{er}}(\dot{n}_{co} - \dot{n}_{eb} + \dot{n}_{cbv} - \dot{n}_{ti}) \tag{A.2}$$

For model consistency it is most convenient to not connect any flow components (valves, blowers etc) in series. Therefore two small extra volumes are modeled solely to avoid this. The first is before the CBV

$$\dot{p}_{cbv} = \frac{RT_{cbv}}{V_{cbv}}(\dot{n}_{comp} - \dot{n}_{ic} - \dot{n}_{cbv}) \tag{A.3}$$

The second is before the EGR cut-out valve (COV).

$$\dot{p}_{cov} = \frac{RT_{cov}}{V_{cov}}(\dot{n}_{eb} - \dot{n}_{cov}) \tag{A.4}$$

A.2.4 Turbocharger

Flows and efficiencies of the compressor and turbine are calculated in the same manner as in [45], where super ellipses fitted to maps from the manufacturer are used for inter- and extrapolation. Parameters for the ellipses from [45] are adjusted in order to get molar rather than mass flow.

As compressor and turbine efficiencies are defined as the ratio between actual power transfer and that of an ideal adiabatic process, they facilitate calculation of temperature after the compressor as well as

power transfers P_{turb} and P_{comp} to and from the rotating part of the turbocharger [12]. P_{turb} and P_{comp} are used in the dynamic equation of the shaft speed ω_{tc}. Note that the mechanical efficiency is included in the turbine efficiency.

$$\dot{\omega}_{tc} = \frac{P_{turb} - P_{comp}}{J_{tc}\omega_{tc}} \tag{A.5}$$

The cylinder by-pass enters the exhaust receiver very near the turbine and the by-pass air passes directly through there without mixing into the exhaust receiver gas (see Figure A.3). Therefore T_{er} is set to equal the cylinder flow temperature only, instead of a mix of T_{co} and T_{cbv}. Turbine inlet temperature T_{ti} is, however, an average of T_{er} and T_{cbv} weighted by the respective flows and heat capacities. The part of the turbine flow that stems from the exhaust receiver (and not the by-pass) is found as $\dot{n}_{co} - \dot{n}_{eb}$ rather than $\dot{n}_{turb} - \dot{n}_{cbv}$ to avoid an algebraic loop between the calculations of T_{ti} and $\dot{n}_{turb}$.

$$T_{ti} = \frac{(\dot{n}_{co} - \dot{n}_{eb})c_{p,er}T_{er} + \dot{n}_{cbv}c_{p,amb}T_{cbv}}{(\dot{n}_{co} - \dot{n}_{eb})c_{p,er} + \dot{n}_{cbv}c_{p,amb}} \tag{A.6}$$

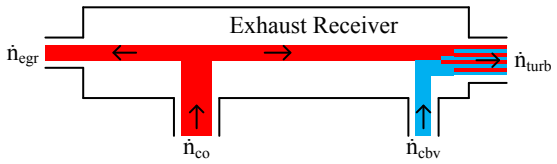

Figure A.3: The cylinder by-pass (CBV) flow mixes directly into the turbine flow and not the exhaust receiver.

A.2.5 EGR Blower

Molar flow through the EGR blower is calculated by assuming a relationship between the non-dimensional parameters head coefficient (Ψ) and flow coefficient (Φ).

$$\Phi = a\left(1 - \left(\frac{\Psi}{b}\right)^n\right)^{\frac{1}{n}} \tag{A.7}$$

where

$$\Psi = 2c_{p,eb}T_{eb} \cdot \frac{\Pi_{eb}^{\frac{\gamma-1}{\gamma}} - 1}{\omega_{eb}^2 r^2} \quad , \quad \Phi = \frac{\dot{n}_{eb}RT_{eb}}{\omega p_{eb}\pi r^3} \tag{A.8}$$

The temperature in the EGR string is assumed to be constant due to the EGR cooler (part of the EGR Unit) .

A.2.6 Valves and Cooler

All valves are modeled as compressible turbulent restrictions with variable openings [12].

$$\dot{n}_v = \frac{A(\alpha)p_{in}}{\sqrt{RT_{in}}}\sqrt{\frac{2\gamma}{\gamma-1}\left(\left(\frac{p_{out}}{p_{in}}\right)^{\frac{2}{\gamma}} - \left(\frac{p_{out}}{p_{in}}\right)^{\frac{\gamma+1}{\gamma}}\right)} \tag{A.9}$$

The cooler is modeled as an incompressible turbulent restriction.

$$\dot{n}_{ic} = A_{ic}\sqrt{\frac{p_{cbv}}{RT_{cbv}}(p_{cbv} - p_{sr})} \tag{A.10}$$

Scavenge receiver temperature T_{sr} is assumed to be constant due to the effectiveness of the cooler.

A.2.7 Cylinders

A mean value approach is used for the flow ($\dot{n}_{ci}$) from the scavenge receiver through the cylinders to the exhaust receiver. The cylinders are modeled as a compressible turbulent restriction (Eq. A.9) but with a fixed opening. The total flow $\dot{n}_{co}$ from cylinder to exhaust receiver is larger than $\dot{n}_{ci}$ due to the addition of and reaction with fuel. As in [45] we assume a lean combustion reaction. Here on the form

$$CH_y + \left(1 + \frac{y}{4}\right) O_2 \rightarrow CO_2 + \frac{y}{2} H_2O \tag{A.11}$$

where the virtual fuel molecule CH_y is introduced to simplify the analysis. The fuel constant y refers to the total ratio of hydrogen to carbon among the different species in the fuel. As an example isooctane C_8H_{18} corresponds to a fuel with $y = 18/8 = 2.25$, and the molar flow of the virtual fuel $CH_{2.25}$ is 8 times that of C_8H_{18}. For every 1 virtual fuel molecule, $1 + \frac{y}{4}$ oxygen molecules are converted to 1 carbon-dioxide and $\frac{y}{2}$ water molecules. Thus if $\dot{n}_f$ denotes the molar flow of CH_y the total flow from cylinder to exhaust receiver is

$$\dot{n}_{co} = \dot{n}_{ci} + \left(-1 - \frac{y}{4} + 1 + \frac{y}{2}\right) \dot{n}_f = \dot{n}_{ci} + \frac{y}{4} \dot{n}_f \tag{A.12}$$

The temperature of flow from cylinders to exhaust receiver is calculated from a modified limited pressure diesel cycle. A detailed explanation is found in [45].

A.2.8 Gas Composition

Scavenge gas composition is the essential variable for the EGR controller and thus also essential to the model. In [43] and[45] oxygen mass fraction of the scavenge and exhaust receivers, respectively, were modeled. In the present paper the molar fraction is used to better relate to the scavenge oxygen sensor signal. Also the two oxygen fraction states are expanded to vectors of gas composition states that includes fractions of both O_2, CO_2 and H_2O. The remaining part of the gas is assumed to be N_2. As the total amount of gas is described by the pressure state (along with temperature and volume) an explicit N_2 state would be redundant. The gas composition vector of the gas in receiver i is defined as

$$X_i = \frac{\begin{bmatrix} n_{i,O_2} & n_{i,CO_2} & n_{i,H_2O} \end{bmatrix}^T}{n_{i,total}} \tag{A.13}$$

The gas composition vector of a flow at position j is defined as

$$Z_j = \frac{\begin{bmatrix} \dot{n}_{j,O_2} & \dot{n}_{j,CO_2} & \dot{n}_{j,H_2O} \end{bmatrix}^T}{\dot{n}_{j,total}} \tag{A.14}$$

The differential equations for the gas composition in the scavenge and exhaust receivers, respectively, are

$$\dot{X}_{sr} = \frac{\dot{n}_{cov}}{n_{sr}} (Z_{cov} - X_{sr}) + \frac{\dot{n}_{ic}}{n_{sr}} (Z_{ic} - X_{sr}) \tag{A.15}$$

$$\dot{X}_{er} = \frac{\dot{n}_{co}}{n_{er}} (Z_{co} - X_{er}) \tag{A.16}$$

where n_{sr} and n_{er} are calculated from the pressure states, temperatures and the ideal gas law. The composition Z_{ic} of the cooler flow equals that of ambient air X_a.

The composition Z_{co} of the flow out of the cylinders is based on $\dot{n}_{ci}$ (with composition $Z_{ci} = X_{sr}$) and the effect of the fuel

$$Z_{co} = \frac{\dot{n}_{ci} X_{sr} + \dot{n}_f \Gamma}{\dot{n}_{co}} \quad , \quad \Gamma = \begin{bmatrix} -1 - \frac{y}{4} \\ 1 \\ \frac{y}{2} \end{bmatrix} \tag{A.17}$$

where Γ is a constant vector that relates to the combustion reaction.

Assuming that the gas composition of the recirculated gas does not change in the EGR unit and that the volume between EGR blower and COV is small enough to be neglected for the composition dynamics leads to

$$Z_{cov} = X_{er} \tag{A.18}$$

Using this and equations A.12 and A.17 we can rewrite equations A.15 and A.16 as

$$\dot{X}_{sr} = \frac{\dot{n}_{cov}}{n_{sr}}(X_{er} - X_{sr}) + \frac{\dot{n}_{ic}}{n_{sr}}(X_a - X_{sr}) \tag{A.19}$$

$$\dot{X}_{er} = \frac{\dot{n}_{ci}}{n_{er}}(X_{sr} - X_{er}) + \frac{\dot{n}_f}{n_{er}}\left(\Gamma - \frac{y}{4}X_{er}\right) \tag{A.20}$$

It is possible to include sulfur content in the fuel by using the virtual fuel molecule CH_yS_z instead and extending the combustion reaction and the composition vectors to include SO_2. Composition changes in the EGR unit (sulfur removal and humidity changes) can be included by changing the assumption expressed by Equation A.18. For clarity reasons these extensions have not been included here.

A.2.9 Oxygen Sensor

A ZrO_2 type sensor measures the molar oxygen fraction in the scavenge receiver. The pressure, temperature and gas composition is not ideal for such a sensor so in order to increase accuracy and decrease sensor wear a rather complex gas extraction system has been designed by MDT. The resulting dynamic properties of this sensor setup is difficult to model accurately. Good results have been obtained by modeling it as a time delay and a first order filtering effect

$$\tau_{Fb} \cdot \dot{O}_{sr,Fb}(t) = O_{sr}(t - \Delta t_{Fb}) - O_{sr,Fb}(t) \tag{A.21}$$

where O_{sr} is the actual oxygen fraction, $O_{sr,Fb}$ is the measurement, τ_{Fb} is the sensor time constant and Δt_{Fb} is the sensor time delay. The values of τ_{Fb} and Δt_{Fb} are both expected to lie in the range 10-20 seconds depending on level of clogging in the gas extraction system and pressure conditions in the receiver.

A.2.10 MVEM Validation

The MVEM is validated in [45] and found to represent the main system behavior. The changes and additions in the present paper is regarded as technicalities (e.g. mass/molar) that does not affect the overall model validity. The extension of the gas composition model to include CO_2, H_2O and N_2 is difficult to validate as only the O_2 fraction is measured. Therefore the MVEM model is not further validated here. The reduced version is, however, validated against both the MVEM and two engines in a later section.

A disadvantage of the MVEM model is that it was parameterized and validated against data where the engine was running at the upper half of the load region. The problematic fast loading transients mainly occur at the lower half. While the overall model structure is valid at low loads the extrapolation accuracy in some of the flow components is unknown.

A.2.11 Model Structure

The MVEM has 11 states of which 4 are pressures, 1 is the turbocharger speed and the remaining 6 are gas composition. The pressure and TC speed states are coupled through the flow elements as shown in Figure A.4. These states affect the gas composition states whereas the gas composition states only affect the pressures and TC speed through gas property changes, an effect that is negligible in this regard. The MVEM can therefore be separated into two cascaded systems as shown in Figure A.4 where the pressure, flow and TC speed part provides inputs to the gas composition part of the model.

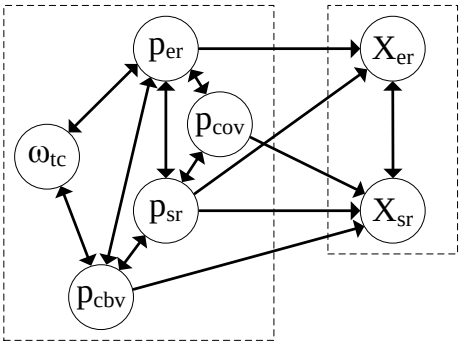

Figure A.4: A digraph shows the couplings between states in the MVEM model. The model can be separated in two cascaded systems as the gas composition states only affect each other.

A.3 Control-Oriented Model

The COM is a dynamic model of the scavenge oxygen level that is simpler than the standard MVEM. The MVEM is used as a starting point, but only the gas composition part is considered. This section shows how to simplify the model by removing dynamics that is not essential for the gas composition and how to estimate the inputs.

A.3.1 Model Reduction

Reduction of the gas composition part can be achieved by removal of non-essential dynamics. A complete state decoupling by diagonalization is difficult due to the system nonlinearity, but a fast mode can be decoupled by triangularization of the system matrix. Simulation of the MVEM model shows that a few terms can be neglected, allowing us to rewrite the remainder of the model into a simple form with first order dynamics.

First the gas composition model is written in the form of a time-varying state space model

$$\begin{bmatrix} \dot{X}_{sr} \\ \dot{X}_{er} \end{bmatrix} = \begin{bmatrix} -\frac{\dot{n}_{cov}+\dot{n}_{ic}}{n_{sr}} & \frac{\dot{n}_{cov}}{n_{sr}} \\ \frac{\dot{n}_{ci}}{n_{er}} & -\frac{\dot{n}_{ci}+\frac{y}{4}\dot{n}_f}{n_{er}} \end{bmatrix} \begin{bmatrix} X_{sr} \\ X_{er} \end{bmatrix} + \begin{bmatrix} \frac{\dot{n}_{ic}}{n_{sr}} X_a \\ \frac{\dot{n}_f}{n_{er}} \Gamma \end{bmatrix} \tag{A.22}$$

or equivalently

$$\dot{X} = A(U)X + K(U) \tag{A.23}$$

where

$$U = \begin{bmatrix} \frac{\dot{n}_{cov}+\dot{n}_{ic}}{n_{sr}} \\ \frac{\dot{n}_{cov}}{n_{sr}} \\ \frac{\dot{n}_{ci}+\frac{y}{4}\dot{n}_f}{n_{er}} \\ \frac{\dot{n}_{ci}}{n_{er}} \end{bmatrix} = \begin{bmatrix} U_1 \\ U_2 \\ U_3 \\ U_4 \end{bmatrix} \quad , \tag{A.24}$$

$$A(U) = \begin{bmatrix} -U_1 & U_2 \\ U_4 & -U_3 \end{bmatrix} \quad , \quad K(U) = \begin{bmatrix} (U_1 - U_2)X_a \\ (U_3 - U_4)\frac{4}{y}\Gamma \end{bmatrix} \tag{A.25}$$

If U were assumed to be constant, the model in equation A.23 could be separated into decoupled states by a state transformation

$$\tilde{X} = \begin{bmatrix} \tilde{X}_1 \\ \tilde{X}_2 \end{bmatrix} \quad , \quad X = E\tilde{X} \quad , \quad \tilde{X} = E^{-1}X \tag{A.26}$$

where the transformation matrix E is chosen as the gathered eigenvectors of A. This transformation results in a diagonal system matrix $E^{-1}AE$ so the system is split into two decoupled states. In the present case U is the system input and cannot be assumed to be constant. The transformed system matrix becomes

$E^{-1}(AE-\dot{E})$ which is not generally diagonal. It is, however, possible to design the transformation matrix in a way that makes A triangular, thus decoupling part of the system. Choose

$$E = E(U) = \begin{bmatrix} \frac{U_2}{\lambda_1+U_1} & \frac{U_2}{\lambda_2+U_1} \\ 1 & 1+\psi(t) \end{bmatrix} \tag{A.27}$$

where the eigenvalues of A are

$$\lambda_1 = \lambda_1(U) = -\frac{U_1+U_3+\sqrt{(U_1-U_3)^2+4U_2U_4}}{2} \tag{A.28}$$

$$\lambda_2 = \lambda_2(U) = -\frac{U_1+U_3-\sqrt{(U_1-U_3)^2+4U_2U_4}}{2} \tag{A.29}$$

and $\psi(t)$ is an auxiliary state that behaves according to

$$\dot{\psi} = -\psi^2(\lambda_2+U_1) - \psi(2\lambda_2+U_3+U_1+U_5) - U_5 \tag{A.30}$$

U_5 is defined by the relative change of U and λ_2

$$U_5 = \frac{\dot{\lambda}_2+\dot{U}_1}{\lambda_2+U_1} - \frac{\dot{U}_2}{U_2} \tag{A.31}$$

Now the transformed system can be written on the form

$$\begin{bmatrix} \dot{\tilde{X}}_1 \\ \dot{\tilde{X}}_2 \end{bmatrix} = \begin{bmatrix} \tilde{a}_{11} & 0 \\ \tilde{a}_{21} & \tilde{a}_{22} \end{bmatrix} \begin{bmatrix} \tilde{X}_1 \\ \tilde{X}_2 \end{bmatrix} + E^{-1}K \tag{A.32}$$

where the terms $\tilde{a}_{ii}$ are time-varying. The triangular form of the system matrix is a salient feature of the model in A.32 as the zero in the $\tilde{a}_{12}$ position shows that in the transformed system model, the state $\tilde{X}_1$ is not affected by changes in $\tilde{X}_2$.

The reduction now proceeds with the help of the MVEM model. Wide range simulations where U is varied at realistic rates show that the auxiliary state ψ remains small enough to be negligible (Figure A.5), considering the form of the equations where it appears. The difference between $\tilde{a}_{11}$ and λ_1 is also negligible and both varies in the range [-1;-0.5]. This corresponds to a mode of the system with a time constant $\tau_1 = \frac{1}{-\lambda_1}$ varying in the range 1-2 seconds which is faster than the desired range of the model (Figure A.6). To simplify the model these dynamics are neglected and removed. The removal is achieved

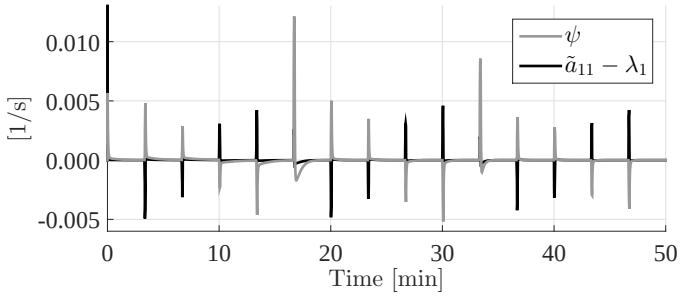

Figure A.5: The figure shows the magnitude of the terms ψ and $\tilde{a}_{11}-\lambda_1$. Both terms remain close to 0 during a simulation of the MVEM in a wide range of engine loads and EGR blower speeds with realistic input rates and they can therefore be neglected in the model.

by setting $\dot{\tilde{X}}_1 = 0$ and solving for $\tilde{X}_1$ in Equation A.32.

$$\tilde{X}_1 = -\frac{(U_1-U_2)X_a - \frac{U_2}{\lambda_2+U_1}(U_3-U_4)\frac{4}{y}\Gamma}{U_2\left(\frac{1}{\lambda_1+U_1}-\frac{1}{\lambda_2+U_1}\right)\lambda_1} \tag{A.33}$$

From the transformation in Equation A.26 we can express $\tilde{X}_1$ in terms of the original states

$$\tilde{X}_1 = \frac{(1+\psi)X_{sr} - \frac{U_2}{\lambda_2+U_1}X_{er}}{U_2\left(\frac{1+\psi}{\lambda_1+U_1} - \frac{1}{\lambda_2+U_1}\right)} \tag{A.34}$$

Combining Equations A.33 and A.34 while neglecting ψ we can solve for X_{er} in terms of U and X_{sr}.

$$X_{er} = \left(X_{sr} + \frac{K_1 - \frac{U_2}{\lambda_2+U_1}K_2}{\lambda_1}\right)\frac{\lambda_2+U_1}{U_2} \tag{A.35}$$

Using this result in Equation A.22 with the definition of U and rewriting leads to

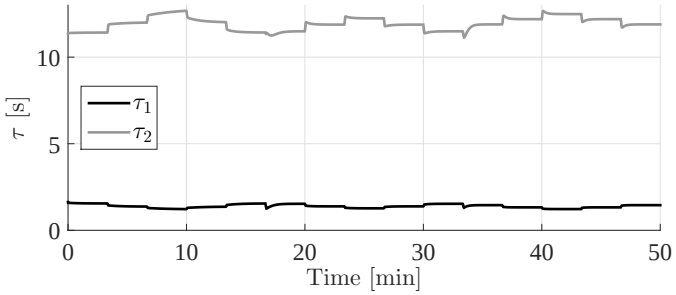

Figure A.6: Time constants τ_1 and τ_2 of the gas mixing process vary slightly during simulation over a wide engine load and EGR flow range.

$$\tau_2\dot{X}_{sr} = -X_s + \frac{X_a(\dot{n}_{ci} + \frac{y}{4}\dot{n}_f)\dot{n}_{ic} + \Gamma\dot{n}_{cov}\dot{n}_f}{(\dot{n}_{cov}+\dot{n}_{ic})(\dot{n}_{ci}+\frac{y}{4}\dot{n}_f) - \dot{n}_{cov}\dot{n}_{ci}} \tag{A.36}$$

where $\tau_2 = \frac{1}{-\lambda_2}$. Simulations show τ_2 to vary in the range 11-13 seconds, depending on engine load and EGR flow (Figure A.6). Equation A.36 with a constant $\tau_2 = 12$ seconds is a reasonable model of X_{sr}. Further simplification can be achieved by neglecting the filling and emptying dynamics of the scavenge receiver, by setting

$$\dot{n}_{ci} = \dot{n}_{cov} + \dot{n}_{ic} \tag{A.37}$$

which leads to

$$\tau_2\dot{X}_{sr} = -X_{sr} + X_a + \frac{\left(\Gamma - X_a\frac{y}{4}\right)\dot{n}_f\dot{n}_{cov}}{\left(\dot{n}_{ic}+\frac{y}{4}\dot{n}_f\right)\left(\dot{n}_{ic}+\dot{n}_{cov}\right)} \tag{A.38}$$

Equation A.38 represents the behavour of X_{sr} with only the most dominating dynamics included. One fast mode stemming from the coupling of the two receivers is removed as well as the filling and emptying dynamics of the scavenge receiver. Steady state output is maintained. The final model has the form of three parallel first order Hammerstein models where fuel, EGR and intercooler flows act as inputs. The only parameters are ambient air composition, ratio of hydrogen to carbon atoms in the fuel and a time constant.

A.3.2 Input Approximation

Having developed a simple model of the gas composition dynamics we now turn to the inputs of this model. The composition Z_a of the ambient air flow and the fuel composition ratio y can be considered as known constant parameters, whereas the three gas flows $\dot{n}_f$, $\dot{n}_{cov}$ and $\dot{n}_{ic}$ need to be estimated from signals that are available to the controller if the COM is to be used in an engine control system. The final setup can be seen in Figure A.7.

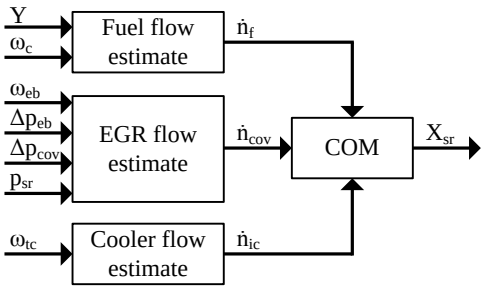

Figure A.7: Overview of the control-oriented model with its input estimates and the signals used.

A.3.2.1 Fuel Flow

The fuel flow is a control input from the governor and it can be calculated as proportional to the product of engine speed ω_c and governor index Y with reasonable accuracy.

$$\dot{n}_f = k_f \omega_c Y \tag{A.39}$$

The constant of proportionality k_f can be found from engine shop test data where a fuel flow measurement is available.

A.3.2.2 COV Flow

The cut-out valve is modeled as a compressible turbulent restriction with variable opening in the MVEM. Equation A.9 could theoretically provide a simple way to estimate the flow. In practice, however, the COV is fully open during normal operation and does not provide enough restriction to induce a significant pressure difference. This is obviously a design choice in order to avoid counteracting the EGR blower. Speaking of which, the EGR blower provides the preferred alternative for EGR flow estimation (Equations A.7 and A.8). Output pressure is calculated as scavenge pressure plus pressure difference over the COV. Input pressure is then found using the differential pressure over the blower. EGR flow temperature is assumed constant $T_{egr} = 300$ K. The relation between Ψ and Φ is parameterized using data made available from the blower manufacturer.

A.3.2.3 Cooler Flow

In the MVEM model the cooler is modeled as an incompressible turbulent restriction. Equation A.10 should be adequate for flow estimation. Unfortunately the pressure difference over the cooler is not a commonly available signal. Also, the restriction provided by the cooler might be too small to provide adequate signal to noise ratio of the estimate. As an alternative the cooler flow can be estimated as the difference between compressor and CBV flows. However, the MVEM models for these flows require even more pressure signals as well as temperatures and a compressor flow map.

As a consequence we resort to a more crude estimation of the cooler flow inspired by the model used in [30]. Here it was argued that the compressor operates very close to a single line on a compressor map with almost constant efficiency. This facilitates modeling of the compressor flow as a simple function of ω_{tc} or p_{sr} only, even during transients. Such a model was applied to an engine with neither EGR nor CBV. These additions each add an additional degree of freedom to the system and might degrade performance of the simple flow estimate.

The accuracy of this simple model as well as the effect of introducing EGR and CBV is investigated by simulation of the MVEM. Figure A.8 shows $\dot{m}_{ic}$ as a function of ω_{tc} when keeping the CBV opening constant and varying either the engine load (43-100%) or the EGR blower speed (within the relevant range). Figure

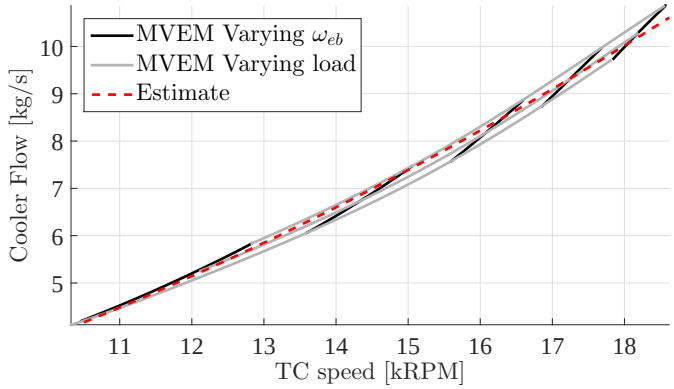

Figure A.8: Simulation and estimation of cooler flow $\dot{n}_{ic}$ with constant CBV opening and varying engine load (43-100%) and EGR blower speed.

A.8 also shows an estimate on the form

$$\dot{n}_{ic} = \theta \cdot \left((1-\phi)\omega_{tc} + \phi\omega_{tc}^2\right) \tag{A.40}$$

where θ and ϕ are constants. The simulations show that variation of the EGR flow only slightly degrades the accuracy of the flow estimate. Problems arise when varying the CBV opening as seen in Figure A.9. Clearly, the cooler flow is not well described as a function of only ω_{tc} in this case. We do not pursue to improve the estimation method here but only state that it works poorly when varying the CBV opening. Future research might solve this issue, but for now it is not deemed critical as the CBV is closed in the low engine load region where rapid load transients occur during maneuvering. The MVEM model is parameterized for the high load region where the CBV is normally open and therefore the investigation has been included here.

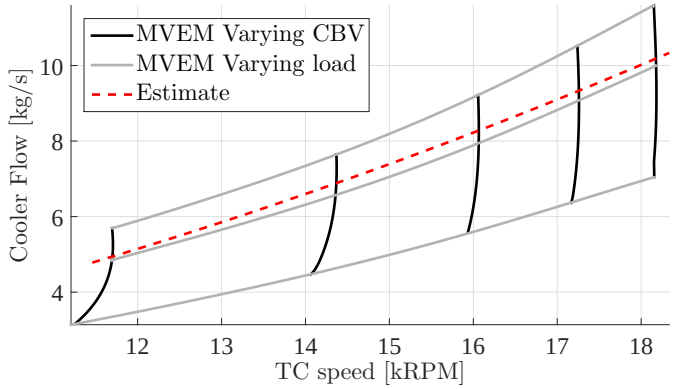

Figure A.9: Simulation and estimation of cooler flow $\dot{n}_{ic}$ with constant EGR blower speed opening and varying engine load (43-100%) and CBV opening (0-100%).

The dominating dynamics for the cooler flow is due to the turbocharger inertia. This is naturally captured by basing the flow estimate on ω_{tc}. Figure A.10 show a comparison between MVEM and Equation A.40 in a scenario where engine load and EGR blower speed are changed in steps. The estimate replicates the MVEM well in transients and only seems to deviate slightly in steady state.

A.3.3 Operating Region

Equation A.38 is valid throughout the load region, as long as the combustion is lean. Regarding the input approximation, the fuel flow estimate is valid globally. The provided EGR blower maps can be

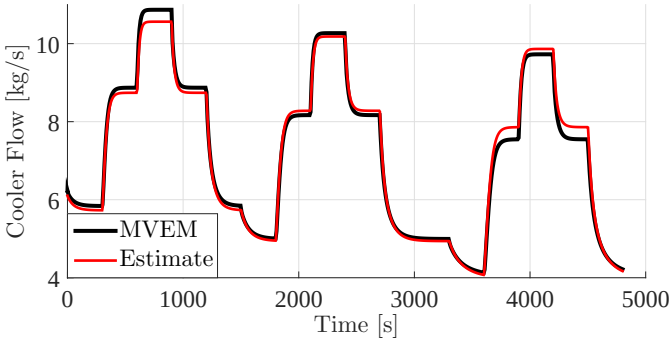

Figure A.10: Simulation and estimation of cooler flow while changing engine load (43-69-100%) and EGR blower speed in steps.

extrapolated to the conditions present at low load. The cooler flow estimate is unable to represent variation of the CBV opening. As the CBV is always fully closed at low loads, the consequence of this deficiency is limited with regards to EGR controller synthesis when the aim is to design a controller that is able to deal with fast loading transients, which mainly occur at low loads. On the other hand, the cooler flow estimate is subjected to extrapolation into the low load region and possible disturbance from the auxiliary blowers (not shown) which increase scavenge pressure and flow in the low load region. Comparison to experimental data (Section A.4) shows the model to be robust against this.

A.4 Validation of Control-Oriented Model

In this section the control-oriented model is validated by comparing the output to a simulation of the full MVEM model and measurement data from two engines. In the latter cases the dynamics of the scavenge oxygen sensor naturally influence the results. This is compensated by increasing the time constant in the COM and adding a time delay.

A.4.1 Comparison of COM and MVEM

The MVEM model allows us to verify the consequences of the simplifications done to the model. Matlab Simulink is used for simulation of the MVEM. Dynamic simulation of pressure in volumes that are small relative to the flows can be difficult for the solver, but Simulink's implicit ode15s solver is able to simulate the MVEM at more than 200x real time on a standard PC.

Figure A.11 shows a comparison of the scavenge oxygen level simulated by the full MVEM and the COM, respectively. The scenarios are EGR blower speed steps at three different engine loads. It can be seen that the removal of fast dynamics in gas mixing and removal of filling and emptying dynamics of the scavenge receiver has almost no consequence for the accuracy. The most significant decrease in accuracy comes from the simplification of compressor flow estimation which has an influence on the steady state accuracy but does not change the dynamics significantly. Figure A.12 shows a similar comparison but this time the blower speed is kept constant while the engine load is changed in steps (between 43, 69 and 100%). Here the dynamics differ slightly due to neglection of scavenge receiver filling and emptying. This effect is most evident during a load change, where the scavenge pressure changes. Deviation due to the cooler flow model is also seen at certain steady state points.

A.4.2 Comparison of COM and Test Engine

To further validate the control-oriented model it is applied to data recorded from two engines. The first is the 4T50ME-X test engine situated in the MDT Diesel Research Center in Copenhagen. The oxygen

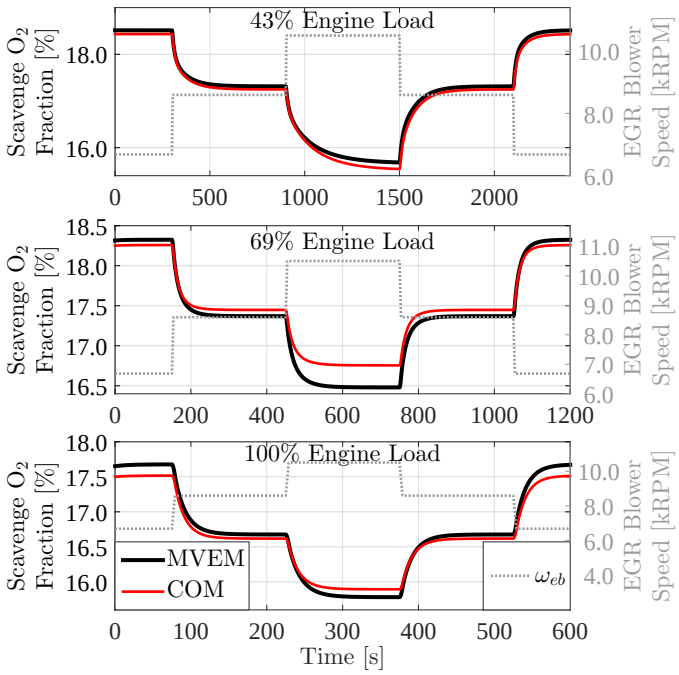

Figure A.11: Comparison of O_{sr} simulated by MVEM and COM during steps of EGR blower speed at engine loads 43, 69 and 100%.

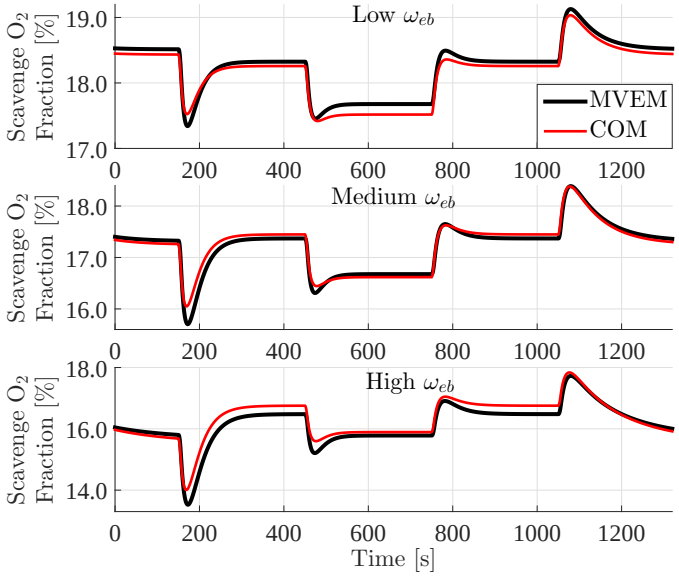

Figure A.12: Comparison of O_{sr} simulated by MVEM and COM during steps of engine load (43-69-100-69-43%) at different EGR blower speeds.

sensor dynamics are incorporated by increasing the model time constant and adding a 10 second time delay. Here the first scenarios are also EGR blower speed steps at constant load (50, 75 and 100%), see Figure A.13. The COM captures both the dynamics and steady state well over this wide load range. At 100% load the COM seems to have a slight lag. This indicates that the sensor delay is shorter than 10 seconds at this load.

Figure A.14 shows the COM applied to a number of engine RPM setpoint ramps in the low load range. Here the auxiliary blowers are activated but the model is able to replicate the O_{sr} behavior anyway.

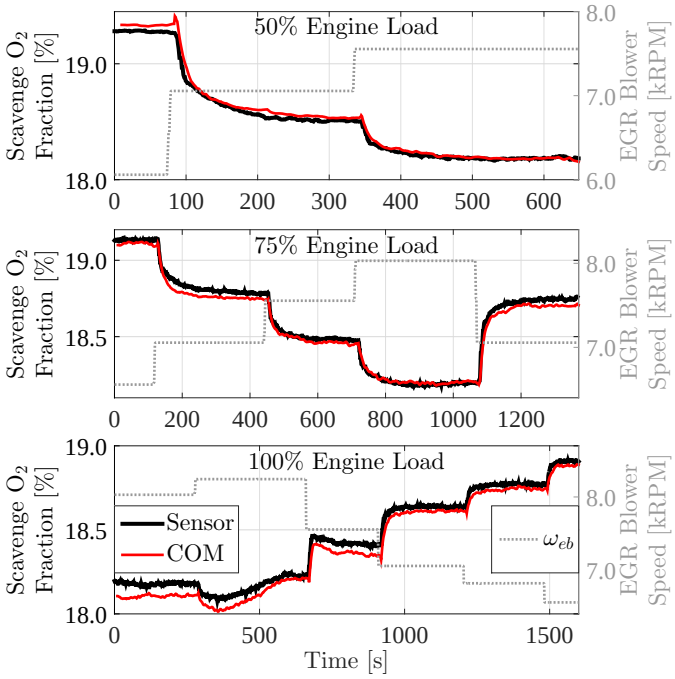

Figure A.13: Comparison of O_{sr} measured on test engine and estimated by COM during steps of EGR blower speed at engine loads 50, 75 and 100%.

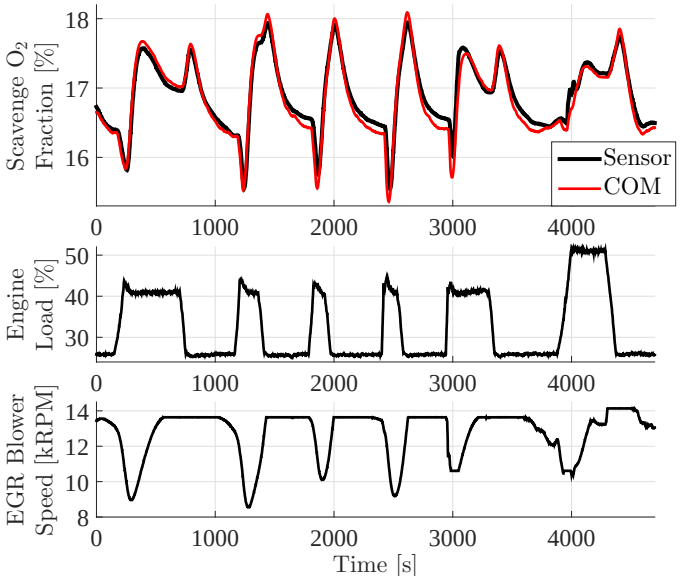

Figure A.14: Comparison of O_{sr} measured on test engine and estimated by COM during a series of engine RPM setpoint changes.

A.4.3 Comparison of COM and Vessel Engine

The MVEM and the COM are models of the 4T50ME-X test engine. In order to validate the generality of the model, it is also applied to the 6S80ME-C9.2 engine installed on the container vessel Maersk Cardiff. The most basic parameters of the vessel engine is provided in Table A.2. A similar scenario as previously is shown in Figure A.15 where the EGR blower speed is varied stepwise in different load ranges. However, as this is from a vessel the governor does not keep a constant load and especially at the higher load ranges it is seen to affect O_{sr} significantly. The COM is able to replicate the O_{sr} behavior as it takes advantage of the load signal. Again the sensor delay seems to be slightly smaller than estimated at 80% load.

Table A.2: Parameters of vessel engine

Number of cylinders	6	$[-]$
Bore	0.8	$[m]$
Stroke	3.45	$[m]$
Scavenge pressure at MCR	3.0	$[bar]$
Engine speed at MCR	73.9	$[RPM]$
Effective power at MCR	23.0	$[MW]$

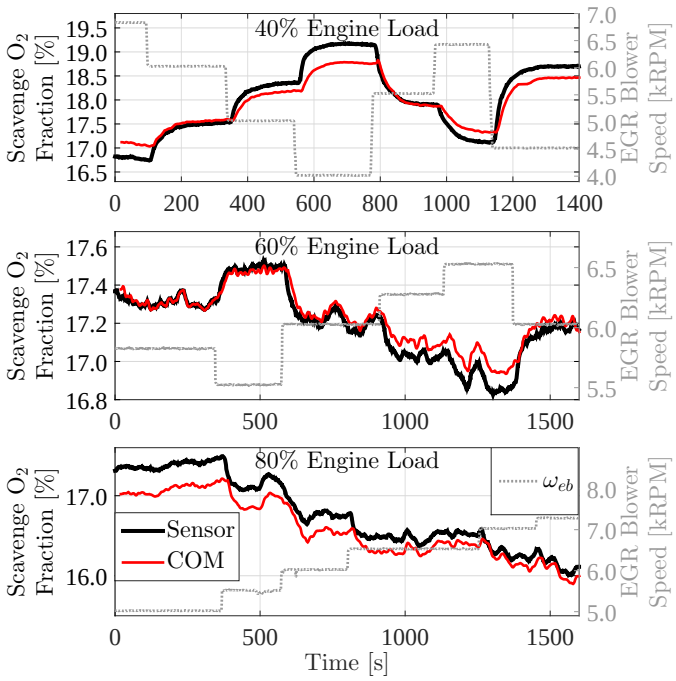

Figure A.15: Comparison of O_{sr} measured on vessel engine and estimated by COM during steps of EGR blower speed at engine loads 40, 60 and 80%.

Figure A.16 shows the COM applied to a number of RPM setpoint steps in the low load range on the vessel engine. Most of the O_{sr} behavior is replicated but the COM deviates somewhat from the steady state values of the sensor.

A.5 Conclusions

This paper presented a mean value molar model of scavenge oxygen fraction in large two-stroke crosshead diesel engines with Exhaust Gas Recirculation (EGR). The purpose of the model was simulation and design of EGR closed loop control for steady state as well as transient loading conditions. The paper showed in theory and practice that our simplified nonlinear model captures all essential dynamics that is needed for EGR control.

The nonlinear control-oriented model of the molar oxygen fraction in the scavenge receiver was developed by model reduction of the gas composition part of a mean value model. Model reduction was done by transforming the system to disclose non-dominant dynamics and perform model reduction to leave the steady state response untouched. The resulting model consisted of three parallel first order Hammerstein systems with inputs being fuel flow, EGR flow and intercooler flow, and it was shown how these quantities were estimated from commonly available signals.

The performance of the control-oriented model was validated by comparison to the output of a complete

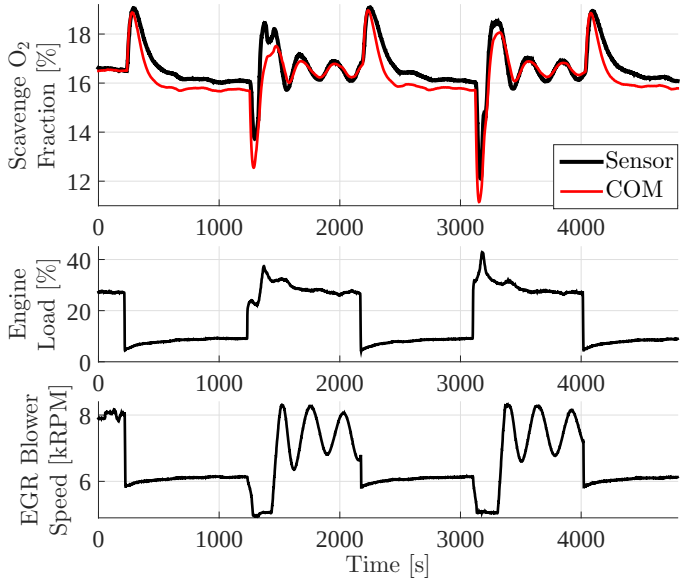

Figure A.16: Comparison of O_{sr} measured on vessel engine and estimated by COM during a series of engine RPM setpoint changes.

MVEM model, to measurement series from a test engine and to recordings from a vessel engine in various scenarios. The model was found to capture the gas mixing dynamics well and was able to replicate the steady state response convincingly in the relevant range of operation.

The control-oriented model presented here was employed for successful observer and controller designs, which will be published separately.

Paper B

Adaptive Observer for Nonlinearly Parameterised Hammerstein System with Sensor Delay - Applied to Ship Emissions Reduction

Kræn Vodder Nielsen[*1,2], Mogens Blanke[2,3], Lars Eriksson[4]

[1] MAN Diesel & Turbo, Teglholmsgade 41, 2450 København SV, Denmark [2]Department of Electrical Engineering, Automation and Control Group, Technical University of Denmark, Elektrovej Building 326, 2800, Kgs. Lyngby, Denmark

[3]AMOS CoE, Institute of Technical Cybernetics, Norwegian University of Science and Technology, 7491 Trondheim, Norway

[4]Vehicular Systems, Department of Electrical Engineering, Linköping University, 58183 Linköping, Sweden

Abstract:
Taking offspring in a problem of ship emission reduction by exhaust gas recirculation control for large diesel engines, an underlying generic estimation challenge is formulated as a problem of joint state and parameter estimation for a class of multiple-input single-output Hammerstein systems with first order dynamics, sensor delay and a bounded time-varying parameter in the nonlinear part. The paper suggests a novel scheme for this estimation problem that guarantees exponential convergence to an interval that depends on the sensitivity of the system. The system is allowed to be nonlinear parameterized and time dependent, which are characteristics of the industrial problem we study. The approach requires the input nonlinearity to be a sector nonlinearity in the time-varying parameter. Salient features of the approach include simplicity of design and implementation. The efficacy of the adaptive observer is shown on simulated cases, on tests with a large diesel engine on test bed and on tests with a container vessel.

K. V. Nielsen, M. Blanke, and L. Eriksson. “Adaptive Observer for Nonlinear Parameterised Hammerstein System with Sensor Delay - a Technology for Ship Emissions Reduction”. *Transactions on Control Systems Technology* (2016). Submitted

[*]Principal corresponding author. Tel.: +45 33851909; E-mail: kraenv.nielsen@man.eu

B.1 Introduction

This paper considers observer design for a class of systems where a bounded time-varying parameter enters the model nonlinearly. The motivation for this problem is a case of emission reduction for large diesel engines, where accurate estimation of gas composition in the scavenging air path of the engine is essential. The dynamics of this problem are described by a nonlinear model that is nonlinearly parameterized, time-varying and includes sensor delay. Literature mainly deals with systems that are either linear in the unknown parameters or where the contribution from time dependent inputs and the unknown parameters, respectively, enter in a simple affine manner in the system equations. This is not the case for the emission control problem at hand, so a solution is needed for estimation of parameter and state in a nonlinear parameterized Hammerstein system, with time-varying elements.

An overview of several nonlinear observer design methods was presented by [62] who also defined a terminology to distinguish between adaptive observers and joint state and parameter observers. An early approach for joint state and parameter observer design for nonlinear systems was to apply an Extended Kalman Filter augmenting the state vector by the unknown parameters. This approach has problems with divergence and bias as shown in [63], who also suggested a solution for linear systems. Extension to a class of nonlinear systems was done in [64], but still for problems that were linear in the parameters. Gradient based estimators for affine systems were treated in numerous articles and in textbooks, including [65]. For nonlinearly parameterized systems, [66] showed that the gradient methods are insufficient and can lead to divergence in observers, and a min-max problem design was introduced to ensure global stability. In the present paper a guarantee of exponential convergence is essential to ensure robustness of the estimator candidates as the method is to be rolled out on a large industrial scale.

Nonlinearly parameterized perturbations were studied for a large class of nonlinear systems in [67], who also presented a stepwise design. This method was combined with a high-gain observer in [68] to generalise the design to output feedback. [69] used an observer design framework known as *Immersion & Invariance* for nonlinearly parameterised systems, under a monotonicity constraint, by adding nonlinear dynamic scaling, the purpose of which was to avoid solving partial differential equations. An uncertainty-set-based algorithm for parameter estimation was presented in [70]. This algorithm included estimates of the parameters and of the maximal set of feasible parameters. In case of nonconvex problems, the algorithm was shown capable of detecting if a local minimum was reached instead of a global one. This and most other results in literature apply to systems that fulfill some convexity or monotonicity requirements. [71] overcame this by combining traditional observer design with explorative search for part of the parameter vector. Yet another extension was presented in [72] who used virtual update laws in the design of observers where the parameter estimates include direct terms from the measurements. This facilitated implementation of update laws that are dependent on time derivatives of measurements without explicitly calculating the derivatives. Off-line estimation for multiple-input single-output (MISO) Hammerstein models were treated in [73] where the suggested approach was shown to be superior to linear methods for a chemical distillation process and a heat exchanger. The iterative approach of [74] was used for estimating the parameters of both the nonlinear and the linear parts. A recursive identification method was analyzed by [75]. A state observer for an extended Hammerstein model of an engine test bench was presented by [76]. Parameter estimation of Hammerstein systems was treated in e.g. [77] and [78] but also these works addressed off-line identification rather than real-time estimation. In contrast, [79] presented adaptive control and real-time parameter estimation for a certain class of Hammerstein systems where the nonlinear part is linear in the unknown parameters.

This text first motivates the industrial estimation challenge from which a generic model and an estimation problem is formulated. The paper then presents both *a parameter estimator* and *a joint state and parameter observer* design for MISO Hammerstein models with first order dynamics and sensor delay. An

adaptive observer is suggested that estimates the state and a time-varying parameter of the nonlinear part. Explicit calculation of derivatives is avoided by using virtual update laws inspired by [72]. Exponential convergence bounds and minimum convergence rates[2] are derived for the observer errors. The parameter error converges at least exponentially to the bounds of the time-varying parameter. A benefit of the suggested observer is shown to be the simplicity of design, of implementation and of tuning. Formal proofs for convergence and error bounds are included in the paper on conditions of fairly weak requirements on the nonlinear part of the Hammerstein model. Whereas an analytical analysis on the effect of disturbances has not been performed, the application to a real world problem demonstrates the performance of the method.

The paper first introduces the industrial case of marine emission reduction by exhaust gas recirculation in Section B.2 and generalizes the underlying oxygen estimation problem to be one of estimating state and parameter in a nonlinear parameterized first order MISO Hammerstein system with sensor delay. An adaptive observer solution is then suggested in Section B.4 along with derivation of bounds and minimum convergence rates for the observer errors. The design is favorably compared to an existing but far more complex design from [68] in Section B.5 and a simulation example follows in Section B.6. The suggested observer is then applied to a high fidelity simulation of a large marine diesel engine, and to data from marine prime mover diesels on a test bed and at sea. The results show that the suggested approach is solid and yet simple to implement and therefore has the potential to become enabling technology in estimation based control of emissions from large two-stroke diesel engines.

B.2 The Oxygen Estimation Problem in Emission Control

Increased environmental concern has led the International Maritime Organization to restrict the emissions from marine diesel engines [2]. The Tier III standard, that applies to vessels built after 1st of January 2016, severely restricts NO_x emission in specified NO_x Emission Control Areas (NECAs). The North American coastal area is such a NECA and the North Sea and Baltic Sea are expected to become NECAs [54]. The Tier III standard specifies a reduction by a factor of four compared to the Tier II standard, thus requiring significant modifications to the engines.

NO_x formation in a diesel engine mainly occurs during combustion where high temperatures lead to reactions between nitrogen and oxygen, known as the Zeldovich mechanism [11]. One method of decreasing NO_x formation is to install an Exhaust Gas Recirculation (EGR) system to increase heat capacity and decrease oxygen availability in the combustion. The result is lower peak combustion temperatures and thus less NO_x formation. A simplified overview of the airflow of a high pressure EGR system is shown in Figure A.1. The speed of the EGR blower is used to regulate the amount of low oxygen exhaust gas that is recirculated to the scavenge receiver. Fixed gain feedback control is used to reach a setpoint for scavenge receiver oxygen fraction (O_{sr}). The pressure, temperature and gas composition of the scavenge receiver necessitates a gas extraction system in order to reliably measure O_{sr}. The gas extraction results in a measurement delay of about 20 seconds. In steady running conditions the feedback controller performs adequately in spite of this delay but in some engine loading transients O_{sr} drops excessively and the lack of oxygen causes formation of thick black smoke for more than half a minute. This is not acceptable as excessive soot formation might damage the engine and since loading transients frequently occur during maneuvering close to ports where visible smoke is restricted.

As EGR systems have only recently been added to marine two-strokes, most literature in EGR control applies to four-stroke automotive engines, where EGR is often accompanied by a variable-geometry turbocharger. High-fidelity modeling of such a system was treated in [19] and controller design in [16], [18], [21] and recently [61]. Reduction of smoke in loading transients on marine diesel engine by

[2] Definition 5.10 in [80].

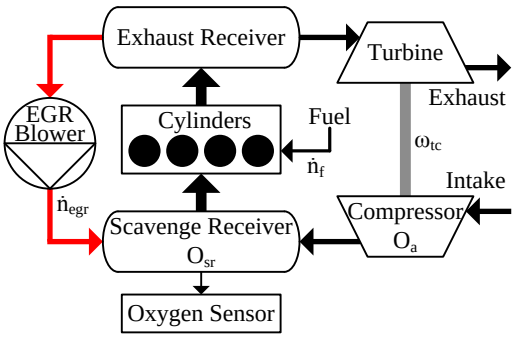

Figure B.1: Airflow of turbocharged diesel engine with high-pressure Exhaust Gas Recirculation (shown in red).

sophisticated control of a variable-geometry turbocharger was seen [33] but this system lacked exhaust gas recirculation. Modeling and observer design for intake manifold oxygen fraction of a diesel engine with EGR was treated in [27] where a Luenberger-like adaptive observer also estimated the fuel blend level.

High fidelity simulation models of the airflow of a marine engine with high pressure EGR were presented in [43], [45] and [49]. SISO control methods for a linearized version of such a model were investigated in [44] where it was found difficult to achieve both performance and robustness. The high-fidelity model from [49] is used in Section B.7 for validation of the observer. A simpler, control-oriented model (COM) of O_{sr} was also proposed in [53] and [49] where it was shown to represent the most essential dynamics. The COM is a first order Hammerstein model (B.1) with molar fuel flow $\dot{n}_f$, molar EGR flow $\dot{n}_{egr}$ and turbocharger speed ω_{tc} as inputs.

$$\tau \dot{O}_{sr} = -O_{sr} + O_a - \frac{(1+\frac{y}{4}(O_a+1))\dot{n}_f \dot{n}_{egr}}{(\theta\beta(\omega_{tc})+\frac{y}{4}\dot{n}_f)(\theta\beta(\omega_{tc})+\dot{n}_{egr})} \tag{B.1}$$

The model includes ambient oxygen fraction O_a, ratio of hydrogen to carbon in the fuel y and a mixing time constant τ as parameters. The product $\theta\beta(\omega_{tc})$ represents the compressor flow where

$$\beta(\omega_{tc}) = (1-\phi)\frac{\omega_{tc}}{1000 \text{ rad/s}} + \phi\left(\frac{\omega_{tc}}{1000 \text{ rad/s}}\right)^2 \tag{B.2}$$

and ϕ is a constant. As the compressor flow model is empirical and represents a substantial simplification of the physics involved in the process, the parameter θ is expected to vary slightly depending on operating region and conditions but stay within an interval ($\theta(t) \in [\bar{\theta}-\kappa; \bar{\theta}+\kappa]$).

The delay of the gas extraction system (Δt) is included in the model as

$$O_{srm}(t) = O_{sr}(t-\Delta t) \tag{B.3}$$

where O_{srm} is the measured scavenge oxygen fraction available to the controller.

A nonlinear parameter estimator of θ for the COM was proposed in [53] but it did not consider the sensor delay, time-variance of θ and convergence bounds were not found. An observer for O_{sr} is desired in order to compensate for the delay, which impedes the EGR controller during engine loading transients.

B.3 A Generic System Model

The observer design proposed in this paper applies to MISO Hammerstein systems with sensor delay of the following form

$$\tau\dot{x}(t) = g(\theta(t), u(t)) - x(t) \tag{B.4a}$$

$$y(t) = x(t-\Delta t) \tag{B.4b}$$

$$\bar{\theta} - \kappa \leq \theta(t) \leq \bar{\theta} + \kappa \tag{B.4c}$$

where $x \in D_x$ is a system state within $D_x \subset R$, $u : [0,\infty) \to D_u$ is a vector of known signals within $D_u \subset R^p$, $g : D_\theta \times D_u \to D_x$ is referred to as the input nonlinearity, τ is a known positive time constant and Δt is a known time delay of the measurement $y \in D_x$. $g(\theta(t),u(t))$ is assumed to be piecewise continuous in t. The time dependency of signals is explicitly expressed when needed.

$\theta(t)$ is a time-varying parameter bounded within an interval $\theta(t) \in [\bar{\theta} - \kappa; \bar{\theta} + \kappa]$, $\kappa \geq 0$. $\bar{\theta}$ defines the middle of the interval and κ is the possible deviation from $\bar{\theta}$. It is not necessary to know the parameters $\bar{\theta}$ and κ. Theorem 1 that the parameter estimate of the proposed observer will converge to the interval.

The input nonlinearity is required to satisfy a sector condition with respect to the parameter estimate error. With estimation errors denoted as $\tilde{x} = \hat{x} - x$, $\tilde{\theta} = \hat{\theta} - \theta$ and $\tilde{g}(\theta,\tilde{\theta},u) = g(\theta + \tilde{\theta},u) - g(\theta,u)$, the condition can be stated as

Property 1

The function $\tilde{g}(\tilde{\theta},u)$ is a sector nonlinearity in $\tilde{\theta}$:

$$\forall \tilde{\theta}, \exists \rho, \exists \gamma > 0 : \gamma\tilde{\theta}^2 \leq \tilde{g}(\theta,\tilde{\theta},u)\tilde{\theta} \leq \rho\tilde{\theta}^2.$$

It can be inferred from Property 1 that $\tilde{g}(\theta,\tilde{\theta},u)$ is monotonically increasing in $\tilde{\theta}$. If g is continuously differentiable this property is satisfied if $\frac{\partial g}{\partial \theta}$ has positive bounds.

B.4 Estimator Design

Definition 1

A parameter estimator for the system defined by (B.4) is

$$\hat{\theta}(t) = k \cdot \left(\tau y(t) + \int_0^t y(t) - g(\hat{\theta}(t),u(t-\Delta t))\,\mathrm{dt} \right) \tag{B.5}$$

where $k > 0$.

Theorem 1

Let the estimator defined by (B.5) be used for estimating the time-varying parameter $\theta(t)$ of the system defined by (B.4). If Property 1 is fulfilled, then $\tilde{\theta}(t)$ is bounded by the relation

$$|\hat{\theta}(t) - \bar{\theta}| \leq \kappa + \left(|\hat{\theta}(0) - \bar{\theta}| - \kappa \right) e^{-k\gamma t} \tag{B.6}$$

Proof of Theorem 1

Differentiating (B.5) with respect to time

$$\dot{\hat{\theta}}(t) = k \cdot \left(\tau\dot{y}(t) + y(t) - g(\hat{\theta}(t),u(t-\Delta t)) \right) \tag{B.7}$$

Using (B.4b) we get

$$\dot{\hat{\theta}}(t) = k \cdot \left(\tau\dot{x}(t-\Delta t) + x(t-\Delta t) - g(\hat{\theta}(t),u(t-\Delta t)) \right) \tag{B.8}$$

From (B.4a), $\tau\dot{x}(t-\Delta t) + x(t-\Delta t) = g(\theta(t-\Delta t),u(t-\Delta t))$, hence

$$\begin{aligned} \dot{\hat{\theta}}(t) = k \cdot \left(g(\theta(t-\Delta t),u(t-\Delta t)) - g(\hat{\theta}(t),u(t-\Delta t)) \right) \\ = -k\tilde{g}(\theta(t-\Delta t),\hat{\theta}(t) - \theta(t-\Delta t),u(t-\Delta t)) \end{aligned} \tag{B.9}$$

The proof now splits into three cases, depending on the size of $\hat{\theta}$.

i) As a first case, assume that the estimate is above the interval ($\hat{\theta} \geq \bar{\theta} + \kappa$).

As $\bar{\theta} + \kappa \geq \theta$ and $\tilde{g}(\theta, \tilde{\theta}, u)$ is monotonically increasing in $\tilde{\theta}$, equation B.9 can be converted to the differential inequality

$$\dot{\hat{\theta}}(t) \leq -k\tilde{g}(\theta(t-\Delta t), \hat{\theta}(t) - (\bar{\theta} + \kappa), u(t-\Delta t)) \tag{B.10}$$

From Property 1 we get

$$\dot{\hat{\theta}}(t) \leq -k\gamma(\hat{\theta}(t) - (\bar{\theta} + \kappa)) \Leftrightarrow \tag{B.11}$$

$$\dot{\hat{\theta}}(t) - (\bar{\theta} + \kappa) \leq -k\gamma\hat{\theta}(t) \tag{B.12}$$

According to the Comparison Principle as seen in [81], the solution to the differential inequality (B.12) is bounded by the solution to the corresponding differential equation, thus

$$\hat{\theta}(t) - (\bar{\theta} + \kappa) \leq \left(\hat{\theta}(0) - (\bar{\theta} + \kappa)\right) e^{-k\gamma t} \Leftrightarrow \tag{B.13}$$

$$\hat{\theta}(t) - \bar{\theta} \leq \kappa + \left(\hat{\theta}(0) - \bar{\theta} - \kappa\right) e^{-k\gamma t} \tag{B.14}$$

As $\hat{\theta} \geq \bar{\theta}$ we get

$$\left|\hat{\theta}(t) - \bar{\theta}\right| \leq \kappa + \left(\left|\hat{\theta}(0) - \bar{\theta}\right| - \kappa\right) e^{-k\gamma t} \tag{B.15}$$

which proves (B.6) for the first case.

ii) In the second case, assume that the estimate is below the interval ($\hat{\theta} \leq \bar{\theta} - \kappa$).

As $\bar{\theta} - \kappa \leq \theta$ and $\tilde{g}(\theta, \tilde{\theta}, u)$ has positive sensitivity to $\tilde{\theta}$, equation B.9 can also be converted to the differential inequality

$$\dot{\hat{\theta}}(t) \geq -k\tilde{g}(\theta(t-\Delta t), \hat{\theta}(t) - (\bar{\theta} - \kappa), u(t-\Delta t)) \tag{B.16}$$

From Property 1 we get

$$\dot{\hat{\theta}}(t) \geq -k\gamma(\hat{\theta}(t) - (\bar{\theta} - \kappa)) \Leftrightarrow \tag{B.17}$$

$$\dot{\hat{\theta}}(t) - (\bar{\theta} - \kappa) \geq -k\gamma\hat{\theta}(t) \tag{B.18}$$

Application of the Comparison Principle again leads to

$$\hat{\theta}(t) - (\bar{\theta} - \kappa) \geq \left(\hat{\theta}(0) - (\bar{\theta} - \kappa)\right) e^{-k\gamma t} \Leftrightarrow \tag{B.19}$$

$$\hat{\theta}(t) - \bar{\theta} \geq -\kappa + \left(\hat{\theta}(0) - \bar{\theta} + \kappa\right) e^{-k\gamma t} \tag{B.20}$$

Since $\hat{\theta} \leq \bar{\theta}$ we get

$$\left|\hat{\theta}(t) - \bar{\theta}\right| \leq \kappa + \left(\left|\hat{\theta}(0) - \bar{\theta}\right| - \kappa\right) e^{-k\gamma t} \tag{B.21}$$

which proves (B.6) for the second case.

iii) The third and last case where the estimate is inside the interval obviously also fulfills (B.6). □

As $|\theta(t) - \bar{\theta}| \leq \kappa$, a consequence of Theorem 1 is that the absolute value of the parameter estimation error will converge toward 2κ or less without overshoot and with a minimum convergence rate of $k\gamma$.

Definition 2

A joint state and parameter observer for the system defined by (B.4) is

$$\dot{\hat{x}} = \frac{1}{\tau}\left(g(\hat{\theta}(t), u(t)) - \hat{x}\right) \tag{B.22a}$$

$$\hat{\theta}(t) = k \cdot \left(\tau y(t) + \int y(t) - g(\hat{\theta}(t), u(t-\Delta t))\,\mathrm{dt}\right) \tag{B.22b}$$

where $k > 0$.

Theorem 2

Let the observer defined by (B.22) be used for observing the state x and the parameter θ of the system defined by (B.4). If Property 1 is fulfilled, then $\tilde{x}$ is bounded by (B.29).

Proof of Theorem 2

The differential equation of the state estimate error is

$$\tau\dot{\tilde{x}} = \tau\dot{\hat{x}} - \tau\dot{x} = -\hat{x} + g(\hat{\theta}(t), u(t)) + x - g(\theta, u(t)) \Leftrightarrow \tag{B.23}$$

$$\tau\dot{\tilde{x}} = -\tilde{x} + \tilde{g}(\theta(t), \tilde{\theta}(t), u(t)) \tag{B.24}$$

From Property 1 we get

$$-\rho\left|\hat{\theta}(t) - \theta\right| \leq \tilde{g}(\theta(t), \tilde{\theta}(t), u(t)) \leq \rho\left|\hat{\theta}(t) - \theta\right| \tag{B.25}$$

Furthermore, from Theorem 1,

$$\left|\hat{\theta}(t) - \theta\right| \leq \left|\hat{\theta}(t) - \bar{\theta}\right| + \kappa \leq 2\kappa + \left(\left|\hat{\theta}(0) - \bar{\theta}\right| - \kappa\right) e^{-k\gamma t} \tag{B.26}$$

Combining (B.25) with (B.26) leads to two differential inequalities

$$\tilde{g}(\theta(t), \tilde{\theta}(t), u(t)) \geq -\rho\left(2\kappa + \left(\left|\hat{\theta}(0) - \bar{\theta}\right| - \kappa\right) e^{-k\gamma t}\right) \tag{B.27a}$$

$$\tilde{g}(\theta(t), \tilde{\theta}(t), u(t)) \leq \rho\left(2\kappa + \left(\left|\hat{\theta}(0) - \bar{\theta}\right| - \kappa\right) e^{-k\gamma t}\right) \tag{B.27b}$$

Inserting these into (B.24)

$$\tau\dot{\tilde{x}} \geq -\tilde{x} - \rho\left(2\kappa + \left(\left|\hat{\theta}(0) - \bar{\theta}\right| - \kappa\right) e^{-k\gamma t}\right) \tag{B.28a}$$

$$\tau\dot{\tilde{x}} \leq -\tilde{x} + \rho\left(2\kappa + \left(\left|\hat{\theta}(0) - \bar{\theta}\right| - \kappa\right) e^{-k\gamma t}\right) \tag{B.28b}$$

Using the Comparison Principle once again allows us to solve the differential inequalities

$$\tilde{x}(t) \geq -2\rho\kappa + (\tilde{x}(0) + 2\rho\kappa) e^{-\frac{t}{\tau}} - \eta\left(e^{-k\gamma t} - e^{-\frac{t}{\tau}}\right) \tag{B.29a}$$

$$\tilde{x}(t) \leq 2\rho\kappa + (\tilde{x}(0) - 2\rho\kappa) e^{-\frac{t}{\tau}} + \eta\left(e^{-k\gamma t} - e^{-\frac{t}{\tau}}\right) \tag{B.29b}$$

where

$$\eta = \frac{\rho\left(\left|\hat{\theta}(0) - \bar{\theta}\right| - \kappa\right)}{1 - k\gamma\tau} \tag{B.30}$$

Thus $|\tilde{x}(t)|$ will converge to $2\rho\kappa$ or lower with a minimum exponential convergence rate λ equal to the rate of the slowest converging term. Therefore $\lambda = \min(k\gamma, \frac{1}{\tau})$. □

Figure B.2 shows an overview of the signal paths when combining control object and sensor with the joint state and parameter observer.

Note that the observer also can be applied to systems where the input nonlinearity has negative sensitivity to parameter estimation errors, opposite to what is specified in Property 1. This is achieved by inverting the sign of the parameter estimator equation. Consider as an example a system on the form (B.4) with

$$g(\theta, u) = -\theta \cdot (u^2 + 1) \tag{B.31}$$

The nonlinearity can be rewritten by defining $\psi = -\theta$ to

$$g_\psi(\psi, u) = \psi \cdot (u^2 + 1) \tag{B.32}$$

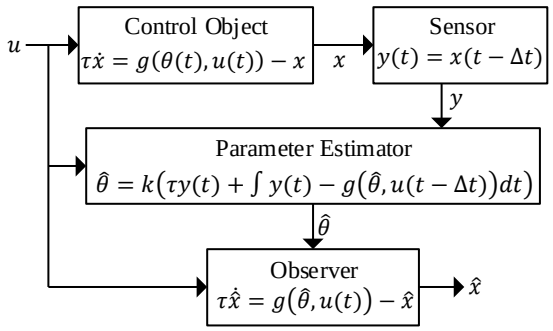

Figure B.2: Overview of the signal paths of the joint parameter and state observer. The parameter estimator uses the inputs and the sensor signal, whereas the observer only uses inputs and estimated parameter.

Now $g_\psi()$ fulfills Property 1 and ψ can be estimated according to Definition 1

$$\hat{\psi}(t) = k \cdot \left(\tau y(t) + \int_0^t y(t) - g_\psi(\hat{\psi}(t), u(t - \Delta t))\,\mathrm{dt} \right) \tag{B.33}$$

As $g_\psi(\psi, u) = g(\theta, u)$ we get

$$\hat{\theta}(t) = -k \cdot \left(\tau y(t) + \int_0^t y(t) - g(\hat{\theta}(t), u(t - \Delta t))\,\mathrm{dt} \right) \tag{B.34}$$

Thus for systems with negative sensitivity to parameter errors the sign of the parameter estimator should be switched.

The choice of observer gain k depends on the application. A high gain leads to fast convergence but also challenges the observer with regards to robustness to model inaccuracy and noise. As the observer has a direct gain from measurement to parameter estimate the observer might not be suited for control objects with significant sensor noise.

Note that when $\theta(t)$ is constant, $\kappa = 0$ and the observer errors converge exponentially to zero.

B.5 Comparison

The strength of the design presented here is the simplicity of the estimator for the case of the MISO Hammerstein system. This is in contrast to the design presented by [67] that solves the parameter estimation problem for a wider class of systems with a more complex estimator. For comparison, the design presented by [67] is applied to the problem solved by the parameter estimator from Definition 1. That is, estimating the parameter θ of the system (B.4). The resulting parameter estimator is[3]

$$\dot{z} = -k_\phi \left(\hat{\phi} - \frac{1}{\tau} y(t) \right) - \frac{1}{\tau} \frac{\partial g}{\partial \theta}(\hat{\theta}, u(t - \Delta t)) \cdot k_\theta \left(\tau\hat{\phi} - g(\hat{\theta}, u(t - \Delta t)) \right) \tag{B.35}$$

$$\hat{\phi} = z + k_\phi \frac{y(t)}{\tau} + \frac{1}{\tau} g(\hat{\theta}, u(t - \Delta t)) \tag{B.36}$$

$$\dot{\hat{\theta}} = k_\theta \left(\tau\hat{\phi} - g(\hat{\theta}, u(t - \Delta t)) \right) \tag{B.37}$$

The difference in complexity is clear when comparing to Definition 1. The estimator from [67] requires online calculation of $\frac{\partial g}{\partial \theta}$, an additional internal state z and an additional tuning parameter. An exponentially converging upper bound of $|\tilde{\theta}|$ was derived in [67], but it depends on the selection of a Lyapunov function and does not rule out the possibility of overshoot.

[3] Design choice for $\dot{\hat{\theta}}$ is based on (B.9).

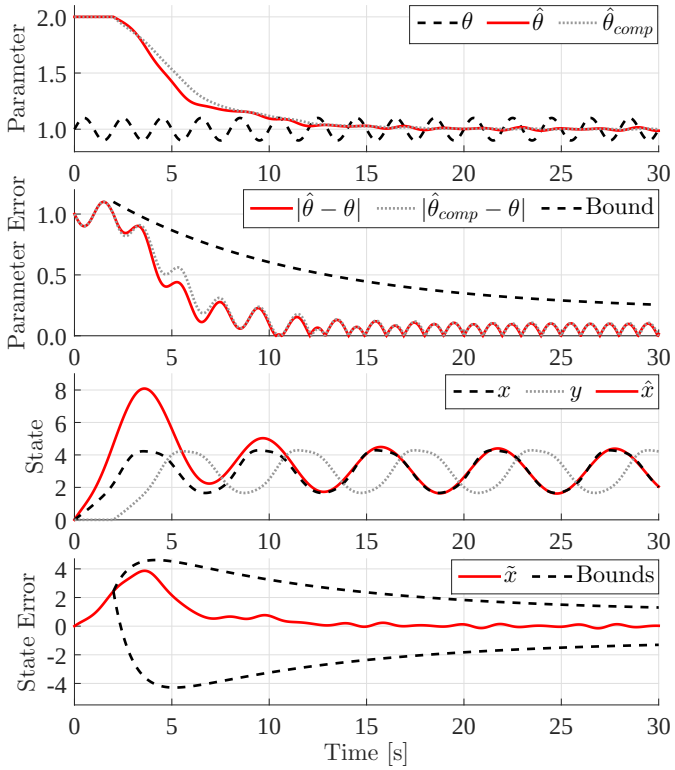

Figure B.3: Simulation of the observer applied to a simple system. The errors converge within the bounds and the state estimate is not delayed like the measurement. The observer performance is similar to that of the more complex parameter estimator ($\hat{\theta}_{comp}$) from Section B.5.

B.6 Simulation Example

This section demonstrates the efficacy of the observer with a simple simulated example. The nonlinear part, $g(\theta,u)$, of the system is defined as

$$g(\theta,u) = \theta \cdot (u^2+1) \tag{B.38}$$

Taking the partial derivative with respect to θ leads to

$$\frac{\partial g(\theta,u)}{\partial \theta} = u^2+1 \tag{B.39}$$

For $|u(t)| \leq 2$ the system fulfills Property 1 with $\gamma = 1$ and $\rho = 5$. Theorem 2 facilitates the design of a joint state and parameter observer with errors that converge exponentially. The system and the observer are simulated with $\tau = 1$ s, $\Delta t = 2$ s, $k = 0.1$, $\theta = 1$, $u(t) = 2\sin(\frac{\pi t}{6})$ and , $\theta(t) = 1+0.1\sin(\pi t)$, thus $\bar{\theta} = 1$ and $\kappa = 0.1$. The simulated observer errors are shown in Figure B.3 along with the calculated bounds. The parameter estimate starts updating after 2 seconds as it needs a recording of the input signals with a length equal to the delay. The bottom plot compares the state to the measurement and the estimate. Figure B.3 also shows the performance of the parameter estimator ($\hat{\theta}_{comp}$) from Section B.5 simulated with similar gains. There is no significant performance difference between the two parameter estimates in this example.

B.7 Adaptive Observer for Oxygen Estimation

The joint state and parameter observer is applied to the EGR system by defining state, measurement and inputs as, respectively

$$x = O_{sr}\ ,\ y = O_{srm}\ ,\ u = \begin{bmatrix} \dot{n}_f & \dot{n}_{egr} & \omega_{tc} \end{bmatrix}^T \tag{B.40}$$

and the input nonlinearity of the Hammerstein model as

$$g(\theta,u) = O_a - \frac{(1+\frac{y}{4}(O_a+1))\dot{n}_f\dot{n}_{egr}}{(\theta\beta(\omega_{tc})+\frac{y}{4}\dot{n}_f)(\theta\beta(\omega_{tc})+\dot{n}_{egr})} \tag{B.41}$$

The values of ρ and γ are found as the limits to

$$\frac{\partial g}{\partial \theta} = \left(1+\frac{y}{4}(O_a+1)\right)\frac{\dot{n}_f\dot{n}_{egr}\beta\left(2\beta+\frac{y}{4}\dot{n}_f+\dot{n}_{egr}\right)}{\left(\theta\beta+\frac{y}{4}\dot{n}_f\right)^2(\theta\beta+\dot{n}_{egr})^2} \tag{B.42}$$

These limits depend on the possible combinations of inputs which are difficult to determine. Conservative values can be calculated by defining independent intervals for the inputs. For a typical engine this approach results in limits of the order $\rho = 10^{-3}$, $\gamma = 10^{-5}$. With an estimator gain of 100 (as used in the experiments) this leads to a convergence bound with a time constant of 15 minutes. This is considered as a theoretical result that guarantees convergence in worst-case rather than an indicator of expected performance, as all simulations and experiments show much faster convergence. A combination of inputs that results in $\gamma = 10^{-5}$ (and thus slow convergence) only exists for short intervals as the inputs to the COM are not independent in the physical system.

The following sections show the observer applied to EGR systems with increasing levels of realism. As the observer has more than enough time for initial convergence during the fixed-input EGR startup phase, our main focus is engine loading transients where the observer has to be robust against model inaccuracy and variations of θ.

B.7.1 Results from Control-Oriented Model

The joint state and parameter observer is first applied to a simulation of the control-oriented EGR model. The scenario is an engine loading transient with subsequent adjustment of turbocharger speed and EGR flow. The value of θ is changed in a step, to illustrate the convergence bounds. Figure B.4 shows the results. $\theta(t)$ is constant after the step at 50 seconds, so the observer errors converge to zero. The convergence bound for this period is shown in Figure B.4. With respect to the oxygen fraction, the observer is able to produce a reasonable instantaneous estimate of the simulated state during the loading transient in spite of the change of θ.

B.7.2 Results from High-Fidelity Simulation

The observer is now applied to a simulation of the high-fidelity model of the full air path of a marine diesel engine with high pressure EGR presented in [49]. This model includes more complex dynamics than the COM and thus challenges the observer robustness. As before the scenario is a load transient, but in this case θ, the turbocharger speed and the EGR flow are simulated by the model. The EGR blower speed is adjusted after the transient. Figure B.5 shows the results. The transition through the operating region makes the simulated θ change. The parameter estimate fluctuates slightly during the first part of the transient and travels outside the interval to which $\theta(t)$ belongs. This is due to the small differences in dynamics between the COM and the high-fidelity model which are not accounted for in the convergence proofs. As before the observer is able to estimate the oxygen fraction without delay and with reasonable accuracy during the transient.

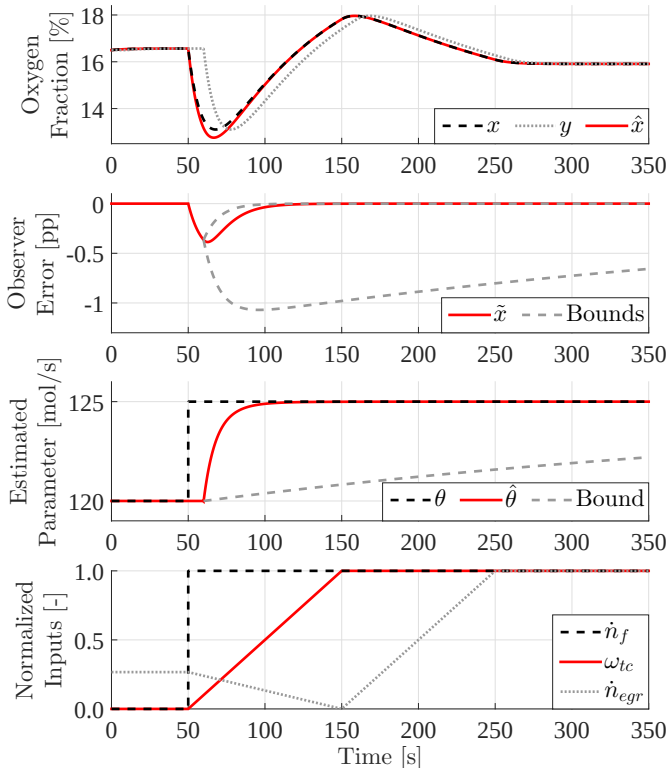

Figure B.4: Results from application of the joint state and parameter observer to a simulation of the control-oriented EGR model.

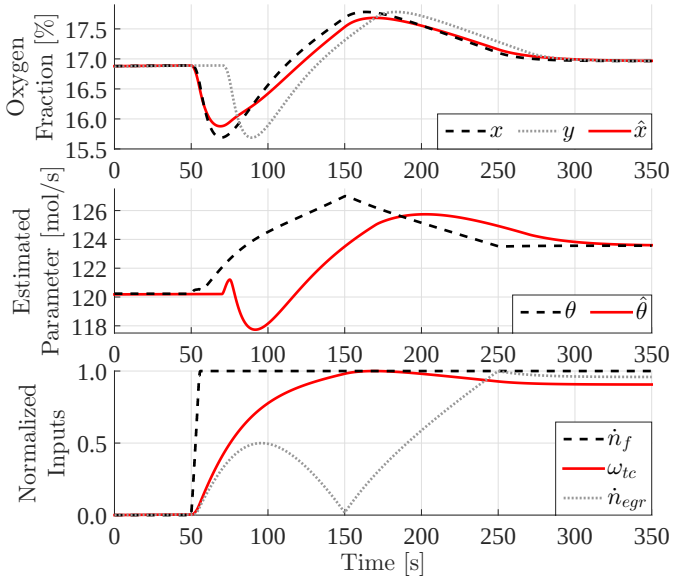

Figure B.5: Results from application of the joint state and parameter observer to a simulation of a high-fidelity model of a diesel engine airpath.

The high-fidelity model depends on turbine and compressor maps for flow calculation. These maps only cover pressure conditions present in the upper half of the engine load region. Research into extrapolation of the model to low load conditions is still ongoing. Most of the problematic loading transients occur in the lower half where auxiliary blowers aid the turbocharger compressor in maintaining scavenge pressure. The validity of the joint state and parameter observer in the low load region is tested experimentally.

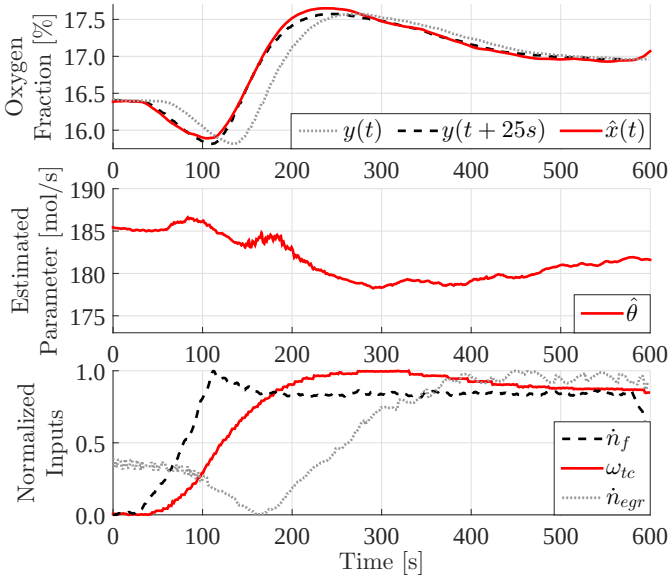

Figure B.6: Results from application of the joint state and parameter observer to an engine load ramp performed on an engine test bed.

B.7.3 Results from Engine Test Bed

The observer is experimentally validated by applying it to data recorded from an engine test bed, in this case the 4T50ME-X large two-stroke engine situated in engine designer MAN Diesel & Turbo's Diesel Research Center in Copenhagen. Figure B.6 shows the result of applying the observer to a load ramp in the lower half of the load range. In this region θ is higher as the auxiliary blowers increase the flow. Small fluctuations occur in the parameter estimate, but the observer is able to predict the measurement with reasonable accuracy in spite of the auxiliary blowers.

B.7.4 Results from Vessel

The final validation is carried out by applying the observer to an example of the unfortunate scenario that it is meant to alleviate. The dataset in question stems from the 4500 TEU container vessel Maersk Cardiff, operating in the South China Sea. When moving at steady state at approximately 10% engine load, the bridge performed an engine speed setpoint step. Engine load peaked at 43% during the transient and stabilized at about 27%. The slow response of the EGR controller led to a severe drop in O_{sr} from 16% to 12% with subsequent oscillations. This drop resulted in formation of thick black exhaust smoke for more than 45 seconds.

Results from application of the observer is shown in Figure B.7. The vessel engine is approximately 3 times larger than the test bed engine, and θ scales similarly. The observer is challenged by the extreme scenario and the input transients, especially in EGR flow, propagates to $\hat{\theta}$. It is difficult to determine whether the fluctuating behavior of $\hat{\theta}$ is due to model inaccuracy or whether it represents actual transient behavior of $\theta(t)$. In any case, the state observer is able to predict the O_{sr} drop 20 seconds before the sensor, with acceptable accuracy. The EGR controller would benefit significantly from this information in order to decrease the EGR flow during the transient and thus avoid unacceptable smoke formation.

B.8 Conclusions

Designs for both a *parameter estimator* and a *joint state and parameter observer* were presented along with derivation of exponentially converging bounds on state and parameter errors. A simulation example

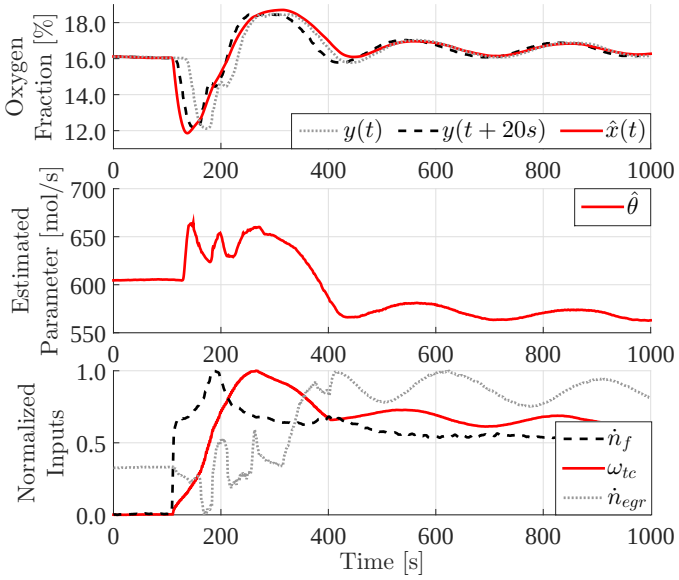

Figure B.7: Results from application of the joint state and parameter observer to an engine speed setpoint step performed on a vessel operating at sea.

illustrated the performance of the resulting observer and it the complexity was favorably compared to the method of [68]. It was shown that while the suggested approach applies to a more narrow class of systems, the present design is simpler and provides better knowledge about error behavior. Application of the observer to a high-pressure exhaust gas recirculation system for large two-stroke diesel engines at test bed and at sea showed that the suggested method is a promising candidate to become enabling technology for estimator-based control of exhaust gas recirculation, and thereby a cornerstone in order for large marine diesel engines to meet strict emission requirements in NO_x and soot formation.

Acknowledgment

This work was partially funded by the Danish Agency for Science, Technology and Innovation, grant number 1355-00071B.

Paper C

Adaptive Feedforward Control of Exhaust Recirculation in Large Diesel Engines

Kræn Vodder Nielsen[*1,2], Mogens Blanke[2,3], Lars Eriksson[4], Morten Vejlgaard-Laursen[1]

[1] MAN Diesel & Turbo, Teglholmsgade 41, 2450 København SV, Denmark [2]Department of Electrical Engineering, Automation and Control Group, Technical University of Denmark, Elektrovej Building 326, 2800, Kgs. Lyngby, Denmark

[3]AMOS CoE, Institute of Technical Cybernetics, Norwegian University of Science and Technology, 7491 Trondheim, Norway

[4]Vehicular Systems, Department of Electrical Engineering, Linköping University, 58183 Linköping, Sweden

Abstract:
Environmental concern has lead the International Maritime Organization to restrict NO_x emissions from marine diesel engines. Exhaust gas recirculation (EGR) systems have been introduced in order to comply to the new standards. Traditional fixed-gain feedback methods are not able to control the EGR system adequately in engine loading transients so alternative methods are needed. This paper presents the design, convergence proofs and experimental validation of an adaptive feedforward controller that significantly improves the performance in loading transients. First the control concept is generalized to a class of first order Hammerstein systems with sensor delay and exponentially converging bounds of the control error are proven analytically. It is then shown how to apply the method to the EGR system of a two-stroke crosshead diesel engine. The controller is validated by closed loop simulation with a mean-value engine model, on an engine test bed and on a vessel operating at sea. A significant reduction of smoke formation during loading transients is observed both visually and with an opacity sensor.

K. V. Nielsen, M. Blanke, L. Eriksson, and M. Vejlgaard-Laursen. "Adaptive Feedforward Control of Exhaust Recirculation in Large Diesel Engines". *Control Engineering Practice* (2016). In review

[*]Principal corresponding author. Tel.: +45 33851909; E-mail: kraenv.nielsen@man.eu

C.1 Introduction

Emissions of CO_2, SO_x and NO_x have in recent years received an ever growing attention due to their environmental effects. The International Maritime Organization (IMO) has introduced a stepwise restriction to NO_x emissions from marine diesel engines, so far culminating in the Tier III standard [2]. For large two-stroke diesel engines this standard dictates a reduction by a factor of four compared to the Tier II standard and applies to vessels built after 1st of January 2016 when operating in specified NO_x Emission Control Areas (NECAs). As for now the North American coastal area is a NECA but serious steps have been taken toward including the North Sea and Baltic Sea as NECAs as well [54]. The substantial reduction specified in the Tier III standard requires significant changes to the modern marine diesel engines and a number of solutions are being investigated and developed into products. This paper focuses on control of high-pressure Exhaust Gas Recirculation (EGR) for large two-stroke diesel engines.

The main source of NO_x emission from a large two-stroke diesel engine is thermal NO_x which is formed during the combustion process, where excessively high peak temperatures lead to reactions between nitrogen and oxygen. These reactions are known as the Zeldovich mechanism [11]. Recirculation of exhaust gas to the combustion process increases heat capacity and decreases the availability of oxygen, resulting in lower peak temperatures during combustion and thus decreased formation of NO_x. A simplified overview of the airflow of a large two-stroke engine with high-pressure EGR developed by MAN Diesel & Turbo is shown in Figure C.1. In the EGR string (on the left) exhaust gas is cleaned and cooled in the EGR Unit, pressurized by the EGR blower and mixed into the scavenge flow.

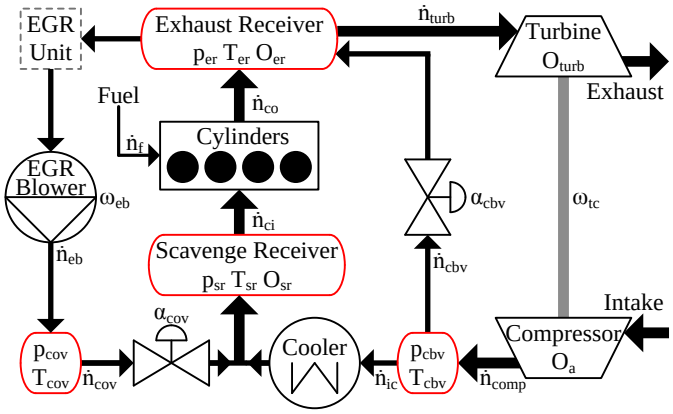

Figure C.1: Overview of main gas flows and components of the engine with exhaust gas recirculation and cylinder by-pass valve.

The amount of air that is to be recirculated in the EGR string is implicitly decided by calculation of a number of operating points in which the NO_x emission is within the legislated limits. These points are characterized by engine load and molar scavenge receiver oxygen fraction (O_{sr}) as seen in Figure C.2. The goal of the EGR controller is then to reach this O_{sr} setpoint given the engine load condition.

The reference EGR controller applies fixed gain propor-tional-integral feedback control. In steady engine load scenarios the O_{sr} setpoint is kept within desired bounds but whenever the engine load (and thus the fuel flow) changes, the EGR controller is in trouble. The slow nature of the system and a significant delay in the measurement of O_{sr} limits the possible disturbance rejection of the feedback control. In fast loading transients the lack of response can result in severe negative peaks in O_{sr} leading to formation of black exhaust smoke for more than 45 seconds. With the PI EGR controller it is necessary to restrict the engine loading rate in order to avoid this smoke. However, such a solution is not viable as the NECAs mainly cover ports and coastal areas where maneuvering capability is essential.

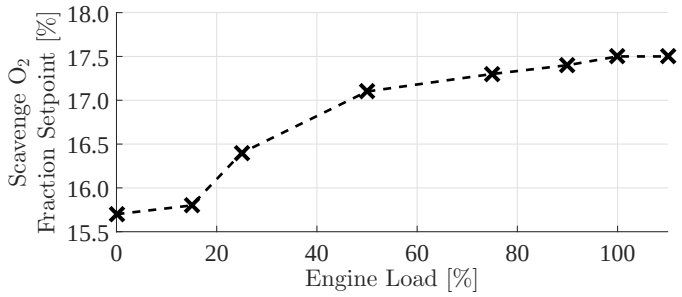

Figure C.2: An example of required scavenge oxygen fraction as a function of engine load. The linearly interpolated commissioning points are specific to the engine.

C.1.1 Literature

Extensive treatment of combustion engine processes and modeling can be found in works such as [11, 12, 14]. Relevant treatment of large two-stroke crosshead engines mainly include governor design (engine speed control) as found in [4, 31, 32, 57, 58]. This led to investigation and development of dynamical models of engine speed response, where turbocharger dynamics were proven to have a significant effect [28, 29, 30]. IMO's stepwise introduction of NO_x emission limits led to research into the use of variable geometry turbines as in [33]. A more recent development and investigation of a large two-stroke engine model without EGR was recently published in [34, 36, 37, 38, 59].

Only few publications have been made about the EGR control for large two-strokes. Hansen et al published two papers about modeling and control, respectively [43, 44]. The model was extended and improved by Alegret et al in [45] by introducing the Cylinder By-pass Valve (CBV), changing the parameter estimation scheme and the development of a new exhaust temperature calculation. The authors of the present paper made a number of further extensions to the same model in [49], where a simpler control-oriented model (COM) of the scavenge oxygen fraction was derived as well. A similar COM had earlier been presented in [53] along with a nonlinear controller. A joint state and parameter observer for the COM was presented in [50].

A much larger amount of publications are available on the EGR control for automotive engines, typically including a VGT [15, 18, 19, 20, 21, 60, 61]. An investigation into the effect of fuel mix on the intake oxygen fraction on an automotive engine with EGR and observer design for this system was published in [26, 27]. The design of EGR control for large two-stroke engines differ from the automotive engine especially in the differences between scavenging of 2-stroke and 4-stroke engines, lack of engine test bed availability (as explained in [4]), system time constants, sensor availability and the general maturity of the field.

C.1.2 Purpose

Existing EGR feedback control is able to control O_{sr} during steady operating conditions but suffers during loading transients. In [44] it was shown that the achievable performance with SISO feedback control is limited. A nonlinear controller with direct use of fuel flow and turbocharger speed signals where suggested in [53] but without thorough validation. The present paper extends the results from [53] significantly. The main contributions of the present paper are

1. The controller concept introduced in [53] is generalized to a class of first order Hammerstein systems that now include sensor delay.

2. Exponentially converging bounds of the control error are proven.

3. The controller is validated by closed loop simulation with an MVEM model, in an engine test bed and on a vessel operating at sea.

C.1.3 Outline of this paper

Section C.2 provides a brief summary of the two EGR models used. Section C.3 presents the new controller concept as generalized to a class of first order Hammerstein models and proves minimum convergence bounds of the control error. The control concept is applied to the control-oriented EGR model in Section C.4. Section C.5 shows the results of closed loop simulation and presents experimental validation both on an engine test bed and on a vessel operating at sea.

C.2 EGR System Models

The controller presented in this paper is designed by the use of mathematical models of the EGR system behavior. A high-fidelity mean-value engine model (MVEM) is used for validation of closed loop properties. Controller synthesis by linearizing a similar MVEM was investigated in [44] where it was shown difficult to achieve both performance and robustness. The MVEM model also served as a basis of a simpler control-oriented model in [49]. In the present paper we design a nonlinear controller based on the COM similar to the controller presented on [53]. The MVEM and the COM are summarized below.

C.2.1 Mean-Value Engine Model

The size and complexity of a two-stroke cross-head marine diesel engine makes practical experiments an expensive and thus scarce resource. Therefore it is highly advantageous to be able to simulate engine behavior when designing controllers. A model of the main gas flows and gas composition of the 4T50ME-X engine located in MDT's Diesel Research Center in Copenhagen was presented in [43]. It had the form of a mean value, filling and emptying model where many parameters were estimated from test data. This model was improved and extended in [45] where the cylinder bypass valve was added and the parameter estimation scheme was changed. A few further changes were made in [49], most notable the change from mass to molar flows and gas composition in order to better relate to the scavenge oxygen sensor. The latter model is used in the present paper for closed loop validation of the EGR controller.

The components represented in the MVEM are shown in Figure C.1. Four volumes (red) are characterized by an isothermal pressure state in each

$$\dot{p}_i = \frac{RT_i}{V_i}\left(\dot{n}_{in} - \dot{n}_{out}\right), \tag{C.1}$$

where $\dot{n}$ represents molar flow. The turbocharger speed is also modeled as a state

$$\dot{\omega}_{tc} = \frac{P_{turb} - P_{comp}}{J_{tc}\omega_{tc}}, \tag{C.2}$$

where P_{turb} and P_{comp} are turbine and compressor power, respectively, and J_{tc} is the moment of inertia of the total rotor system. Molar fractions of O_2 in the scavenge and exhaust receivers are modeled as states

$$\dot{O}_i = \frac{RT_i}{p_i V_i} \sum_{input=j} \dot{n}_j \left(O_j - O_i\right) \tag{C.3}$$

Standard submodels of valves, blower, turbine, compressor and intercooler calculate the molar flow between said volumes based on input and output pressures and in most cases some additional variable or input ε such as valve opening or turbocharger speed

$$\dot{n}_i = f(p_{in}, p_{out}, \varepsilon) \tag{C.4}$$

Note that $\dot{n}_i$ represents a molar flow, not a state of the model. The flow through the cylinder submodel is calculated as the mean of the flow through one engine revolution. A lean combustion reaction of the form

$$CH_y + \left(1 + \frac{y}{4}\right) O_2 \rightarrow CO_2 + \frac{y}{2} H_2O \tag{C.5}$$

is assumed. The virtual fuel molecule CH_y is introduced to simplify the analysis. The fuel constant y refers to the total ratio of hydrogen to carbon among the different species in the fuel. Based on (C.5) the molar fraction of O_2 in the total flow exiting the cylinders is calculated as

$$O_{co} = \frac{\dot{n}_{ci} O_{sr} - \dot{n}_f \left(1 + \frac{y}{4}\right)}{\dot{n}_{ci} + \frac{y}{4} \dot{n}_f}, \tag{C.6}$$

where $\dot{n}_{ci}$ is the total flow entering the cylinders and $\dot{n}_f$ is the molar flow of the virtual fuel molecule CH_y. Outflow temperature from the cylinders are calculated from a modified limited pressure diesel cycle. A detailed explanation is found in [45]. Inputs to the MVEM model are fuel index, engine speed, COV and CBV valve openings and EGR blower speed.

The MVEM model is parameterized to represent the upper half of the engine load region (50-100% load). The system is as such not different in the lower half of the load region, but the compressor, turbine and EGR blower maps do not include this region. Also, when operating in the lower load region the CBV valve is shut and auxiliary blowers (not modeled) aid the compressor in maintaining sufficient scavenge pressure.

C.2.2 Control-Oriented Scavenge Oxygen Model

Where the MVEM is intended to provide a highly accurate description of process physics the control-oriented model only aims at capturing the main dynamics and nonlinearity of the scavenge oxygen fraction. The simplicity and low number of parameters allow the use of the COM directly in the controller.

The COM was first briefly presented in [53]. In [49] it was shown how to derive the COM from the MVEM. The MVEM can be considered as a cascade of two isolated systems: one of pressures/TC-speed and one of O_2 fractions. Reduction of the O_2 fraction system results in a first order Hammerstein model with 3 flows from the pressure/TC-speed system as inputs

$$\tau \dot{O}_{sr} = -O_{sr} + O_a - \frac{(1 + \frac{y}{4}(O_a + 1)) \dot{n}_f \dot{n}_{egr}}{(\dot{n}_{ic} + \frac{y}{4} \dot{n}_f)(\dot{n}_{ic} + \dot{n}_{egr})} \tag{C.7}$$

Equation C.7 is the control-oriented model. It includes ambient oxygen fraction O_a, a fuel dependent constant y and a time constant $\tau \approx 12$ s as parameters. Molar fuel flow $\dot{n}_f$, EGR flow $\dot{n}_{egr}$ and intercooler flow $\dot{n}_{ic}$ are inputs to the model. In order to include the dynamics of the scavenge oxygen sensor a time delay of about 10-20 seconds can be added and the time constant can be increased to 15-20 seconds.

In [49] it was shown how to estimate the three molar flows from signals that are commonly available to the EGR controller. The fuel flow is a control input from the governor and can be calculated as proportional to the product of engine speed ω_c and fuel index Y as

$$\dot{n}_f = k_f \omega_c Y \tag{C.8}$$

EGR flow is estimated by use of an EGR blower map, along with up- and downstream pressures and blower speed. Intercooler flow is estimated as proportional to a polynomial expression β in turbocharger speed ω_{tc}.

$$\dot{n}_{ic} = \theta \cdot \beta(\omega_{tc}) \tag{C.9}$$

where

$$\beta(\omega_{tc}) = (1 - \phi) \frac{\omega_{tc}}{1000 rad/s} + \phi \left(\frac{\omega_{tc}}{1000 rad/s} \right)^2 \tag{C.10}$$

Simulations show that (C.9) is fairly accurate in the upper half of the load range when the CBV opening is kept constant (Figure C.3). However, the parameter θ is not easily obtainable from a priori engine data. Figure C.4 shows an overview of how the flow estimators provide input to the COM. When compared to

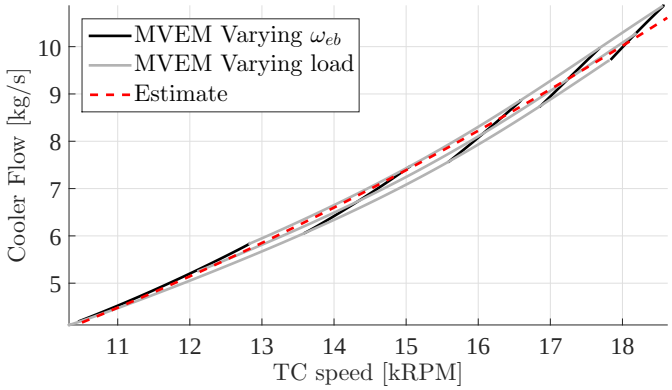

Figure C.3: Simulation and estimation of cooler flow $\dot{m}_{ic}$ with constant CBV opening and varying engine load (43-100%) and EGR blower speed.

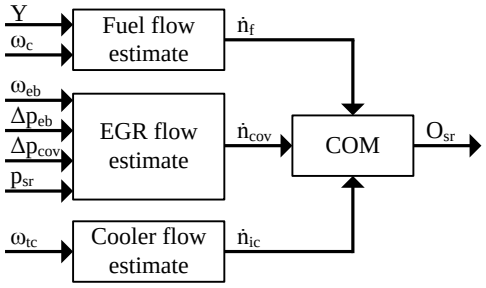

Figure C.4: Overview of the control-oriented model with its input estimates and the signals used.

data from the engine test bed the COM is able to model the scavenge oxygen dynamics well, even in the lower half of the load range and during large load transients as shown in Figure C.5.

C.3 Adaptive Feedforward Controller

This section presents the concept of adaptive feedforward (AFF) control that we later apply to the EGR system. The controller presented here is fit for controlling a certain class of first order Hammerstein systems. An overview of the adaptive feedforward concept is shown in Figure C.6. It consists of an estimator for a time-varying, and bounded, parameter $\theta(t)$ and an inversion of the input nonlinearity.

Model inversion was used for air flow control of automotive engines in [82, 83, 84] in the form of Internal Model Control (IMC). Inversion of the plant model facilitates fast response to fueling transients, but control performance is highly dependent on the correctness of the model and its inverse. The additional feedback part of IMC is avoided with the adaptation element in AFF.

C.3.1 Control Object

The adaptive feedforward controller presented here is fit for a control object that can be modeled as a first order Hammerstein system with a known time constant τ and one time-varying and bounded parameter $\theta(t)$ in the input nonlinearity. A vector of known disturbances $d(t)$ can be included as well

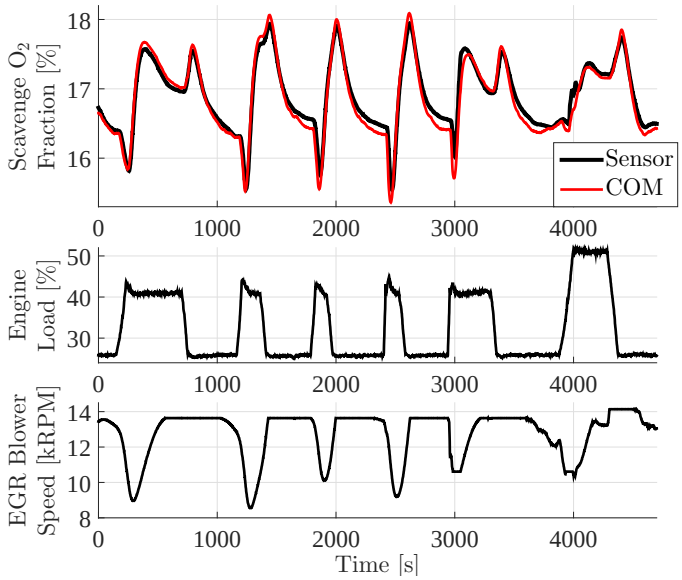

Figure C.5: Comparison of O_{sr} measured on test engine and estimated by COM during a series of engine RPM setpoint changes.

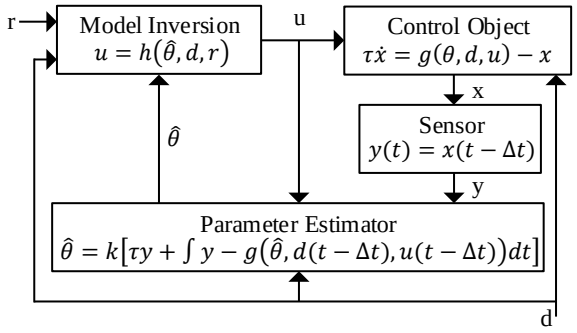

Figure C.6: Control System Structure.

and the controller is specifically efficient in compensating for these due to the feedforward principle. The differential equation that describes the system dynamics is

$$\tau\dot{x}(t) = g(\theta(t), d(t), u(t)) - x(t) \tag{C.11a}$$

$$y(t) = x(t - \Delta t) \tag{C.11b}$$

$$\bar{\theta} - \kappa \leq \theta(t) \leq \bar{\theta} + \kappa \tag{C.11c}$$

where $u(t)$ is the controlled input and $g()$ is the input nonlinearity of the model. The state x is measured as y with delay Δt. The constants $\bar{\theta}$ and κ describes the bounds of the time-varying parameter $\theta(t)$. The input nonlinearity $g()$ must be invertible in the actuated input u. This inverse function is defined as h and we get

$$r = g(\theta, d, h(\theta, d, r)) \tag{C.12}$$

where r belongs to the set of valid setpoints for the controller. Our estimate of the parameter θ is designated $\hat{\theta}$ and we define parameter estimate error $\tilde{\theta} = \hat{\theta} - \theta$. For brevity we furthermore define

$$\tilde{g}(\tilde{\theta}, d, u) = g(\theta + \tilde{\theta}, d, u) - g(\theta, d, y) \tag{C.13}$$

$$\tilde{g}_h(\tilde{\theta},d,r) = g(\theta,d,h(\theta+\tilde{\theta},d,r)) - g(\theta,d,h(\theta,d,r)) \tag{C.14}$$

The input nonlinearity and its inverse must have bounded sensitivity to some of their parameters. The required bounds of the input nonlinearity are stated as

$$\forall\theta_1,\theta_2 \in D_\theta, t \in [0,\infty), \exists\rho, \exists\gamma > 0 : \gamma\tilde{\theta}^2 \leq \tilde{g}(\tilde{\theta},d(t),u(t))\tilde{\theta} \leq \rho\tilde{\theta}^2 \tag{C.15}$$

where α indicates the sign of the sensitivity to θ. This sign must have the same value globally for a specific system. If $g(\theta,d(t),u(t))$ is continuously differential w.r.t. θ, the bounds in (C.15) can be expressed as

$$\gamma \leq \frac{\partial g(\theta,d(t),u(t))}{\partial\theta} \leq \rho \tag{C.16}$$

A bound must also be guaranteed for the sensitivity of the inverse of the input nonlinearity

$$\forall\theta_1,\theta_2 \in D_\theta, t \in [0,\infty), \exists\mu : \left|\tilde{g}_h(\tilde{\theta},d(t),r)\right| \leq \mu\left|\tilde{\theta}\right| \tag{C.17}$$

If $g(\theta,d(t),h(\hat{\theta},d(t),r))$ is continuously differentiable w.r.t. $\hat{\theta}$ the bound in (C.17) can be expressed as

$$\left|\frac{\partial g(\theta,d,h(\hat{\theta},d,r))}{\partial\hat{\theta}}\right| \leq \mu \tag{C.18}$$

If such bounds are guaranteed a controller based on a parameter estimator and inversion of the input nonlinearity can be proven to make the controller error converge at least exponentially to an interval around zero. This is shown in the following sections.

C.3.2 Parameter Estimator

The nonlinear parameter estimator from [50] is used for estimating θ

$$\hat{\theta} = k\left(\tau y(t) + \int y(t) - g(\hat{\theta}(t),d(t-\Delta t),u(t-\Delta t))\,\mathrm{dt}\right) \tag{C.19}$$

where $k > 0$. Note the direct gain from measurement y to estimated parameter $\hat{\theta}$. The estimator described by (C.19) includes an implicit state due to the integral. In [50] it the parameter estimate bounds were proven to be

$$|\hat{\theta}(t) - \bar{\theta}| \leq \kappa + \left(|\hat{\theta}(0) - \bar{\theta}| - \kappa\right)e^{-k\gamma t} \tag{C.20}$$

where $\theta(t) \in [\bar{\theta}-\kappa;\bar{\theta}+\kappa]$ and $\kappa \geq 0]$.

C.3.3 Feedforward

The feedforward part of the controller comprise on inversion of the input nonlinearity using the estimated parameter

$$u = h(\hat{\theta}(t),d(t),r) \tag{C.21}$$

where $\hat{\theta}(t)$ is the parameter estimate from (C.19), $d(t)$ is measured and r is the reference. The controller structure was drawn in Figure C.6.

C.3.3.1 Proof of control error convergence

Define the control error as $\tilde{x} = x - r$, then its time derivative is found with Equation C.11a

$$\tau\dot{\tilde{x}} = \tau\dot{x} = g(\theta,d,h(\hat{\theta},d,r)) - x \tag{C.22}$$

Using (C.12) and (C.14) we get

$$\tau\dot{\tilde{x}} = \tilde{g}_h(\tilde{\theta},d,r) + g(\theta,d,h(\theta,d,r)) - x \Leftrightarrow \tag{C.23}$$

$$\tau\dot{\tilde{x}} = \tilde{g}_h(\tilde{\theta},d,r) + r - x = \tilde{g}_h(\tilde{\theta},d,r) - \tilde{x} \tag{C.24}$$

From (C.17) we get

$$-\mu\left|\hat{\theta}(t)-\theta\right| \leq \tilde{g}_h(\tilde{\theta}(t),d(t),r) \leq \mu\left|\hat{\theta}(t)-\theta\right| \tag{C.25}$$

Furthermore, from Theorem 1,

$$\left|\hat{\theta}(t)-\theta\right| \leq \left|\hat{\theta}(t)-\bar{\theta}\right| + \kappa \leq 2\kappa + \left(\left|\hat{\theta}(0)-\bar{\theta}\right| - \kappa\right)e^{-k\gamma t} \tag{C.26}$$

Combining (C.25) with (C.26) leads to two differential inequalities

$$\tilde{g}_h(\tilde{\theta}(t),d(t),r) \geq -\mu\left(2\kappa + \left(\left|\hat{\theta}(0)-\bar{\theta}\right| - \kappa\right)e^{-k\gamma t}\right) \tag{C.27a}$$

$$\tilde{g}_h(\tilde{\theta}(t),d(t),r) \leq \rho\left(2\kappa + \left(\left|\hat{\theta}(0)-\bar{\theta}\right| - \kappa\right)e^{-k\gamma t}\right) \tag{C.27b}$$

Inserting these into (C.24)

$$\tau\dot{\tilde{x}} \geq -\tilde{x} - \mu\left(2\kappa + \left(\left|\hat{\theta}(0)-\bar{\theta}\right| - \kappa\right)e^{-k\gamma t}\right) \tag{C.28a}$$

$$\tau\dot{\tilde{x}} \leq -\tilde{x} + \mu\left(2\kappa + \left(\left|\hat{\theta}(0)-\bar{\theta}\right| - \kappa\right)e^{-k\gamma t}\right) \tag{C.28b}$$

Using the Comparison Principle from [81] allows us to solve the differential inequalities and get

$$\tilde{x}(t) \geq -2\mu\kappa + (\tilde{x}(0) + 2\mu\kappa)e^{-\frac{t}{\tau}} - \eta\left(e^{-k\gamma t} - e^{-\frac{t}{\tau}}\right) \tag{C.29a}$$

$$\tilde{x}(t) \leq 2\mu\kappa + (\tilde{x}(0) - 2\mu\kappa)e^{-\frac{t}{\tau}} + \eta\left(e^{-k\gamma t} - e^{-\frac{t}{\tau}}\right) \tag{C.29b}$$

where

$$\eta = \frac{\mu\left(\left|\hat{\theta}(0)-\bar{\theta}\right| - \kappa\right)}{1-k\gamma\tau} \tag{C.30}$$

This result in (C.29) means that the absolute value of of the control error converges exponentially to $2\mu\kappa$ or lower with a minimum convergence rate equal to the minimum of $\frac{1}{\tau}$ and $k\gamma$. The control error converges to zero when $\theta(t)$ is constant.

C.4 AFF EGR Control

This section shows how the adaptive feedforward controller concept is applied to the control-oriented model of the EGR system. The resulting AFF EGR controller has similarities to the nonlinear feed forward controller presented in [82], but the adaptation element of the AFF makes additional feedback control unnecessary.

C.4.1 Definitions

The AFF EGR controller consists of the parameter estimator (C.19) and the feedforward (C.21), with the following definitions

$$x = O_{sr} \quad , \quad d = \begin{bmatrix} \dot{m}_f & \omega_{tc} \end{bmatrix}^T \quad , \quad u = \dot{m}_{egr} \tag{C.31}$$

Scavenge oxygen fraction is defined as the state. Fuel flow and turbocharger speed are defined as known disturbances. A flow controller enables us to treat EGR flow as the actuated input. The dynamics of this

inner flow control loop is expected to be fast enough to not reduce performance of the outer oxygen control loop significantly. Simulations and experiments verify this assertion in later sections. The input nonlinearity $g()$ from (C.7) is defined as

$$g(\theta,d,u) = O_a - \frac{(1+\frac{y}{4}(O_a+1))\dot{n}_f\dot{n}_{egr}}{(\theta\beta(\omega_{tc})+\frac{y}{4}\dot{n}_f)(\theta\beta(\omega_{tc})+\dot{n}_{egr})} \tag{C.32}$$

as g has negative sensitivity to θ we invert the sign of the parameter estimator (C.19) (as explained in [50]). The small inaccuracy of (C.9) is compensated by continuously estimating θ as a time-varying parameter. The inversion of $g(\theta,d,u)$ with respect to u is

$$h(\theta,d,r) = \frac{\theta\beta(\omega_{tc})\cdot(O_a-r)}{r-\frac{\theta\beta(\omega_{tc})\cdot O_a-\dot{n}_f\cdot\left(1+\frac{y}{4}\right)}{\theta\beta(\omega_{tc})+\frac{y}{4}\cdot\dot{n}_f}} \tag{C.33}$$

with $r < O_a$. In special cases the right side of Equation (C.33) is outside the actuator limits or even undefined. This is handled as follows

$$u = \begin{cases} h(\hat{\theta},d,r) & \text{if } h(\hat{\theta},d,r) \in [0;u_{max}[\\ u_{max} & \text{otherwise} \end{cases} \tag{C.34}$$

Such special cases relate to the invertibility of $g()$ w.r.t. $\dot{n}_{egr}$. The issue is illustrated in Figure C.7. With $\dot{n}_f$ and $\theta\beta(\omega_{tc})$ fixed, there are limits to how much $g()$ and thus O_{sr} can vary when $\dot{n}_{egr}$ is non-negative

$$g(\theta,d,0) = O_a \tag{C.35}$$

$$\lim_{u\to\infty} g(\theta,d,u) = O_a - \frac{(1+\frac{y}{4}(O_a+1))\dot{n}_f}{\theta\beta(\omega_{tc})+\frac{y}{4}\dot{n}_f} \tag{C.36}$$

A low EGR flow leads to a $g()$ close to O_a. Thus if r is close to O_a the result of the inversion in (C.33) is a low EGR flow setpoint u.

At the other end of the scale, a high EGR flow leads to a $g()$ close to the limit expressed by (C.36). If r is close to this limit but above, the inversion $h()$ results in a high EGR flow. If r is equal to the limit $h()$ is undefined and if r is below the limit, $h()$ is negative. For all three scenarios of a low r, the maximum EGR flow is the best option as it leads to the lowest O_{sr}. Note that even though the result of the inversion is

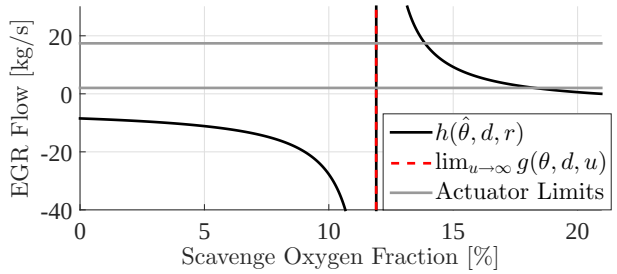

Figure C.7: This figure illustrates the result of inverting the scavenge oxygen model without considering physical limits. Below a certain limit the inverted model dictates a negative EGR flow in order to decrease the oxygen level further. This issue is handled by the controller.

beyond the actuator limits, the parameter estimator will converge as long as $\dot{n}_{egr} > 0$. The minimum EGR flow is positive as the EGR blower is not designed for running in zero or negative flow, but this is handled by the flow controller.

C.4.2 Sensitivity Bounds

The AFF controller presented in Section C.3 requires the functions g and h to fulfill the sensitivity bounds specified in Section C.3.1. With the definitions in (C.32) and (C.33), $g(\theta,d,u)$ and $g(\theta,d,h(\hat{\theta},d,r))$ are continuously differentiable w.r.t. θ and $\hat{\theta}$, respectively. Therefore the bounds can be expressed by (C.16) and (C.18). Partial differentiation leads to

$$\frac{\partial g(\theta,d,u)}{\partial \theta} = \left(1+\frac{y}{4}(O_a+1)\right)\frac{\dot{n}_f\dot{n}_{egr}\beta\left(2\beta+\frac{y}{4}\dot{n}_f+\dot{n}_{egr}\right)}{\left(\theta\beta+\frac{y}{4}\dot{n}_f\right)^2(\theta\beta+\dot{n}_{egr})^2} \tag{C.37}$$

and from the chain rule

$$\frac{\partial g(\theta,d,h(\hat{\theta},d,r))}{\partial \hat{\theta}} = \frac{\partial g(\theta,d,u)}{\partial u}\cdot\frac{\partial h(\hat{\theta},d,r)}{\partial \hat{\theta}} \tag{C.38}$$

where

$$\frac{\partial g(\theta,d,u)}{\partial u} = \frac{\dot{n}_f\left(\frac{y}{4}(O_a+1)+1\right)\theta\beta}{\left(\beta\theta+\frac{y}{4}\dot{n}_f\right)\left(\beta\theta+h(\hat{\theta},d,r)\right)^2} \tag{C.39}$$

and

$$\frac{\partial h(\hat{\theta},d,r)}{\partial \hat{\theta}} = \frac{(r-O_a)\beta\left((r+1)\left(\frac{y}{4}\right)^2+\frac{y}{4}\right)\dot{n}_f^2}{\left(\left(1+(r+1)\frac{y}{4}\right)\dot{n}_f+\hat{\theta}\beta(r-O_a)\right)^2} + \frac{(r-O_a)\left(2\hat{\theta}\beta^2\left(1+(r+1)\frac{y}{4}\right)\dot{n}_f+\hat{\theta}^2\beta^3(r-O_a)\right)}{\left(\left(1+(r+1)\frac{y}{4}\right)\dot{n}_f+\hat{\theta}\beta(r-O_a)\right)^2} \tag{C.40}$$

Unfortunately it is difficult to determine strict limits of γ, ρ and μ due the complex couplings between the variables which appear in (C.37), (C.39) and (C.40). Conservative guesses can be achieved by defining independent intervals for $\dot{n}_f$, $\dot{n}_{egr}$, β, θ and $\hat{\theta}$ and then evaluating the extremes of (C.37) and (C.38). For the engine test bed this results in limits of the order $\gamma = 1.6\cdot10^{-5}\frac{s}{mol}$, $\rho = 2.3\cdot10^{-3}\frac{s}{mol}$ and $\mu = 7\cdot10^{-4}\frac{s}{mol}$.

This value of γ results in a minimum convergence rate of about $1.6\cdot10^{-3}\frac{1}{s}$ if a typical observer gain of $k = 100\frac{mol}{s^2}$ is used. This corresponds to a time constant of about 10 minutes. Thus, even though exponential stability is guaranteed, the convergence is not guaranteed to be fast.

Further insight into the consequences of this issue can be gained by considering the scenarios in which the sensitivity of (C.37) is low. $\frac{\partial g}{\partial \theta}$ reaches its minimum when TC speed is high and fuel flow and EGR flow are low, simultaneously. This can only occur in a fast loading down scenario where the TC speed drops slower than the fuel flow due to the inertia of the rotor and the sensitivity will increase as fast as the TC speed drops. However, in a loading down scenario the response of the AFF controller is to increase the EGR flow, even if $\hat{\theta}$ has not fully converged. The end result is that even though the analytically derived minimum bound of the convergence rate is low, the expected convergence is better. This is also observed in the simulations and experiments in Section C.5.

C.5 Results

The new EGR controller is now validated with an increasing level of realism. At first, closed loop simulation against the COM verifies the convergence properties. Then closed loop simulation against the MVEM to verify robustness toward the simplifications from MVEM to COM. Experimental validation is carried out first on an engine test bed connected to a water brake and finally on a vessel during operation at sea.

C.5.1 Simulation

The models and controllers are implemented and simulated in Matlab Simulink. Dynamic simulation of pressure in the volumes that are small relative to the flow can be difficult for the solver, but Simulink's

implicit ode15s solver is able to simulate the closed loop of the MVEM and AFF EGR controller at more than 80x real time on a standard PC.

C.5.1.1 Simulation with COM

In order to verify the convergence properties proven in Section C.3 the closed loop setup shown in Figure C.6 is simulated with g and h defined by (C.32) and (C.12), respectively, and the parameters shown in Table C.1.

Table C.1: Parameters for closed loop COM simulation

k	100	$[\frac{mol}{s^2}]$	θ	120-125	$[\frac{mol}{s}]$
Δt	10	$[s]$	$\hat{\theta}_0$	120	$[\frac{mol}{s}]$
O_a	20.95	$[\%]$	ϕ	0.54	$[-]$
y	1.78	$[-]$	τ	10	$[s]$

Results from such a simulation are shown in Figure C.8. The convergence bounds are demonstrated with a step of the parameter θ. Notice that the parameter estimate starts converging 10 seconds after the step due to the delay. The scavenge oxygen fraction reaches its setpoint again after about 50-100 seconds after the step. Thus the simulated performance is satisfying whereas the convergence bounds are quite conservative. The AFF controller has the property that if $\theta(t)$ is constant, then $\kappa = 0$ and both parameter error and control error converges to zero. In Figure C.8, θ is constant after 50 seconds and thus the errors converge to zero. These bound are illustrated in Figure C.8.

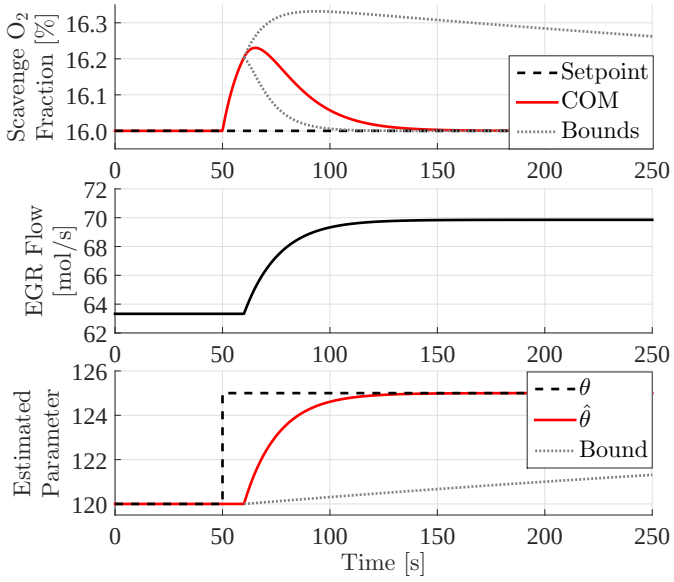

Figure C.8: Closed loop simulation of the control oriented EGR model with AFF controller. The scenario is a step in the parameter θ. The scavenge O_2 fraction converges rapidly but the guaranteed bounds converge slowly.

C.5.1.2 Simulation with MVEM

Simulation with the COM is able to verify the convergence properties proven in the control concept, but simulation with the MVEM is needed to investigate whether the controller is robust toward the assumptions and simplifications made to reduce the MVEM to the COM. This includes the inner loop with EGR flow

control, intercooler flow estimation, cylinder bypass valve and the more complex dynamics included in the MVEM. Furthermore, the MVEM is used for comparison to a PI controller (the reference EGR controller).

The first scenario is load steps with fixed CBV. Engine load is changed in steps as 43-69-100-69-43%. Figure C.9 shows the results. The AFF controller outperforms the PI controller significantly. In the second and third step (highest load) the AFF controller overcompensates due to the simplification of the intercooler flow estimate. The simulated θ changes abruptly at each step and then converges to a steady value. The estimate $\hat{\theta}$ converges to the new steady θ value as after every step.

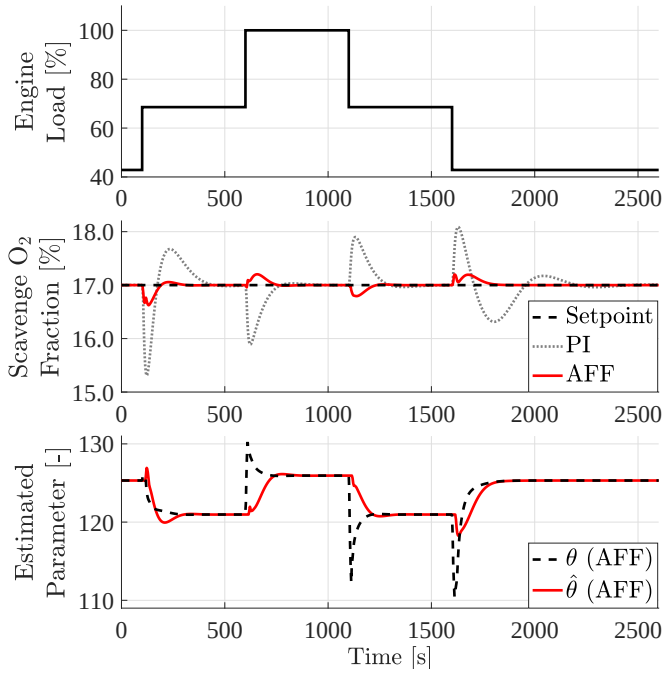

Figure C.9: Comparison of engine load steps with respectively PI and AFF controller, simulated with the MVEM.

The second scenario is CBV opening steps at 69% engine load. Changes in the CBV opening is not included in the cooler flow estimation and is therefore not compensated directly by the feedforward part of the AFF. Instead the parameter estimator has to adapt $\hat{\theta}$ in order to compensate for the steps. The initial responses of the two controllers are similar but the AFF controller converges faster to the setpoint again. The simulated θ now changes even more at each step than in the previous simulation. The estimate $\hat{\theta}$ still converges to the new steady θ value as after every step.

In all simulations $\theta(t)$ is practically constant between the steps. Thus the control error converges to zero between the steps.

C.5.2 Experimental validation

The AFF EGR controller has been implemented as an option in a test version of the MDT EGR control software. This facilitates experimental validation of the design, first in an engine test bed and then on a vessel operating at sea.

C.5.2.1 Experiments on Engine Test Bed

The MVEM and the COM are based on the 4T50ME-X test engine located in the MDT Diesel Research Center in Copenhagen. The engine is fitted to a water brake where the engine load can be adjusted to fit the propeller curve.

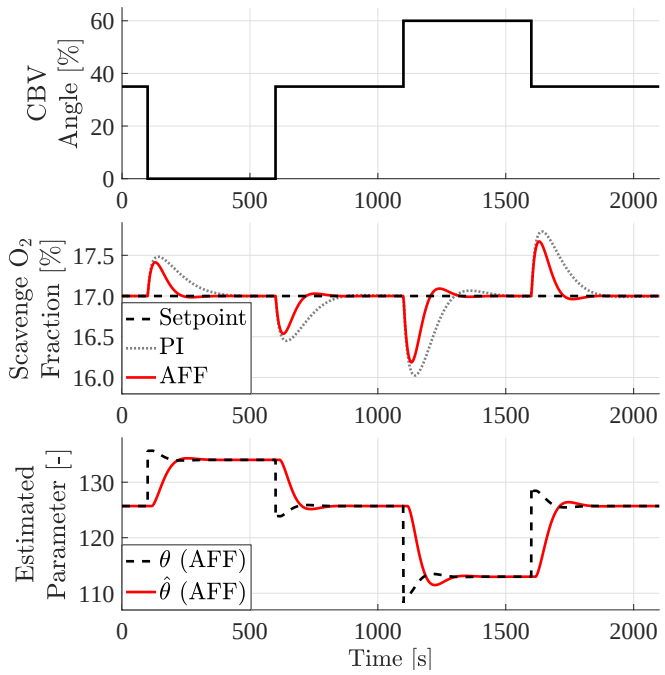

Figure C.10: Comparison of CBV opening steps with PI and AFF EGR controller, respectively, simulated with the MVEM.

In order to compare the AFF EGR controller to the reference PI controller, the two are subjected to similar engine load ramps from 26% to 42% in 80 seconds (Figure C.11). The scavenge oxygen measurement clearly shows the difference in performance. With the PI controller O_{sr} drops from 16.5% to below 15.9% whereas the nonlinear controller only lets O_{sr} drop to 16.4%. The test bed includes an opacity sensor in the chimney. The standard of the facility is that the opacity should remain below 12% and that opacity above 20% is critical. During test the normal level of opacity was 4%. With the PI controller the opacity peaked at 16% during the transient, whereas the AFF peaked at only 8% opacity. These tests showed a great performance improvement from PI to AFF controller. As there are no measurements of the scavenge cooler flow it is not possible to calculate a reliable "true" θ value in this case. It is, however, observed that the estimate $\hat{\theta}$ changes somewhat after the step but otherwise remains within a small interval, as predicted by models and simulations.

C.5.2.2 Experiments on Vessel

To validate the AFF controller further it was tested on the container vessel Maersk Cardiff (with a 6S80ME-C9.2 engine) during operation at sea. A comparison between the two controllers where made, similar to the validation on the engine test bed. However, as the vessel engine drives a propeller rather than a water brake, the load transient scenario is an engine RPM setpoint step instead of a load ramp. The result is seen in Figure C.12. The engine accelerates slightly faster with the AFF controller because the faster decrease of EGR flow results in a faster increase of scavenge pressure and thus a looser fuel index limiter. Another improvement is seen in the measurements of O_{sr}. With the PI controller it drops from 16.1% to below 13% during the transient. The AFF controller manages to keep O_{sr} above 15.9%. The difference is also seen in the opacity measurements which is fully saturated at 100% for 30 seconds with the PI controller whereas it peaks at 91% with the AFF and then drops rapidly again. Note that conditions for opacity measurement son the vessel are not comparable to the conditions on the engine test bed so the absolute values should not be directly compared. The parameter estimate $\hat{\theta}$ increases during the

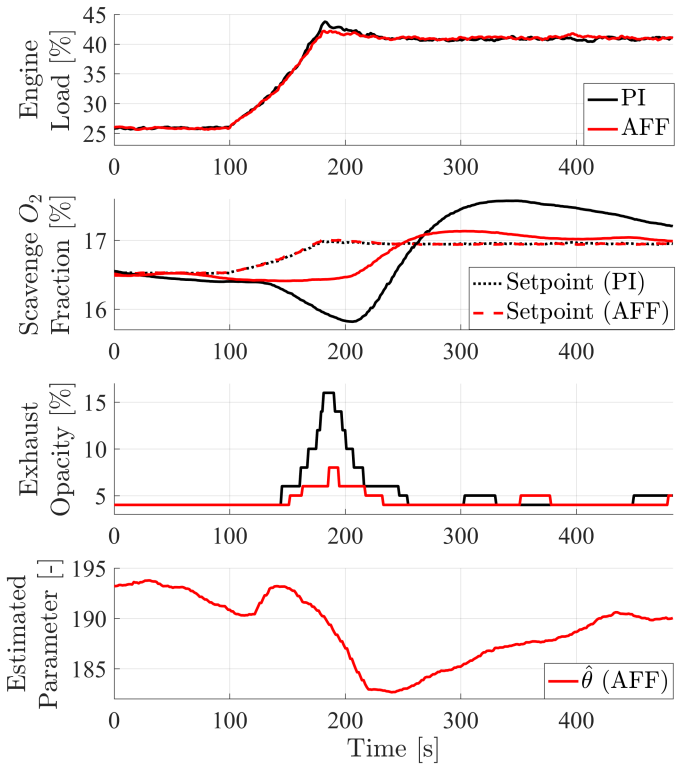

Figure C.11: Comparison of similar engine load ramps with PI and AFF EGR controller, respectively, at engine test bed. A significant difference in scavenge oxygen fraction and exhaust opacity is observed, showing superior performance of the AFF over the reference controller.

acceleration and then decreases to a steady value that is lower than before the step. These variations can be explained by the large decrease of EGR rate during acceleration and the auxiliary blowers which turn of at the final high load. As the actual flow through the scavenge cooler was not measured it is not possible to calculate a "true" θ for comparison.

The exhaust was filmed with a video camera during the transients. Figures C.13 and C.14 show stills from the videos. Thick black smoke was emitted for about 45 seconds in the PI case, whereas a much lighter smoke was emitted for about 20 seconds with the AFF.

Figure C.15 shows a comparison of the steady state behavior of the controllers. The engine is running at ∼10.5% load. An oscillation of 0.3% load occurs with a period of 5 minutes. With the PI controller this load disturbance leads to an oscillation in O_{sr} of 0.08%. The AFF keeps it within 0.03% of the setpoint. If the EGR blower RPM is kept fixed O_{sr} oscillates with amplitude 0.04%. The AFF is seen to change the EGR blower speed faster than the PI in this scenario.

C.6 Conclusions

In this paper an adaptive feedforward controller design was generalized for a class of first order Hammerstein systems and exponential convergence bounds of the control error and a parameter estimate was analytically proven.

Furthermore the concept was applied to control the EGR system of a large two-stroke marine diesel engine. The AFF EGR controller was validated by closed loop simulation with an MVEM model and experiments on an engine test bed and on a vessel operating at sea. The validation showed the AFF controller to be a significant improvement compared to a PI controller in scenarios with large loading

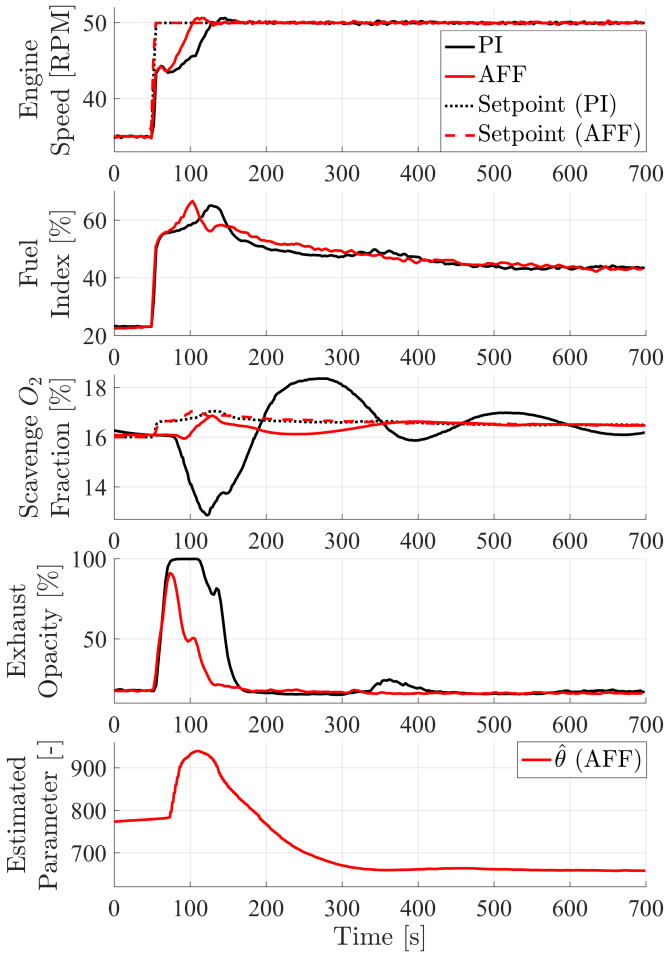

Figure C.12: Comparison of similar engine RPM setpoint step-responses with PI and AFF EGR controller, respectively, on the vessel Maersk Cardiff. A significant difference in scavenge oxygen fraction and exhaust opacity is observed, showing superior performance of the AFF over the reference controller.

transients. Both opacity measurements and visual inspection showed a significant reduction of smoke formation during said transients. In a constant engine speed setpoint scenario the AFF controller also outperformed the PI, with better rejection of the disturbance from load oscillations.

The AFF controller concept enables use of the EGR system during maneuvering, without damaging the engine with soot formation and without violating legislation regarding visible smoke emission.

Acknowledgment

This work was partially funded by the Danish Agency for Science, Technology and Innovation, grant number 1355-00071B.

Figure C.13: Exhaust smoke level with PI controller during engine speed step. Thick black smoke is emitted for 45 seconds.

Figure C.14: Exhaust smoke level with adaptive feedforward controller during engine speed step. Gray smoke is emitted for 20 seconds.

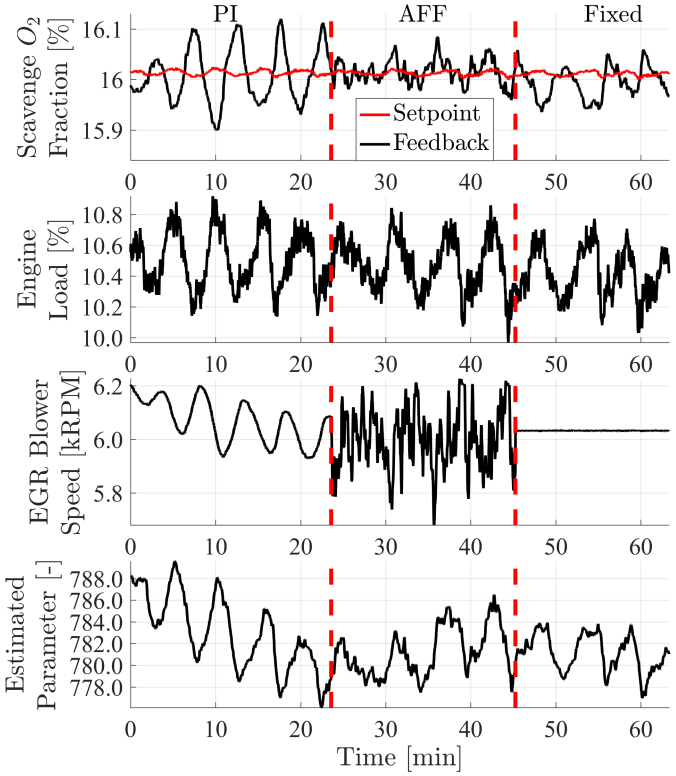

Figure C.15: Comparison of existing PI controller, nonlinear controller and fixed EGR blower speed at close to steady state conditions. A small load oscillation is propagated to the scavenge oxygen level.

Paper D

Diesel Engine Control System to meet Strict Emission Requirements while Maintaining Full Ship Manoeuvring Capability

Kræn Vodder Nielsen[*1,2], Mogens Blanke[2,3], Lars Eriksson[4], Morten Vejlgaard-Laursen[1]

[1] MAN Diesel & Turbo, Teglholmsgade 41, 2450 København SV, Denmark [2]Department of Electrical Engineering, Automation and Control Group, Technical University of Denmark, Elektrovej Building 326, 2800, Kgs. Lyngby, Denmark

[3]AMOS CoE, Institute of Technical Cybernetics, Norwegian University of Science and Technology, 7491 Trondheim, Norway

[4]Vehicular Systems, Department of Electrical Engineering, Linköping University, 58183 Linköping, Sweden

Abstract:
Recent restrictions of NO_x emissions from marine vessels have led to the development of exhaust gas recirculation (EGR) for large two-stroke diesel engines. Meanwhile, the same engines have been downsized and derated to optimize fuel efficiency. The smaller engines reduce the possible vessel acceleration, and to counteract this, the engine controller must be improved to fully utilize the physical potential of the engine.

A fuel index limiter based on air/fuel ratio has recently been developed; unfortunately it does not apply to engines with EGR. This paper presents two methods for extending this limiter to be based on oxygen/fuel ratio which is appropriate for EGR engines. The methods are validated through simulations with a mean-value engine model and on a vessel operating at sea. Validations are performed for combinations of the two methods with both traditional proportional-integral EGR control and with the new faster adaptive feedforward EGR control. The experiments show that the extended limiters reduce exhaust smoke formation during acceleration to a minimum, and when combined with adaptive feedforward EGR control, the engine acceleration capability is maintained. During an engine speed step from 35 to 50 RPM, the peak exhaust opacity only increased 5 percentage points when using the proposed limiter, whereas it increased 70 percentage points without the limiter.

K. V. Nielsen, M. Blanke, L. Eriksson, and M. Vejlgaard-Laursen. "Diesel Engine Control System to meet Strict Emission Requirements while Maintaining Full Ship Manoeuvring Capability". *Applied Energy* (2016). Submitted

[*]Principal corresponding author. Tel.: +45 33851909; E-mail: kraenv.nielsen@man.eu

D.1 Introduction

Nitrogen oxide (NO_x) emissions from combustion engines harm the environment and human health because these emissions contribute to the formation of smog, acid rain and tropospheric ozone. Increasingly strict emission limits have been adopted by the United Nations agency International Maritime Organization (IMO), which have thus far culminated in the Tier III standard [2]. This standard restricts NO_x emissions from slow-speed two-stroke crosshead diesel engines to 3.4 g/kWh. This emissions limit corresponds to a four-fold reduction compared to the earlier Tier II standard. This restriction applies to vessels constructed after the 1st of January 2016 when entering designated NO_x emission control areas (NECAs). Currently (2016), the US and Canadian coasts, Puerto Rico and the US Virgin Islands are NECAs. The North and Baltic Seas will be established as NECAs beginning in 2021. This factor of four reduction in emissions requires new approaches to engine design. Several methods are being developed and introduced to the market. This paper focuses on the control of large two-stroke diesel engines with high-pressure EGR.

The main source of NO_x from a large two-stroke diesel engine is thermal NO_x, which is formed during combustion where high peak temperatures lead to thermal formation of NO_x, e.g. modeled using the Zeldovich mechanism[11]. An EGR system reduces the peak combustion temperature by recirculating exhaust gas to increase heat capacity and decrease oxygen availability in the combustion chamber. Figure D.1 shows the components of the main gas flow in a diesel engine with high-pressure EGR developed by MAN Diesel & Turbo. Intake air is compressed and cooled prior to entering the cylinder. Part of the hot exhaust gas is cleaned and cooled by the EGR unit, pressurized by the EGR blower and reintroduced to the scavenge receiver. The remaining part drives the turbocharger. The EGR blower speed is controlled by an EGR control system that seeks to reach a load-dependent setpoint for the oxygen fraction in the scavenge receiver [49].

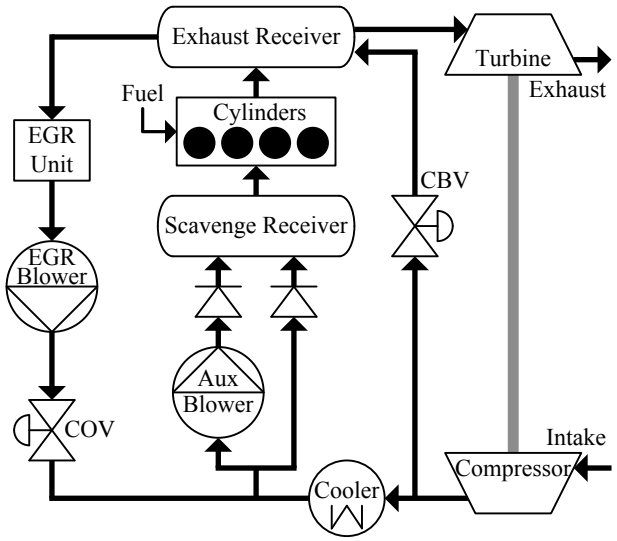

Figure D.1: Overview of main gas flows and components of a large two-stroke diesel engine with high-pressure exhaust gas recirculation and cylinder by-pass valve.

In addition to reducing emissions, increased awareness of fuel efficiency has led to downsizing and derating of large two-stroke engines. The smaller engines are efficient in steady-state scenarios, but the decreased power availability makes the vessels less maneuverable. At low loads the engine performance is limited by the "turbo-lag" phenomenon, in which an increase in exhaust energy due to increased fuel input must accelerate the turbocharger before more oxygen is available in the combustion chamber to react with a larger amount of fuel. An excess of fuel leads to the formation of black smoke, which is damaging

to the engine, a waste of fuel and prohibited by legislative authorities. Traditionally, this is avoided by implementing a fuel index limiter in the governor based on a fixed function of scavenge pressure. The fuel index indicates the amount of fuel injected per combustion event. Basing the limit solely on the scavenge pressure tends to result in a rather conservative estimate. Therefore, a new fuel index limiter has been developed that is based on a more advanced estimate of the air/fuel ratio.

Recirculation of exhaust gases decreases the oxygen fraction in the scavenge air; therefore, the standard fuel index limiters based on either scavenge pressure or air/fuel ratio do not apply to this configuration. Using such limiters during large accelerations leads to excessive smoke formation since some oxygen in the scavenge flow is replaced by burned gases. In early EGR engines with slow EGR controllers, the scavenge oxygen level would actually decrease during acceleration, but recent developments of fast controllers have solved this issue. Nevertheless, even with the fastest EGR controller, there is still a limit to how fast more fuel can be burned due to the turbocharger dynamics. In this paper, the limit is calculated based on the oxygen/fuel ratio in order to maximize maneuverability while guaranteeing smoke-free acceleration.

D.1.1 Literature

Combustion engine processes and modeling are extensively treated in [11, 12, 14]. The literature on the control of large two-stroke engines primarily addresses engine speed controllers (governors), as reported in [4, 31, 32, 57, 58]. Modeling of the engine speed in response to fuel index showed that the turbocharger dynamics had a significant effect [28, 29, 30]. The first NO_x emission limits led to the use of variable geometry turbochargers, which required better control schemes to avoid smoke generation during loading transients [33]. Advanced injection timing has also been shown to decrease the formation of NO_x [85]. Mean-value modeling of a modern two-stroke engine without EGR was reported by [34] and this model was used for several investigations in [36, 37, 38, 59]. A combustion model that showed the NO_x reduction potential of EGR was published in [86].

Fuel index limiters have not received considerable attention in the literature. This subject was briefly mentioned in [4]. A new air/fuel ratio limiter was presented in [87] and [39].

A number of papers on the control of EGR on large two-stroke engines have been published, starting with [43], where a mean-value model of a large two-stroke engine with high-pressure EGR was developed. Achievable EGR control performance with SISO design was investigated in [44] based on a linearization of the MVEM. An extended and improved version of the model was reported in [45] where the parameterization method was alsorevised. The authors of the present paper first proposed a simplified scavenge oxygen model and nonlinear adaptive EGR controller in [53]. A control-oriented scavenge oxygen model was analytically derived from the MVEM model in [49], and a joint state and parameter estimator for this model was presented in [50] along with a proof of exponential convergence. An adaptive feedforward EGR controller based on an inversion of the control-oriented oxygen model was presented in [51] along with convergence proofs and results from a seatrial that showed significant improvement compared to a PI controller.

EGR control for four-stroke automotive engines is more common in the literature [15, 18, 19, 20, 21, 60, 61] compared to marine two-stroke engines. These approaches cannot be directly transferred due to the differences in engine airflow setup and scavenging in 2-stroke and 4-stroke engines, system time constants, sensor setup, control objective and engine test bed availability [4, 86].

D.1.2 Contributions

The main contributions of the present paper are as follows

1. Two methods are proposed that extend an existing fuel index limiter to engines with EGR systems.

2. The methods are validated in a simulation with a high-fidelity mean-value engine model and on a vessel operating at sea. Several combinations of limiters and EGR controllers are compared.

The engine control system proposed herein optimizes vessel maneuverability without smoke formation when using diesel engines with EGR as a prime mover. This enables the application of EGR on downsized engines for improved fuel efficiency while complying with the new Tier III NO_x emission restrictions.

D.1.3 Outline of this Paper

Section D.2 introduces the traditional and recent versions of fuel index limiters and explains why they do not apply to engines with exhaust gas recirculation. Section D.3 briefly summarizes the dynamical models of the engine and EGR system that we later use for the simulation and control design. Section D.4 presents the two novel methods of how the air/fuel limiter can be extended to apply to engines with EGR. Both methods are validated through simulations and a sea trial in Section D.5.

D.2 Speed Governor with Fuel Index Limiters

The purpose of a diesel engine governor is to control the engine speed to a specified setpoint using feedback from a measurement of engine speed and actuation via the fuel index. This is similar to cruise control in an automobile. Governors have evolved from the fly-weight speed governor employed by James Watt for reciprocating steam engines to complex mechanical governors with both proportional, integral and derivative control functions and finally to the modern electronic governors, where even more advanced control methods are implemented in software. A basic function is still a feedback controller designed from knowledge of the dynamic behavior from fuel index to engine speed near steady state.

During load transients, the engine can reach unwanted combinations of states and input that the main feedback design does not take into account. Artificial actuator saturation is therefore implemented in the governor software. This is referred to as a fuel index limiter. The setup is shown in Figure D.2.

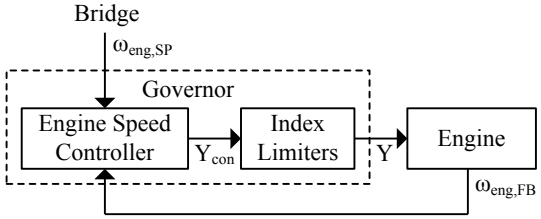

Figure D.2: An engine speed setpoint is set by the bridge. The index limiters ensure that the output from the engine speed controller does not make the engine reach unwanted regions of operation (to limit, e.g., smoke formation and shaft stress).

The possible combinations of engine speed and produced power are restricted by such a limiter. If the engine power is increased too fast compared to the resulting increase in engine speed, then the specified shafting system bearing strength is exceeded. Therefore, a torque-based limiter is applied to the fuel index. This is generally the most restrictive limiter at high loads, where power and torque are high.

At low loads, the achieved torques are lower and instead the availability of oxygen during combustion becomes critical. Part of the energy released from the fuel during combustion drives the turbocharger. If the fuel index is increased too fast compared to the resulting increase in turbocharger speed (and thus the scavenge/boost pressure), then there is not sufficient oxygen for the complete combustion of fuel. This situation is traditionally avoided by applying a fuel index limit based on scavenge pressure (scavenge pressure limiter). However, although the amount of trapped air is related to the scavenge pressure, other

factors can change the relationship, particularly during transients. Combined with little to no tuning for the specific engine, the scavenge pressure limiter ends up being conservative.

IMO's introduction of restrictions on the energy efficiency design index (EEDI) [88] has led to downsizing and derating of ship engines to optimize fuel efficiency [39]. Consequently, this has decreased the acceleration capability of the affected ships. To compensate, MAN Diesel & Turbo has introduced a software upgrade to their engine controllers referred to as Dynamic Limiter Function (DLF) [39]. The purpose of this upgrade is to allow the engine controller to optimize specifically for acceleration when needed. This is achieved by changing the exhaust valve timing and by replacing the scavenge pressure limiter with a more precise fuel index limiter based on the trapped air mass in the combustion chamber.

A fuel index limiter based on trapped air mass can be derived by specifying a limit to the air/fuel ratio (λ_A) of the combustion process, which is defined as

$$\lambda_A = \frac{m_{trap}}{m_f} = \frac{m_{trap}}{k_{fm} Y} \tag{D.1}$$

where m_{trap} denotes the mass of gas trapped in the cylinder and m_f is the mass of fuel. The latter is proportional to fuel index Y. If the limit of the air/fuel ratio is denoted as λ_{LA}, then we can solve (D.1) for the limit to the fuel index

$$Y_{LA} = \frac{m_{trap}}{k_{fm} \lambda_{LA}} \tag{D.2}$$

DLF with the Y_{LA} limiter has been proven on a number of vessels. It allows for faster acceleration without smoke formation. However, it does not apply to engines with exhaust gas recirculation. An underlying assumption of Y_{LA} is that the scavenge air has a constant oxygen fraction equal to that of ambient air. When EGR is applied the scavenge oxygen fraction is decreased from 21% to 16-18% and smoke formation can occur even though the $\frac{m_{trap}}{m_f}$ ratio is within the specified limit. Figure D.3 shows an example.

Figure D.3: Exhaust smoke on a vessel with DLF and EGR during engine speed step. Thick black smoke is emitted for 45 seconds. In this test, the Y_{LA} limiter was used in combination with PI EGR control.

D.3 EGR System Models

This section first presents the dynamic model used to simulate the effect of EGR on the gas composition and flows in a large two-stroke diesel engine. Second, a control-oriented model of the molar scavenge oxygen fraction used for control design is presented. Finally, two generations of EGR controllers are introduced.

D.3.1 Mean-Value Engine Model

The dynamic simulation model used here was presented in [49]. It is a filling and emptying model with a mean-value assumption for the flow through the cylinders. It represents the 4T50ME-X engine located in MDT's Diesel Research Center in Copenhagen. An overview of the modeled components is presented in Figure D.4. The model has four pressure states, a turbocharger speed state and six gas composition states. In this paper we only use the two oxygen fraction states rather than all six gas compositions.

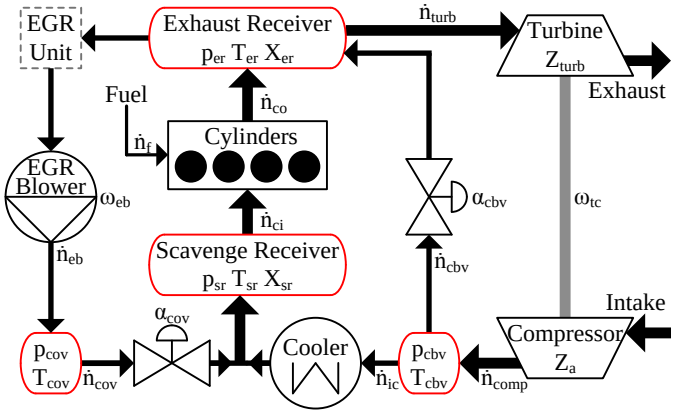

Figure D.4: Overview of gas flows and components modeled in the mean-value engine model.

Absolute pressures in the volumes marked in red in Figure D.4 are modeled isothermally as

$$\dot{p}_i = \frac{RT_i}{V_i}\left(\dot{n}_{in} - \dot{n}_{out}\right) \tag{D.3}$$

where $\dot{n}_i$ indicates molar gas flow. Turbocharger speed is modeled based on the turbine power P_{turb}, compressor power P_{comp} and turbocharger moment of inertia J_{tc}

$$\dot{\omega}_{tc} = \frac{P_{turb} - P_{comp}}{J_{tc}\omega_{tc}}, \tag{D.4}$$

The molar gas composition fractions of the receivers are calculated based on the input flow and composition and the receiver pressure. The dynamic equation for the oxygen fractions in the volumes is

$$\dot{O}_i = \frac{RT_i}{p_i V_i}\sum_{input=j}\dot{n}_j\left(O_j - O_i\right) \tag{D.5}$$

Gas flows through the components between volumes are calculated from the input and output pressures of the component and in some cases an additional input ε (e.g. valve opening or turbocharger speed).

$$\dot{n}_i = f(p_{in}, p_{out}, \varepsilon) \tag{D.6}$$

In the cylinder component, the following lean combustion reaction is assumed

$$CH_y + \left(1 + \frac{y}{4}\right)O_2 \rightarrow CO_2 + \frac{y}{2}H_2O \tag{D.7}$$

Here, the virtual fuel molecule CH_y is used, where y is the average ratio of hydrogen atoms to carbon atoms in the fuel. From (D.7), the oxygen fraction of the flow exiting the cylinders is calculated as

$$O_{co} = \frac{\dot{n}_{ci}O_{sr} - \dot{n}_f\left(1 + \frac{y}{4}\right)}{\dot{n}_{ci} + \frac{y}{4}\dot{n}_f}, \tag{D.8}$$

The temperature of this flow is modeled on a modified limited-pressure diesel cycle. Details on this calculation were presented in [45].

A simple model of crankshaft speed is adapted from [30]. The dynamic equation is

$$\dot{\omega}_c = \frac{P_{ind} - P_{fric} - P_{prop}}{J_c \omega_c} \tag{D.9}$$

where P_{ind} is indicated power, P_{fric} is internal friction power, P_{prop} is power delivered to the propeller and J_c is the moment of inertia of the crankshaft-propeller system. To estimate the indicated power, the molar fuel flow $\dot{n}_f$ is calculated as being proportional to the product of engine speed and fuel index

$$\dot{n}_f = k_f \omega_c Y \tag{D.10}$$

The indicated power is determined from the heat of combustion of fuel per unit mass (k_{hc}) and thermal efficiency η

$$P_{ind} = k_{hc} \dot{m}_f \eta = k_{hc} M_f k_f Y \omega_c \eta \tag{D.11}$$

where M_f is the molar mass of the virtual fuel molecule CH_y. Friction power is proportional to crankshaft speed

$$P_{fric} = k_{fric} \omega_c \tag{D.12}$$

The power delivered to the turbine is modeled with a constant propeller curve. Changes in ship speed are not modeled because these dynamics are assumed to be too slow to affect the limiters

$$P_{prop} = k_{prop} \omega_c^3 \tag{D.13}$$

The state vector of the full model is

$$x = \begin{bmatrix} p_{sr} & p_{er} & p_{cbv} & p_{cov} & \omega_{tc} & \omega_c & O_{sr} & O_{sr} \end{bmatrix}^T \tag{D.14}$$

The dynamic model is expressed in state space form as

$$\dot{x} = f(x, Y, \omega_{eb}, \alpha_{cov}) \tag{D.15}$$

The MVEM model is designed for the 50-100% load range. It therefore does not include the auxiliary blower shown in Figure D.1. This is unfortunate for the use in this paper because hard accelerations with smoke formation normally occur in the 5-50% range. However, most of the engine behavior is similar throughout the load range; therefore, the model is still used for validation here.

D.3.2 Control-Oriented Scavenge Oxygen Model

The AFF EGR controller presented in [51] and one of the extensions presented in this paper are based on a control-oriented model (COM) of the molar scavenge oxygen fraction that was presented in [49]. The COM is a first-order Hammerstein model with three molar flows as input

$$\tau \dot{O}_{sr} = -O_{sr} + g(\dot{n}_f, \dot{n}_{ic}, \dot{n}_{egr}) \tag{D.16}$$

In addition to the three flows, the input nonlinearity includes two parameters

$$g(\dot{n}_f, \dot{n}_{ic}, \dot{n}_{egr}) = O_a - \frac{(1 + \frac{y}{4}(O_a + 1))\dot{n}_f \dot{n}_{egr}}{(\dot{n}_{ic} + \frac{y}{4}\dot{n}_f)(\dot{n}_{ic} + \dot{n}_{egr})} \tag{D.17}$$

O_a is the ambient oxygen fraction, and y is the fuel constant also used in the MVEM. The flows are as shown in Figure D.4. The fuel flow $\dot{n}_f$ is found from (D.10). The EGR flow $\dot{n}_{egr} \approx \dot{n}_{eb}$ is calculated from the input and output pressures and blower speed using a blower map provided by the manufacturer of the EGR blower. The cooler flow is approximated based on the turbocharger speed as

$$\dot{n}_{ic} = \theta \cdot \beta(\omega_{tc}), \quad \beta(\omega_{tc}) = (1 - \phi)\omega_{tc} + \phi \omega_{tc}^2 \tag{D.18}$$

where the parameter θ can be found using the nonlinear parameter estimator presented in [50].

D.3.3 EGR Controllers

The extended limiters have to work in parallel with the EGR controller, and significant couplings between the two are expected. The goal of the EGR controller is to make the scavenge oxygen fraction reach a load-dependent setpoint by varying the EGR blower speed and the COV opening angle. Two generations of EGR controllers are used in this work. These controllers were compared in [51] without extensions to the index limiter. The first generation is the proportional-integral (PI) EGR controller that struggles during transients due to the slow process and sensors dynamics. The well-known simple structure of the controller is illustrated in Figure D.5.

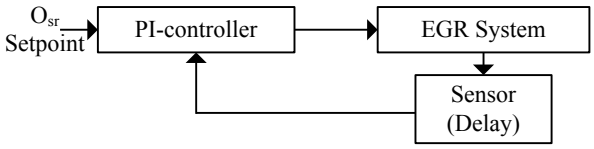

Figure D.5: The PI EGR controller is a simple and well-known approach to regulate the scavenge oxygen fraction to its setpoint. The sensor and process dynamics make it vulnerable to engine load transients.

The second generation is the adaptive feedforward (AFF) EGR controller. The structure of this controller is shown in Figure D.6. The AFF is based on an inversion of the input nonlinearity of the COM and a parameter estimator that ensures convergence of the measured scavenge oxygen error. Exponential convergence was proven in [51]. The AFF utilizes the known fuel flow and turbocharger speed in the inverted model and therefore reacts rapidly to load transients.

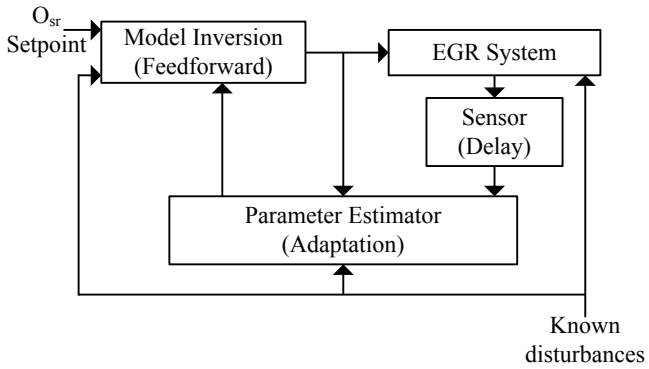

Figure D.6: The adaptive feedforward EGR controller allows for rapid reactions to load changes. A parameter estimator ensures convergence of the controller error.

Although the AFF outperforms the PI in loading transients, it also makes the control software more complex and less intuitive. The combination of a PI EGR controller with a simple extension of the fuel index limiter might be the preferable solution, depending on the performance.

D.4 EGR Fuel Index Limiters

The Y_{LA} limiter does not apply to engines with EGR, because the assumption of a constant scavenge oxygen fraction is violated. This section presents two methods for extending the limiter to represent an oxygen/fuel limiter rather than an air/fuel limiter. The concept of an oxygen/fuel limiter is explained first.

D.4.1 Oxygen Fuel Limiter

On an engine without EGR, the limit to the air/fuel ratio ensures that sufficient oxygen is available for combustion of the fuel. Without EGR, the scavenge air has a constant oxygen fraction equal to that of the ambient air. Therefore, it does not matter whether the limit is specified as air/fuel or oxygen/fuel. With EGR, the scavenge oxygen fraction varies, and therefore, it is necessary to limit the oxygen/fuel ratio λ_O rather than the air/fuel ratio λ_A. The oxygen/fuel ratio is defined as

$$\lambda_O = \frac{m_{O,trap}}{m_f} = \frac{n_{O_2,trap} M_{O_2} N}{k_f Y M_f} \tag{D.19}$$

where $m_{O_2,trap}$ is the mass of oxygen trapped in the cylinder, M_{O_2} is the molar mass of O_2, N is the number of cylinders, and (D.10) is used to substitute molar fuel flow. Using the molar scavenge oxygen fraction O_{sr}, we can rewrite the equation as

$$\lambda_O = \frac{n_{trap} O_{sr} M_{O_2} N}{k_f Y M_f} \tag{D.20}$$

Converting back to the mass of trapped gas rather than moles, the air/fuel ratio appears as

$$\lambda_O = \frac{m_{trap} N}{k_f Y M_f} \cdot \frac{O_{sr} M_{O_2}}{M_{trap}} = \lambda_A \frac{O_{sr} M_{O_2}}{M_{trap}} \tag{D.21}$$

As shown above, the ratios scale with the scavenge oxygen fraction, but the additional constant $\frac{M_{O_2}}{M_{trap}}$ is necessary because we use a molar oxygen fraction to scale a mass-based ratio. This result can be used for rewriting the existing limit λ_{LA} to the oxygen/fuel ratio limit λ_{LO}

$$\lambda_{LO} = \lambda_{LA} \frac{O_a M_{O_2}}{M_{trap}} \tag{D.22}$$

Furthermore, from (D.21), we can express a fuel index limit based on oxygen/fuel ratio as

$$Y_{LO} = \frac{N m_{trap} O_{sr} M_{O_2}}{k_f \lambda_{LO} M_f M_{trap}} \tag{D.23}$$

Inserting the result from (D.22), we obtain

$$Y_{LO} = \frac{N m_{trap} O_{sr} M_{O_2}}{k_f \lambda_{LA} \frac{O_a M_{O_2}}{M_{trap}} M_f M_{trap}} = \frac{N m_{trap} O_{sr}}{k_f \lambda_{LA} M_f O_a} \tag{D.24}$$

From (D.2) and (D.10) we obtain

$$\lambda_{LA} = \frac{N m_{trap}}{k_f M_f Y_{LA}} \tag{D.25}$$

We now insert this into (D.24) to derive a simple method of extending Y_{LA} to Y_{LO}

$$Y_{LO} = \frac{N m_{trap} O_{sr}}{k_f \frac{N m_{trap}}{k_f M_f Y_{LA}} M_f O_a} = Y_{LA} \frac{O_{sr}}{O_a} \tag{D.26}$$

This result shows that the existing air/fuel ratio limiter Y_{LA} (that assumes no EGR) can be converted to an oxygen/fuel ratio limiter Y_{LO} by scaling with the instantaneous value of $\frac{O_{sr}}{O_a}$. This makes intuitive sense because $\frac{O_{sr}}{O_a}$ is the ratio of available oxygen compared to "no-EGR" conditions.

D.4.2 Y_{LOS} - Oxygen/Fuel Limiter based on O_2-Sensor

The first method of extending the air/fuel limiter to an oxygen/fuel ratio is to use the output of the oxygen sensor mounted in the scavenge receiver

$$Y_{LOS} = Y_{LA} \cdot \frac{O_{sr,sens}}{O_a} \tag{D.27}$$

This is a simple and intuitive method of converting the limiter. However, it has two possible drawbacks. First, it relies on the scavenge oxygen sensor which is known to have a time delay of 10-20 seconds and a first-order filtering effect with a time constant in the same range. Therefore, if the scavenge oxygen content changes during acceleration, the limiter conversion will be inaccurate. Second, an increase in the fuel index will lead to a decrease in the scavenge oxygen fraction, until the EGR controller has compensated by lowering the EGR rate. The O_{sr} decrease negatively affects the index limiter. Thus, a negative loop from fuel index through scavenge oxygen back to fuel index has been created. Combined with the sensor and process dynamics, such a loop could possibly lead to degradation of acceleration performance and, in the worst case, to oscillations of fuel index during acceleration, rather than a steady increase. This phenomenon is referred to as limiter loop oscillations (LLO) in the remainder of the text.

D.4.3 Y_{LOM} - Oxygen/Fuel Limiter based on O_2-Model

The second method of extending the limiter is focused on handling the LLO issue explained above. The control-oriented model of scavenge oxygen from Section D.3.2 is used for the conversion in (D.26). The dynamics of the COM mostly represent sensor dynamics, and these are discarded, leaving only the input nonlinearity $g(\dot{n}_f, \dot{n}_{ic}, \dot{n}_{egr})$

$$Y_{LOM} = Y_{LA} \cdot \frac{g(\dot{n}_f, \dot{n}_{ic}, \dot{n}_{egr})}{O_a} \tag{D.28}$$

Fuel flow $\dot{n}_f$ is derived from the fuel index and engine speed as in (D.10)

$$Y_{LOM} = Y_{LA} \cdot \frac{g(k_f \cdot \omega_{eng} \cdot Y, \dot{n}_{ic}, \dot{n}_{egr})}{O_a} \tag{D.29}$$

This equation represents a static version of the limiter loop because Y is used to calculate the limit to itself. This can be solved by noting that $Y \leq Y_{LOM}$; thus, on the limit, we must have $Y = Y_{LOM}$, leading to

$$Y_{LOM} = Y_{LA} \cdot \frac{g(k_f \cdot \omega_{eng} \cdot Y_{LOM}, \dot{n}_{ic}, \dot{n}_{egr})}{O_a} \tag{D.30}$$

Inserting the expression for $g()$ leads to a 2nd-order equation in Y_{LOM}

$$k_f \omega_c \left(\frac{y}{4} - \frac{1 + \frac{y}{4}(O_a + 1)}{O_a} \cdot \frac{\dot{n}_{egr}}{\dot{n}_{ic} + \dot{n}_{egr}} \right) Y_{LOM} - \frac{\dot{n}_{ic}}{Y_{LA}} Y_{LOM} - \frac{\frac{y}{4} k_f \omega_c}{Y_{LA}} Y_{LOM}^2 + \dot{n}_{ic} = 0 \tag{D.31}$$

EGR flow $\dot{n}_{egr}$ is found from the blower speed, up- and downstream pressures and a blower map. Cooler flow $\dot{n}_{ic}$ is calculated with (C.9), where θ is the output of the parameter estimator from [50]

$$\hat{\theta} = k \left(\tau O_{sr,meas} + \int O_{sr,meas} - g(\dot{n}_f, \dot{n}_{ic}(\hat{\theta}), \dot{n}_{egr}) \, \mathrm{dt} \right) \tag{D.32}$$

where $k > 0$ and τ represents the time constant of gas mixing and sensor dynamics. The estimator error was proven to converge exponentially to a small region around zero in [50]. When the 3 flows are determined, Equation (D.31) can be solved, and the positive solution is then used as a fuel index limiter.

The limiter Y_{LOM} has the advantage that it is not directly influenced by the delay of the scavenge oxygen sensor; it is only indirectly influenced through the parameter estimator. It avoids the LLO issue by stating it as a static equation and solving it. The drawbacks are that the calculations are less intuitive and that the process dynamics is ignored. This index limiter is initially conservative because it sets the limit so low that it will not have to decrease the limit during acceleration due to drops in O_{sr}. After the initial step of fuel index, this limiter tends to increase rapidly as it reacts instantaneously to changes in EGR and cooler flow.

Figure D.7 shows an overview of the governor, EGR controller and engine setup.

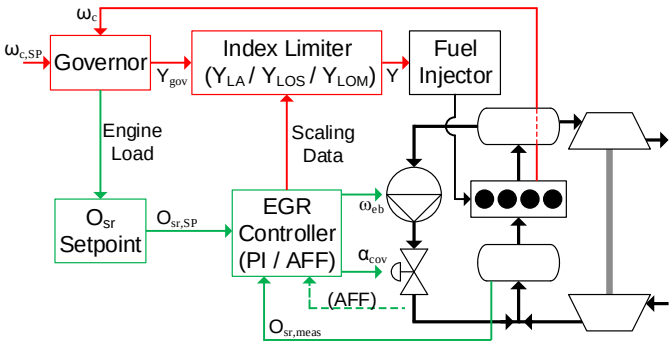

Figure D.7: Overview of the governor (red) and EGR (green) control systems. The two systems control coupled variables of the same process and interact through the engine load signal and data for scaling of the index limiter. The dashed green line refers to TC speed, EGR flow and fuel flow data used by the AFF EGR controller.

D.5 Results

The two methods of limiter extension are validated through simulations with the MVEM and in acceleration tests on a vessel operating at sea. Combinations of the two methods with both generations of EGR controllers are tested.

D.5.1 Simulation

The mean-value engine model described in Section D.3.1 is used for validation of the proposed limiters. The MVEM is implemented in MATLAB Simulink along with the two generations of EGR controllers: the slow PI controller and the fast adaptive feedforward controller (AFF). The air/fuel ratio is calculated internally in the MVEM and used with Equation (D.2) to provide Y_{LA}. Calculation of Y_{LOS} and Y_{LOM} is also implemented to test the limiters in closed loop.

The first scenario is a loading transient where the fuel index setpoint is changed from 60 to 100%. The engine load (power) changes from 43 to 100% during the transient. The limiter extensions Y_{LOS} and Y_{LOM} are simulated in a closed loop one at a time, combined with the fast AFF EGR controller. The goal is to increase the fuel index limit (and thereby ω_c) as fast as possible without exceeding the oxygen fuel equivalence ratio limit specified as 1.1. Figure D.8 presents the result. Y_{LOM} begins at a lower value than Y_{LOS} due to the solution of LLO, but the limits quickly converge during the transient, and no significant performance difference is observed. The AFF EGR controller is able to keep O_{sr} almost constant despite of the increased fuel flow and thereby effectively prevents LLO and issues with sensor delay. Both methods make the oxygen/fuel equivalence ratio saturate at 1.1 as specified.

The MVEM only simulates the high-load region where the turbocharger response is faster than in the low-load region where fast accelerations with subsequent smoke formation occur. The slow TC response worsens the potential scavenge oxygen peaks and therefore also the potential LLO. To simulate the worst case conditions for the limiters, the index setpoint step from 60 to 100% is simulated again, but with the TC moment of inertia in the MVEM tripled to slow the response, with faster O_2 sensor dynamics and with the slow PI EGR controller. The result is presented in Figure D.9. Y_{LOS} now shows a small "overshoot" for 20 seconds before converging with Y_{LOM}. The oxygen/fuel equivalence ratio exceeds its limit during this overshoot, whereas for Y_{LOM}, the behavior is slightly on the conservative side.

The conclusions of the simulations are that the limiter extensions perform similarly well in the simulation of a load transient in the high-load range with use of the AFF EGR controller. With slower turbocharger dynamics, faster sensor dynamics and combined with the PI EGR controller, the Y_{LO1} limiter causes slight LLO and violates the oxygen/fuel limit.

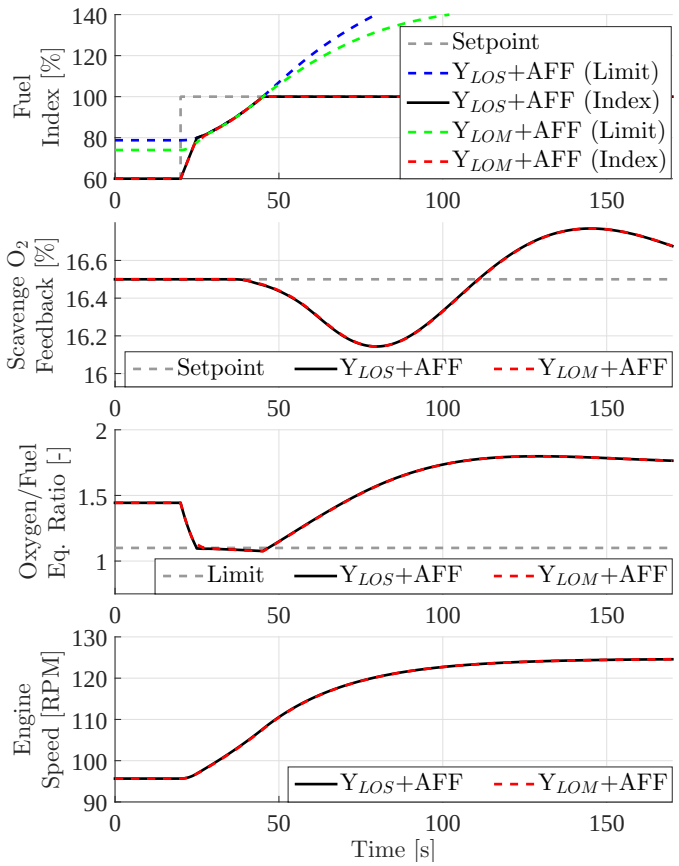

Figure D.8: Closed loop simulations of MVEM with AFF EGR controller and either Y_{LOS} or Y_{LOM} during transient from 43 to 100% load. The limiters show similar performance, and both saturate the oxyen/fuel equivalence ratio at the limit of 1.1.

D.5.2 Experimental Validation

The limiters were experimentally validated on the container vessel Maersk Cardiff during operation in the South China Sea. A series of similar large engine speed setpoint steps where conducted in the maneuvering range with different combinations of index limiters and EGR controllers.

Y_{LOS} was tested with both PI and AFF, whereas Y_{LOM} was only tested with AFF EGR control. Figure D.10 presents the results. Y_{LOS}+PI clearly causes sufficient LLO to degrade engine acceleration. With Y_{LOS}+AFF the LLO is less significant and with Y_{LOM}+AFF it is completely avoided. The latter solution catches up to Y_{LOS}+AFF approximately 45 RPM and provides the fastest acceleration to 50 RPM.

An opacimeter mounted in the exhaust outlet allowed for comparison of smoke formation. Furthermore, the exhaust outlet was recorded with a video camera to provide visual validation. Figure D.11 shows the engine speeds and opacity responses of 5 combinations of limiters and EGR control. Combining the AFF EGR control with an extended limiter clearly causes the least smoke formation, whereas the first approach with PI EGR control and no extension performs poorly. Figure D.12 shows stills from the videos of the exhaust outlet during these steps. Clearly visible smoke formation occurs during steps with the non-extended Y_{LA} limiter, whereas the extended limiters reduce the visible smoke to a minimum. Table D.1 summarizes the conclusions from the experiments.

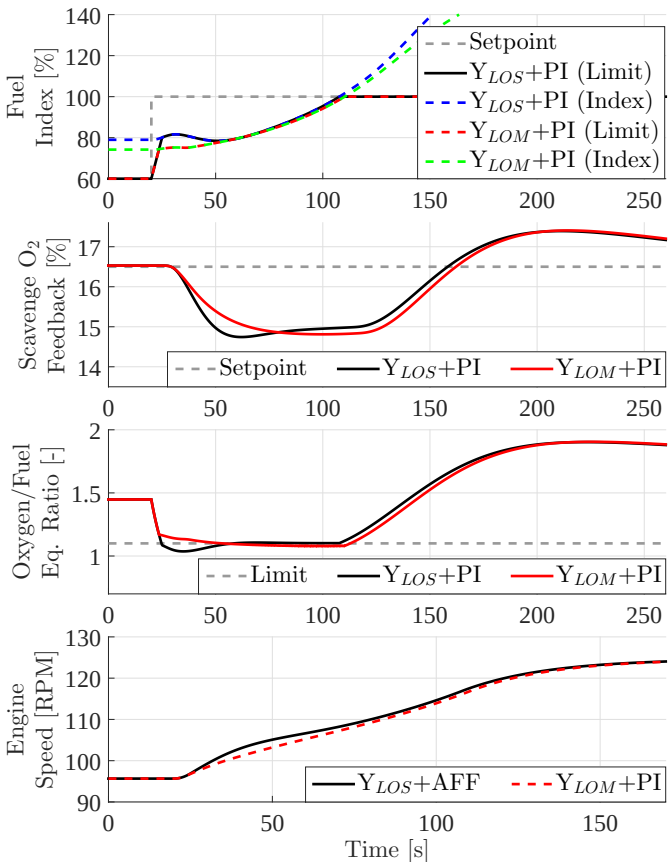

Figure D.9: Closed loop simulations of MVEM with PI EGR controller and either Y_{LOS} or Y_{LOM} during transient from 43 to 100% load. For this simulation, the TC moment of inertia was tripled and O_2 sensor dynamics were artificially fast to induce the worst case with respect to limiter oscillation. Y_{LOS} causes slight LLO and violation of the oxygen/fuel limit.

Table D.1: Conclusions from the experiments. The best performance is achieved by combining the Y_{LOM} limiter with AFF EGR control.

	Y_{LOS}	Y_{LOM}
PI	Slight smoke formation. Reduced acceleration.	Not tested.
AFF	No smoke formation. Good acceleration.	No smoke formation. Best acceleration.

D.6 Conclusions

This paper presented two methods for extending a fuel index limiter based on air/fuel ratio to a limiter based on oxygen/fuel ratio for application to diesel engines with exhaust gas recirculation. The first method was based on a measurement of the scavenge oxygen fraction. The second method was based on a control-oriented model of the scavenge oxygen fraction.

Closed loop simulations with a mean-value engine model showed that the two methods performed similarly well in the high-load range when combined with a fast adaptive feedforward EGR controller. In a simulation of the worst case conditions (with slow model dynamics and a PI EGR controller), the extension based on the oxygen sensor oscillated slightly.

Sea trial experiments showed very significant smoke reduction when using the proposed limiters. The best acceleration performance was achieved by combining the limiter extension based on the control-

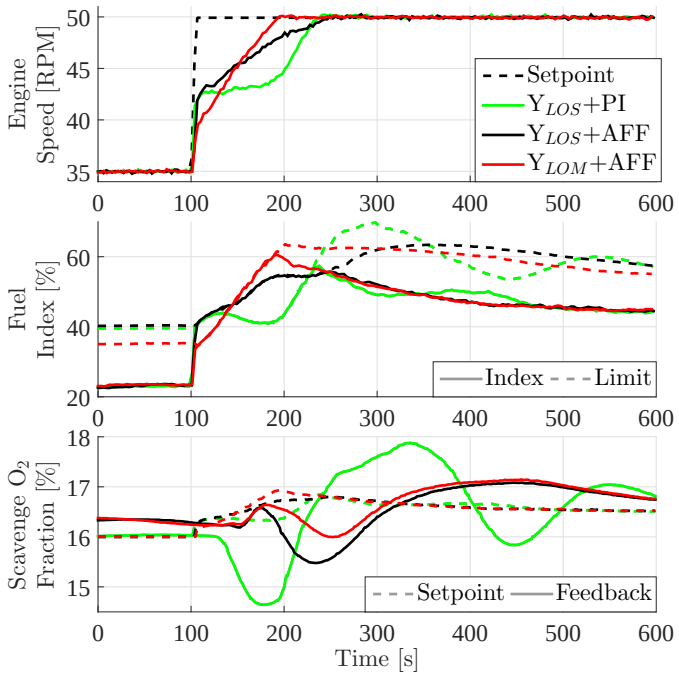

Figure D.10: A comparison of 3 similar engine speed setpoint steps performed on the vessel Maersk Cardiff with different combinations of limiters and EGR controllers. The Y_{LOM} combined with AFF EGR controller provides the fastest acceleration from 35 to 50 RPM.

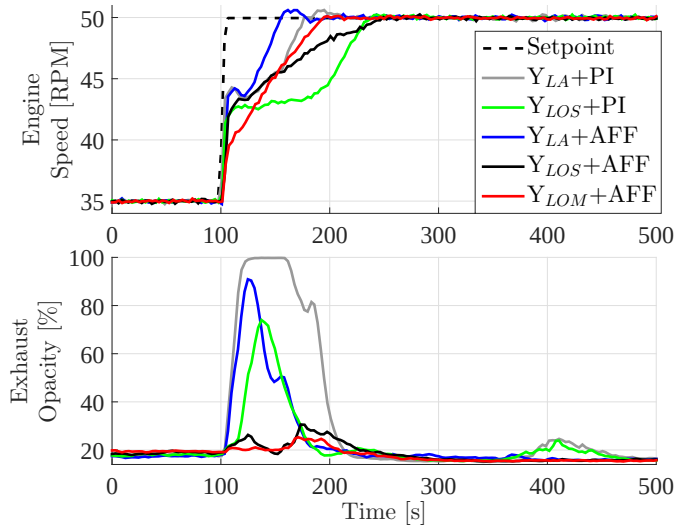

Figure D.11: A comparison of engine speed and smoke for 5 similar engine speed setpoint steps performed on the vessel Maersk Cardiff with different combinations of limiters and EGR controllers. Acceleration performance slightly degrades when basing the limiter conversion on the oxygen sensor (Y_{LOS}).

oriented model with the adaptive feedforward EGR controller.

The advances described in this paper enable the EGR technology to reduce NO_x emissions from large diesel engines. The sophisticated engine control methods facilitate the application of EGR systems on downsized diesel engines for simultaneous maximization of fuel efficiency and minimization of NO_x emissions while maintaining optimal vessel maneuverability without damaging the engine. The limiters proposed here are currently being implemented in commercially available EGR control software along with

(a) Y_{LA}+PI. Thick black smoke is emitted for 45 seconds.

(b) Y_{LA}+AFF. The smoke level is reduced compared to the PI controller but still visible.

(c) Y_{LOS}+PI. Smoke formation is close to invisible.

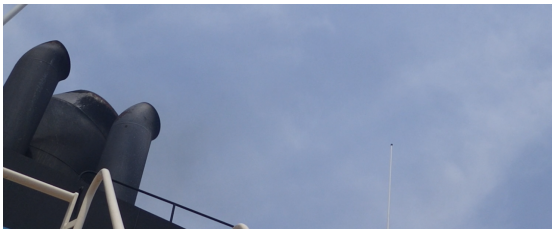

(d) Y_{LOS}+AFF. No visible smoke.

(e) Y_{LOM}+AFF. No visible smoke.

Figure D.12: Exhaust smoke on a vessel with during accelerations from 35 to 50 RPM, with various combinations of fuel index limiters and EGR controllers.

the adaptive feedforward EGR controller.

Acknowledgment

This work was partially funded by the Danish Agency for Science, Technology and Innovation, grant number 1355-00071B.

We thank MAN Diesel & Turbo and Maersk Line for supporting the experiments on the vessel Maersk Cardiff.

Paper E

Nonlinear Adaptive Control of Exhaust Gas Recirculation for Large Diesel Engines

Kræn Vodder Nielsen[*1,2], Mogens Blanke[2,3], Morten Vejlgaard-Laursen[1]

[1] MAN Diesel & Turbo, Teglholmsgade 41, 2450 København SV, Denmark [2]Department of Electrical Engineering, Automation and Control Group, Technical University of Denmark, Elektrovej Building 326, 2800, Kgs. Lyngby, Denmark

[3]AMOS CoE, Institute of Technical Cybernetics, Norwegian University of Science and Technology, 7491 Trondheim, Norway

Abstract:
A nonlinear adaptive controller is proposed for the exhaust gas recirculation system on large two-stroke diesel engines. The control design is based on a control oriented model of the nonlinear dynamics at hand that incorporates fuel flow and turbocharger speed changes as known disturbances to the exhaust gas recirculation.

The paper provides proof of exponential stability for closed loop control of the model given. Difficulties in the system include that certain disturbance levels will make a desired setpoint in O_2 unreachable, for reasons of the physics of the system, and it is proven that the proposed control will make the system converge exponentially to the best achievable state. Simulation examples confirm convergence and good disturbance rejection over relevant operational ranges of the engine.

K. V. Nielsen, M. Blanke, and M. Vejlgaard-Laursen. "Nonlinear Adaptive Control of Exhaust Gas Recirculation for Large Diesel Engines". *IFAC-PapersOnLine* 48.16 (2015). 10th IFAC Conference on Manoeuvring and Control of Marine Craft, MCMC 2015 Copenhagen, 24-26 August 2015, pp. 254 –260. DOI: 10.1016/j.ifacol.2015.10.289

[*]Principal corresponding author. Tel.: +45 33851909; E-mail: kraenv.nielsen@man.eu

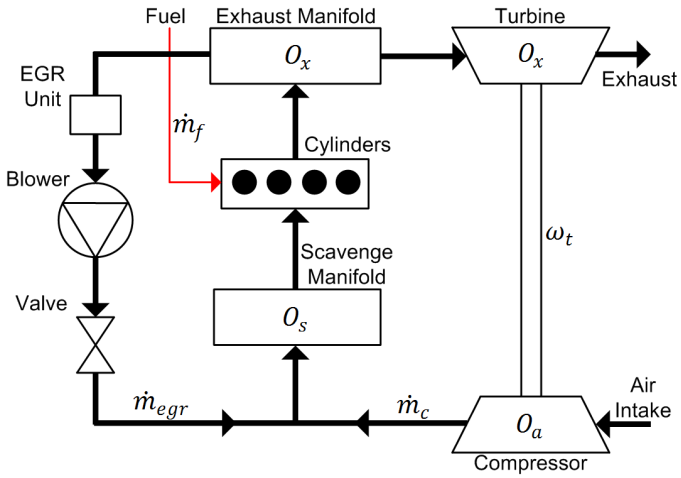

Figure E.1: Simplified overview of engine gas flows.

E.1 Introduction

Emissions from diesel engines are subject to restriction due to awareness of environmental effects of the emissions. The Tier III restrictions, limiting the emission of NO_x from marine diesels in selected areas, as was presented by the International Maritime Organization, [2] will be introduced in 2016. The IMO Tier III rules for environmental protection specifies a reduction of 76% of NO_x emission compared to the Tier II standard in specified Emission Control Areas, including most of the North American coastal areas, among others. This motivates the ship industry to develop technologies that reduce the emissions of NO_x.

One of such technologies is Exhaust Gas Recirculation (EGR), which has been applied to four-stroke engines in the automotive industry for several decades. The principle is to recirculate part of the exhaust gas into the engine intake. This decreases the oxygen content and increases the heat capacity of the scavenging gas. In turn the peak temperatures during combustion are decreased, resulting in a decrease in the formation of NO_x during combustion. Unfortunately, lowering the oxygen content of the scavenging gas also affects the combustion efficiency. At excessively low scavenge air oxygen levels, the engine will produce visible smoke. Thus the optimal scavenging oxygen level is a compromise between fuel economy, smoke formation and NO_x emissions.

To prepare for the Tier III restrictions, engine designer MAN Diesel & Turbo (MDT) has introduced EGR technology on their large two-stroke marine diesel engines. Other technologies for NO_x reduction are also being used, but the scope of this paper is the control of the EGR system. As the scavenge pressure of a two-stroke engine is higher than the exhaust pressure, a blower is used in the EGR string to provide a pressure increase. The blower speed must be carefully controlled to obtain an EGR flow that leads to the appropriate amount of oxygen in the scavenging gas. A simplified schematic of the engine air path is shown in Figure E.1. Some components that are not essential to the paper have been omitted from the Figure. The EGR unit shown in the Figure removes corrosive SO_x and cools the recirculated gas.

The overall control objective is to obtain feedback control of the oxygen concentration O_s in the scavenge manifold using either the speed setpoint of the EGR blower or the opening of the EGR valve as actuator input. This method has been applied to several engine setups. During stationary running conditions existing fixed gain control has shown ability to keep O_s adequately close to a setpoint. However, this feedback control, being based on an O_s measurement with inherent sensor dynamics and measurement delay, is an essential limitation for performance. This becomes an issue when handling hard acceleration of the ship and in high sea conditions where waves have significant impact as a fluctuating load torque on

the propeller shaft [44]. In both these conditions the engine RPM controller adjusts the flow of fuel into the cylinders and thus changes the appropriate EGR flow. The slow nature of the system and difficulties inherent to measuring oxygen concentration in the scavenge manifold makes the control system react slowly to such disturbances. To avoid smoke formation from too low oxygen, it is currently necessary to limit the possible ship acceleration when the EGR system is running. Such a limitation is undesirable and far from possible in all operating situations. Therefore, an alternative control concept is needed that can cope with pressure dependent sensor measurement delay, sensor dynamics and the nonlinear dynamics of the gas recirculation system, and yet provide a high performance closed loop control.

A clear difference between the EGR control system developed by MDT and the EGR systems in the automotive industry is the effort available for commissioning an EGR controller for an engine configuration. Each automotive engine design is thoroughly tested on a test bench before releasing for large scale production. In opposition to this the specific large two-stroke engine designs are produced in very low numbers, they are sometimes not tested until the first engine is produced and even then very limited test time is available due to very high test running cost. It is furthermore possible that a large two-stroke engine will be reconfigured during its time of operation. The consequences of these practical issues are that manual tuning for the individual design is not applicable and that observer design based on a priori data is impractical. This means that the control design must be robust not only towards changes in system behaviour but also towards imprecise design data.

Numerous examples of modelling and control of EGR systems for automotive engines exist in literature. Notable examples are [19], [20] and [15]. [16] proposed nonlinear control of automotive EGR systems using a control Lyapunov function. Modelling of large two-stroke engines have been treated in both classical literature, e.g. [29], [30] and more recently in [34] and [43] though only the latter includes an EGR system. [44] presented EGR control design with SISO methods and feed forward of the fuel index. The main issues were found to be parameter sensitivity and the dead time of the oxygen sensor.

This paper introduces an adaptive nonlinear controller for the EGR system, based on a system model that is significantly simpler than traditional mean value models. The control law incorporates known disturbances for faster rejection of these. Exponential stability of the simplified closed loop system is proven by Lyapunov's direct method. Simulation examples confirm convergence and disturbance rejection properties of the controller.

The control oriented model of the EGR system behavior is briefly introduced in Section E.2. Control design and stability proofs are found in Section E.3. The closed loop system of the simple EGR model and the controller is simulated in Section E.5 followed by a discussion of the validity of the results in Section E.6.

E.2 System Model

This section introduces a model of the scavenge oxygen dynamics in the EGR system. The model is intended as a simplification that is useful for controller design as opposed to conventional mean value approaches that represent a more sophisticated replication of physical processes. In the simple model, the nonlinearities of the stationary system response is used as an input nonlinearity to a first order system. The end result is a first order Hammerstein system with multiple inputs and one output.

E.2.1 Static Model

The static model of the scavenge manifold oxygen fraction assumes that the ambient oxygen fraction O_a, compressor mass flow $\dot{m}_c$, recirculated mass flow $\dot{m}_{egr}$ and fuel mass flow $\dot{m}_f$ are known.

During stationary conditions, the oxygen fraction in the exhaust O_x is a function of compressor flow, ambient oxygen fraction, fuel flow $\dot{m}_f$ and stoichiometric oxygen-to-fuel ratio k_f. Assuming a complete,

lean combustion, O_x is modelled as in [43].

$$O_x = \frac{\dot{m}_c O_a - \dot{m}_f k_f}{\dot{m}_c + m_f} \tag{E.1}$$

The oxygen fraction in the scavenge manifold O_s at stationary state is the average of ambient and exhaust oxygen weighted by compressor flow and recirculated flow $\dot{m}_{egr}$, respectively.

$$O_s = \frac{\dot{m}_c O_a + \dot{m}_{egr} O_x}{\dot{m}_c + \dot{m}_{egr}} \tag{E.2}$$

Combining (E.1) and (E.2) leads to a static model of O_s, based on the 3 major flows.

$$O_s = O_a - (O_a + k_f)\frac{\dot{m}_f}{\dot{m}_c + \dot{m}_f} \cdot \frac{\dot{m}_{egr}}{\dot{m}_c + \dot{m}_{egr}} \tag{E.3}$$

Isolating the recirculated flow in (E.3) leads to an expression that is useful for the control design.

$$\dot{m}_{egr} = \frac{\dot{m}_c(O_a - O_s)}{O_s - \frac{\dot{m}_c O_a - \dot{m}_f k_f}{\dot{m}_c + \dot{m}_f}} = \frac{\dot{m}_c(O_a - O_s)}{O_s - O_x} \tag{E.4}$$

The recirculated flow and the fuel flow are both assumed to be available to the controller, but the compressor flow is not. Estimation from a compressor map is ruled out as maps that covers all operating points are not practically available for each engine. Instead the flow is approximated as a simple function of compressor speed ω_t

$$\dot{m}_c = \omega_t^a \cdot \theta \quad , \quad a \in [1:2] \quad , \quad \theta > 0 \tag{E.5}$$

where a and θ are constants. A similar approximation was done by [30] where the compressor flow was approximated as a function of the scavenge pressure. Introduction of EGR adds to the inaccuracy of (E.5) and θ is expected to change slightly depending on the operating point. The constant a depends on the specific engine.

E.2.2 Dynamic Model

In traditional models the turbocharger dynamics receive great emphasis due to their significant contribution to the system behaviour as was shown by [29]. In the present paper the turbocharger speed ω_t is treated as a known disturbance rather than a state, thus avoiding the interdependency between fuel flow and turbocharger speed. The focus of this model is the oxygen fractions, thus the main dynamics are the mixing of gas in the manifolds. Furthermore the scavenge oxygen sensor is expected to contribute with varying time delay and first order dynamics.

Neglecting the pure time delay, the mixing and sensor dynamics are lumped together as a single first order system in this approach to obtain the simplest model. A known time constant τ is assumed. The nonlinearity expressed in the static model is treated as an input nonlinearity and the result is a first order Hammerstein system with multiple inputs and one output.

The recirculated flow is treated as an actuated input u, whereas fuel flow and turbine speed are gathered in the vector signal d as known disturbances.

$$u = \dot{m}_{egr} \quad , \quad d(t) = \begin{bmatrix} \dot{m}_f \\ \omega_{tc} \end{bmatrix} \tag{E.6}$$

The measured scavenge oxygen fraction is the state variable and a reference value r between zero and ambient oxygen fraction is also defined.

$$x = O_s \quad , \quad r = O_{s,ref} \quad , \quad 0 < r < O_a \tag{E.7}$$

Combining (E.3) and (E.5) the static expression of the scavenge oxygen fraction is a function g of the input, known disturbances and unknown parameter θ.

$$g(\theta,d,u) = O_a - (O_a + k_f)\frac{\dot{m}_f}{\omega_t^a\theta + \dot{m}_f} \cdot \frac{\dot{m}_{egr}}{\omega_t^a\theta + \dot{m}_{egr}} \tag{E.8}$$

The Hammerstein system with the static expression as input nonlinearity and known time constant τ is then

$$\tau\dot{x} = g(\theta,d,u) - x \tag{E.9}$$

E.3 Controller

This paper proposes a nonlinear adaptive controller. The control law is based on Equation (E.4) which is an inversion of the input nonlinearity of the Hammerstein system. The inversion is defined as

$$h(\theta,d,r) = \frac{\omega_t^a\theta(O_a - O_{s,ref})}{O_{s,ref} - \frac{\omega_t^a\theta\cdot O_a - \dot{m}_f k_f}{\omega_t^a\theta + \dot{m}_f}} \tag{E.10}$$

As the parameter θ is expected to vary slightly depending on the operating point a nonlinear parameter estimator continuously provides an estimate $\hat{\theta}$ for use in the control law. The estimator is similar to the ones proposed by [72] in the way a direct term makes the time derivative of the estimate depend on the time derivative of a measurement without explicitly having to differentiate any signals. The proposed controller is

$$\hat{\theta} = k \cdot \left(\tau x + \int x - g(\hat{\theta},d,u)\,dt\right) \tag{E.11}$$

$$u = \begin{cases} h(\hat{\theta},d,r) & \text{if } h(\hat{\theta},d,r) \in [0;u_{max}] \\ u_{max} & \text{otherwise} \end{cases} \tag{E.12}$$

where k is an observer gain and u_{max} is the highest possible EGR flow.

The conditional form of the control law is necessary in the case where it is not physically possible to invert the static model, based on the known disturbances and the estimated parameter.

The proposed controller specifies a setpoint of the EGR flow and assumes that the current EGR flow is known. Thus an inner loop that controls the blower speed and valve opening based on a measurement or an estimate of the flow is required. This inner loop is not treated further in this paper.

E.4 Stability Analysis

This section investigates the stability properties of the closed loop system. The parameter estimator (E.11) and control law (E.12) are assumed to act on the Hammerstein system (E.9). The reference value r is constant.

The analysis considers the convergence of the control error $\tilde{x} = x - r$ and the parameter estimation error $\tilde{\theta} = \hat{\theta} - \theta$.

The stability analysis is divided into two parts, each dealing with one of the two cases of the control law. Before the analysis it is necessary to introduce two positive limits γ_g and γ_η regarding the sensitivity of the functions g and h

$$\frac{\partial g(\hat{\theta},d,u)}{\partial\hat{\theta}} \geq \gamma_g \quad , \quad \left|\frac{\partial g(\theta,d,h(\hat{\theta},d,r))}{\partial\hat{\theta}}\right| \leq \gamma_\eta \tag{E.13}$$

The validity of these limits will be revisited in the last part of the analysis.

E.4.1 First Case

Lyapunov's direct method is used to prove exponential stability when

$$h(\hat{\theta},d,r) \in [0;u_{max}] \tag{E.14}$$

The dynamics of the system state, given the control law are

$$\tau\dot{x} = g(\theta,d,h(\hat{\theta},d,r)) - x \tag{E.15}$$

Note that h inverts g in the actuated input

$$r = g(\theta,d,h(\theta,d,r)) \tag{E.16}$$

From (E.15) and (E.16), with constant r

$$\tau\dot{\tilde{x}} = g(\theta,d,h(\hat{\theta},d,r)) - g(\theta,d,h(\theta,d,r)) + r - x \tag{E.17}$$

$$\Leftrightarrow \tau\dot{\tilde{x}} = \eta(\tilde{\theta},d) - \tilde{x} \tag{E.18}$$

where

$$\eta(t,\tilde{\theta}) = g(\theta,d,h(\theta+\tilde{\theta},d,r)) - g(\theta,d,h(\theta,d,r)) \tag{E.19}$$

From (E.9), $\tau\dot{x}+x = g(\theta,d,u)$, hence the dynamics of the parameter estimator error are

$$\begin{aligned}\dot{\tilde{\theta}} = \dot{\hat{\theta}} &= k\cdot\left(\tau\dot{x}+x-g(\hat{\theta},d,u)\right)\\ &= k\cdot\left(g(\theta,d,u)-g(\theta+\tilde{\theta},d,u)\right) = -k\tilde{g}(\tilde{\theta},d)\end{aligned} \tag{E.20}$$

where

$$\tilde{g}(t,\tilde{\theta}) = g(\theta+\tilde{\theta},d,h(\theta+\tilde{\theta},d,r)) - g(\theta,d,h(\theta+\tilde{\theta},d,r)) \tag{E.21}$$

The time derivative of the observer error $e = \begin{bmatrix}\tilde{x} & \tilde{\theta}\end{bmatrix}^T$ is defined as $f(t,e)$

$$\dot{e} = \begin{bmatrix}\frac{1}{\tau}\left(\eta(t,\tilde{\theta})-\tilde{x}\right)\\ -k\tilde{g}(t,\tilde{\theta})\end{bmatrix} = f(t,e) \tag{E.22}$$

A Lyapunov function V is chosen, where c is a constant

$$V = \frac{1}{2}\tilde{x}^2 + \left(\frac{\gamma_\eta^2}{8k\gamma_g\tau(1-\tau c)} + \frac{c}{2k\gamma_g}\right)\tilde{\theta}^2 \quad , \quad 0 < c < \frac{1}{\tau} \tag{E.23}$$

The derivative of V is

$$\begin{aligned}\frac{\partial V}{\partial t} + \frac{\partial V}{\partial e}f(t,e) = \tilde{x}\frac{1}{\tau}&\left(\eta(t,\tilde{\theta})-\tilde{x}\right)\\ &-\left(\frac{\gamma_\eta^2}{4k\gamma_g\tau(1-\tau c)} + \frac{c}{k\gamma_g}\right)\tilde{\theta}\cdot k\tilde{g}(t,\tilde{\theta})\\ &= -\left(\frac{1}{\tau}-c\right)\tilde{x}^2 - c\tilde{x}^2 + \frac{1}{\tau}\tilde{x}\eta(t,\tilde{\theta})\\ &-\left(\frac{\gamma_\eta^2}{4\gamma_g\tau(1-\tau c)} + \frac{c}{\gamma_g}\right)\tilde{\theta}\tilde{g}(t,\tilde{\theta})\end{aligned} \tag{E.24}$$

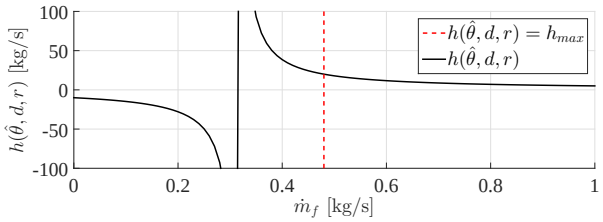

Figure E.2: Example of $h(\hat{\theta},d,r)$ when varying $\dot{m}_f$.

The contributions from $\tilde{g}(t,\tilde{\theta})$ and $\eta(t,\tilde{\theta})$ are limited by use of the conditions (E.13)

$$\tilde{\theta}\cdot\tilde{g}(t,\tilde{\theta}) = \tilde{\theta}\cdot\int_{\theta}^{\theta+\tilde{\theta}}\frac{\partial g(s,d,u)}{\partial s}ds \geq \gamma_g\tilde{\theta}^2 \tag{E.25}$$

$$\left|\eta(t,\tilde{\theta})\right| = \left|\int_{\theta}^{\theta+\tilde{\theta}}\frac{\partial g(\theta,d,h(s,d,y))}{\partial s}ds\right| \leq \gamma_\eta\left|\tilde{\theta}\right| \tag{E.26}$$

Thus

$$\begin{aligned}\frac{\partial V}{\partial t}+\frac{\partial V}{\partial e}f(t,e) \leq &-\left(\frac{1}{\tau}-c\right)\cdot \\ &\left(\tilde{x}^2+\frac{\gamma_\eta^2}{4\tau^2(\frac{1}{\tau}-c)^2}\tilde{\theta}^2-\frac{\gamma_\eta}{\tau}|\tilde{x}|\cdot|\tilde{\theta}|\right)-c\left(\tilde{x}^2+\tilde{\theta}^2\right) \\ &=-\left(\frac{1}{\tau}-c\right)\left(\tilde{x}-\frac{\gamma_\eta}{2\tau(\frac{1}{\tau}-c)}\tilde{\theta}\right)^2-c||e||^2 \leq -c||e||^2\end{aligned} \tag{E.27}$$

Theorem 4.10 in [81] implies exponential stability of $e=0$ when both conditions (E.13) apply.

E.4.2 Second Case

This part of the stability analysis considers the case where

$$h(\hat{\theta},d,r) \notin [0;u_{max}] \tag{E.28}$$

that is, when the static system is not invertible within the actuator limits. More insight into when this occurs can be gained by reviewing the equations defining the system. By (E.1), $O_x < O_a$ when all signals and parameters are positive. O_s is a weighted average of O_a and O_x, hence $O_s \in]O_x;O_a]$. Small EGR flows are required for O_s close to O_a and large EGR flows are required for O_s close to O_x. No physically possible values of EGR flow result in O_s equal to or lower than O_x. As $O_{s,ref} < O_a$, problems with inverting the system only occurs when $O_{s,ref}$ is low compared to O_x.

Figures E.2 and E.3 illustrates the issue of mathematically inverting the system with examples of $h(\hat{\theta},d,r)$, when varying $\dot{m}_f$ and $\hat{\theta}\omega_t^a$, respectively. The reference value is fixed at 17% in both cases.

Normal operation occurs at the rightmost part of Figure E.2. Lowering the fuel flow increases the exhaust oxygen fraction and thus calls for a higher EGR flow to reach the reference value r. The dashed line indicates the value of $\dot{m}_f$ for which the maximum EGR flow (in this case 20 kg/s) is reached. The required EGR flow approaches infinity as the estimated exhaust oxygen fraction approaches the reference value. The result is a vertical asymptote in Figure E.2. For all values of $\dot{m}_f$ below the dashed line, the best option available to the controller is the maximum EGR flow. Beyond the asymptote, the values of h are negative. Care must be taken when implementing the control law as the asymptote represents an undefined value of h. This is solved by evaluating whether the denominator of (E.10) is close to 0.

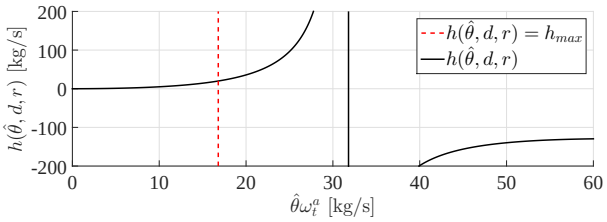

Figure E.3: Example of $h(\hat{\theta},d,r)$ when varying $\hat{\theta}\omega_t^a$.

Figure E.3 depicts $h(\hat{\theta},d,r)$ when varying the estimated compressor flow $\omega_t^a\hat{\theta}$. Normal operation occurs at the leftmost part of the figure. Higher estimated compressor flow result in higher exhaust oxygen fraction and thus requires a higher EGR flow. As above, the point where the maximum EGR flow is reached is marked with a dashed line and the vertical asymptote indicates the point where the estimated exhaust oxygen fraction equals the reference value. Again, for all values of $\omega_t^a\hat{\theta}$ beyond the dashed line, the best option available to the controller is the maximum EGR flow.

It is important to distinguish between the case where the actual static system is non-invertible and the case where only the estimated static system is non-invertible. In the first case, the maximum EGR flow is the optimal choice. For both cases it is important that $\tilde{\theta}$ converges to 0 such that the control law converges to either the correct system inversion or the maximum flow. The isolated convergence of $\tilde{\theta}$ is proven using Lyapunov's direct method.

The following Lyapunov function is chosen

$$V = \frac{1}{2}\tilde{\theta}^2 \tag{E.29}$$

The first sensitivity condition implies

$$\frac{\partial V}{\partial t} + \frac{\partial V}{\partial e} f(t,e) = -k\tilde{\theta}\tilde{g}(t,\tilde{\theta}) \leq -k\gamma_g\tilde{\theta}^2 \tag{E.30}$$

From Theorem 4.10 in [81] $\tilde{\theta}$ will converge exponentially toward 0. Thus, the convergence depends on the first sensitivity condition rather than the control law.

E.4.3 Sensitivity Conditions Revisited

The lower limit of the sensitivity of $g(\theta,d,u)$ to θ is used in both cases of the stability analysis.

$$\frac{\partial g(\theta,d,u)}{\partial \theta} = \left(O_a + k_f\right) \frac{\left(2\omega_t^a\theta + \dot{m}_f + \dot{m}_{egr}\right)\dot{m}_f\dot{m}_{egr}\omega_t^a}{\left(\omega_t^a\theta + \dot{m}_f\right)^2\left(\omega_t^a\theta + \dot{m}_{egr}\right)^2} \tag{E.31}$$

If positive lower and upper limits are defined for all parameters and signals, a lower limit (γ_g) of the sensitivity exists. Thus first sensitivity condition is only satisfied if the EGR flow has a positive lower limit. Considering (E.10), the commanded EGR flow is positive, unless either the estimated compressor flow is zero or if $O_{s,ref}$ equals O_a. Thus the estimated parameter must be initialised with positive value and will not converge when $r = O_a$.

The second sensitivity condition is only used for the first part of the stability analysis. It specifies an upper bound to the absolute value of the sensitivity of $g(\theta,d,h(\hat{\theta},d,r))$ to $\hat{\theta}$. With the chain rule

$$\left|\frac{\partial g(\theta,d,h(\hat{\theta},d,r))}{\partial \hat{\theta}}\right| \leq \left|\frac{\partial g}{\partial u}(\theta,d,h(\hat{\theta},d,r))\right| \cdot \left|\frac{\partial h}{\partial \hat{\theta}}(\hat{\theta},d,r)\right| \tag{E.32}$$

The first term on the right side is

$$\left|\frac{\partial g}{\partial u}(\theta,d,h(\hat{\theta},d,r))\right| = \left|\frac{\dot{m}_f(O_a+k_f)\omega_t^a\theta}{(\omega_t^a\theta+\dot{m}_f)(\omega_t^a\theta+h(\hat{\theta},d,r))^2}\right| \tag{E.33}$$

As all signals and parameters have positive lower and upper bounds, an upper bound to the expression exists.

The second term on the right hand side of (E.32) is

$$\left|\frac{\partial h}{\partial \hat{\theta}}(\hat{\theta},d,r)\right| = \left|\frac{\left(\hat{\theta}^2\omega_t^{2a}(O_a-r)-(k_f+r)(2\dot{m}_f\hat{\theta}\omega_t^a+\dot{m}_f^2)\right)(O_a-r)\omega_t^a}{\left((\hat{\theta}\omega_t^a+\dot{m}_f)r-\hat{\theta}\omega_t^aO_a+\dot{m}_fk_f)\right)^2}\right| \tag{E.34}$$

All signals and parameters have positive bounds, except for $\hat{\theta}$. The denominator is only zero when

$$r = \frac{\hat{\theta}\omega_t^aO_a-\dot{m}_fk_f}{\hat{\theta}\omega_t^a+\dot{m}_f} \tag{E.35}$$

From ($E.1$), the equation above applies when the reference value is equal to the estimated exhaust oxygen fraction. This corresponds to the vertical asymptotes in Figures E.2 and E.3 and therefore does not apply in the first case of the stability analysis. Thus a positive lower limit must exist for the denominator of (E.34). Furthermore, as both the numerator and the denominator of (E.34) are second order polynomials in $\hat{\theta}$ an upper limit of (E.34) exists. Having bounded both terms on the right hand side of (E.32), an upper (γ_η) limit to the sensitivity exists and the second sensitivity condition applies in the first case of the stability analysis.

E.5 Simulation

The convergence of the state and parameter errors are illustrated by two simulation examples. The disturbance signals and model parameters are within the range of values of a real system. Table E.1 shows the values along with the gain k of the parameter estimator.

Table E.1: Parameters used for simulation:

O_a	23 %	r	17 %
τ	15 s	k_f	3.4
$\dot{m}_f$	1-3 kg/s	θ	2 g/RPM
$\dot{m}_{egr,max}$	20 kg/s	ω_t	10 kRPM
a	1	k	20 (g/RPM)/s

In a real engine the turbocharger speed is affected by the fuel and EGR flows. This effect is not present in the simulation here as both fuel flow and turbocharger speed are kept constant except for a single step in fuel flow in the second simulation.

E.5.1 Convergence during Start-up

The first example illustrates the convergence of state and parameter errors during start-up of the EGR system. The initial parameter estimate is 5 times the actual parameter to show convergence under the second case of the control law. Simulated scavenge oxygen fraction, EGR flow and the estimated parameter are shown in Figures E.4, E.5 and E.6.

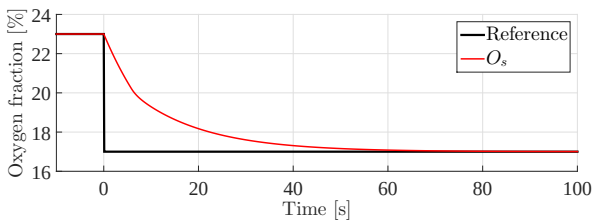

Figure E.4: Simulation of O_s during EGR system start-up.

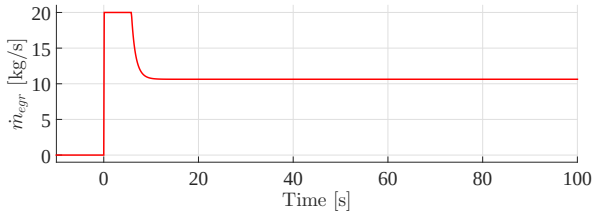

Figure E.5: Simulation of $\dot{m}_{egr}$ during EGR system start-up.

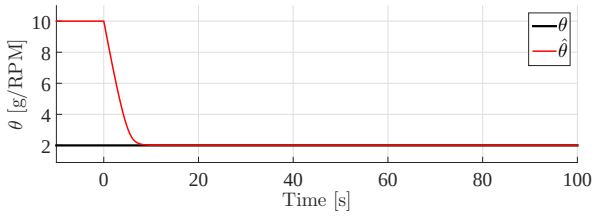

Figure E.6: Simulation of $\hat{\theta}$ during EGR system start-up.

An EGR system start-up is simulated as a step response in the reference $O_{s,ref}$ from 23% (ambient) to 17% at time 0 seconds. After the step, O_s converges to the new reference value without overshoot. EGR flow is zero before the step as this keeps O_s at the ambient level no matter what positive value the compressor flow has. Without EGR flow, the model loses sensitivity to $\hat{\theta}$ so the parameter does not converge. Immediately after the step, the erroneous parameter estimate causes maximum EGR flow. The parameter estimate and thus the EGR flow converges after about 10 seconds to their final values without any overshoot.

E.5.2 Disturbance Step

The second simulation example illustrates how the controller handles a fuel flow step from 1 to 3 kg/s when the parameter estimate has converged. Figures E.7 and E.8 show simulated O_s and $\dot{m}_{egr}$, respectively (dashed lines). The combination of perfect input inversion and no actuator dynamics makes the controller compensate perfectly for the step. A simulation that includes first order actuator dynamics of the form

$$\tau_{act}\frac{d\dot{m}_{egr}}{dt} = u - \dot{m}_{egr} \tag{E.36}$$

with $\tau_{act} = 2s$, is also shown. The actuator dynamics make O_s deviate to just below 16% before converging to the reference value without overshoot. The parameter estimate (not shown) is not affected by the step in any of the cases as the estimate will converge as long as the EGR flow is positive.

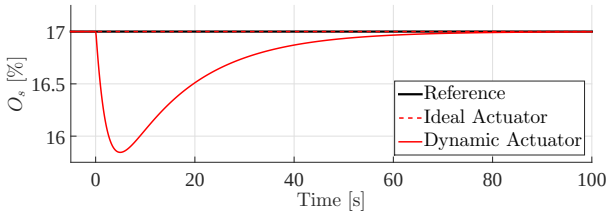

Figure E.7: Simulation of O_s during fuel flow step.

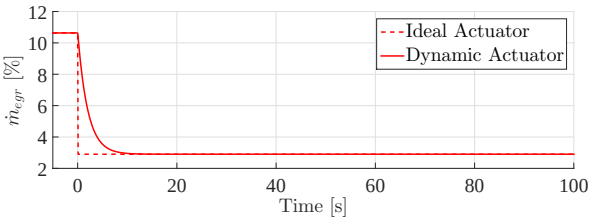

Figure E.8: Simulation of $\dot{m}_{egr}$ during fuel flow step.

E.6 Discussion of Validity

The intention of the presented design approach is to model the essential system behaviour and develop a controller that is robust toward the remaining unmodelled dynamics. The most significant simplifications are the compressor flow model and the assumption of first order dynamics. The approximate time constant might vary slightly depending on the operating point. Also, as the dynamics depend on the specific O_s sensor, this assumption should be revisited with an analysis of the behaviour of specific sensor types. Compensation for the time delay of the O_s measurement is also an issue. Exponential convergence of the control error is a positive indication of robustness of the proposed controller towards unmodelled dynamics. However, a thorough study of the control performance when simulating control of a more sophisticated model is regarded as a necessary step before introducing the method in practice.

Estimation and control of the EGR mass flow is a prerequisite for the proposed controller. Although this increases the controller complexity further, it also facilitates a control structure where the overall O_s controller is not dependent on whether the EGR flow is actuated by varying the blower speed or the valve opening.

E.7 Conclusion

A Hammerstein model was developed of the scavenge oxygen fraction of an EGR system. The model is intended for control design rather than accurate simulation. A nonlinear adaptive controller was proposed based on the simple model of the scavenge oxygen fraction. A controller was developed that inverts the input nonlinearity of the Hammerstein model and continuously estimates a parameter that change with the operating point of the turbocharger. The parameter estimator includes a tuning parameter whereas the control law requires no tuning and can be parameterized purely on overall engine metadata. Exponential convergence of control and parameter errors where proven with Lyapunov's direct method. Certain disturbance values were shown to make the O_2 setpoint unreachable and it was proven that the system converges to the optimal state when using the proposed controller. Simulations confirmed convergence and good compensation of known disturbances also when actuator dynamics was included.

Bibliography

[1] R. J. Blaszczak. *Nitrogen Oxide (NOx), Why and How They Are Controlled*. Technical Bulletin, US Environmental Protection Agency. 1999.

[2] International Maritime Organization. *Marpol ANNEX VI and NTC 2008, 2013: With Guidelines for Implementation*. 2013.

[3] *Marine Environment Protection Committee (MEPC), 70th session, 24-28 October 2016*. http://www.imo.org/en/MediaCentre/MeetingSummaries/MEPC/Pages/MEPC-70th-session.aspx. Accessed: 2016-11-26.

[4] N. Xiros. *Robust Control of Diesel Ship Propulsion*. Springer London, 2002.

[5] K. Kuiken. *Diesel Engines for Ship Propulsion and Power Plants I-II*. Target Global Energy Training, 2008.

[6] MAN Diesel & Turbo. *Marine Engine IMO Tier II and Tier III Programme 2nd Edition*. 2016.

[7] Winterthur Gas & Diesel. *Low-speed Engines*. (Engine Programme). 2016.

[8] Mitsubishi Heavy Industries. "Development of Selective Catalytic Reduction for Low-speed Marine Diesel Engines, Super-clean Marine Diesel R&D Project for the IMO NOx Tier III Regulations". *Mitsubishi Heavy Industries Technical Review* 47.3 (2010), pp. 48–52.

[9] Mitsubishi Heavy Industries. "The World's First Onboard Verification Test of UE Engine with Low Pressure EGR complied with IMO's NOx Tier III Regulations". *Mitsubishi Heavy Industries Technical Review* 53.2 (2016), pp. 40–47.

[10] Kawasaki Heavy Industries, Ltd. *K-ECOS, Kawasaki-ECO System, IMO NOx Tier 3 Compliant Environmentally-friendly Low Emission System*. 2016.

[11] J. B. Heywood. *Internal combustion engine fundamentals*. McGraw-Hill, 1988, 29+930 s.

[12] L. Eriksson and L. Nielsen. *Modeling and control of engines and drivelines*. English. Wiley, 2014, 567 pages.

[13] J. Kaltoft and M. Preem. "Development of Integrated EGR System for Two-Stroke Diesel Engines" (2013). 27th CIMAC World Congress on Combustion Engine.

[14] L. Guzzella and C. H. Onder. *Introduction to modeling and control of internal combustion engine systems*. English. Springer-Verlag, 2010, XII, 354 s.

[15] M. J. van Nieuwstadt, I. V. Kolmanovsky, P. E. Moraal, A. Stefanopoulou, and M. Jankovic. "EGR-VGT control schemes: Experimental comparison for a high-speed diesel engine". English. *IEEE Control Systems Magazine* 20.3 (2000), pp. 63–79.

[16] M. Jankovic, M. Jankovic, and I. Kolmanovsky. "Constructive Lyapunov control design for turbocharged diesel engines". English. *IEEE Transactions On Control Systems Technology* 8.2 (2000), pp. 288–299.

[17] M. Ammann, N. P. Fekete, L. Guzzella, and A. H. Glattfelder. "Model-Based Control of the VGT and EGR in a Turbocharged Common-Rail Diesel Engine: Theory and Passenger Car Implementation". *SAE Technical Papers* (2003). DOI: 10.4271/2003-01-0357.

[18] J. Wahlström, L. Eriksson, and L. Nielsen. "EGR-VGT Control and Tuning for Pumping Work Minimization and Emission Control". und. *IEEE Transactions on Control Systems Technology* 18.4 (2010), pp. 993–1003. DOI: 10.1109/TCST.2009.2031473.

[19] J. Wahlström and L. Eriksson. “Modelling diesel engines with a variable-geometry turbocharger and exhaust gas recirculation by optimization of model parameters for capturing non-linear system dynamics”. *Proceedings of the Institution of Mechanical Engineers, Part D, Journal of Automobile Engineering* 225.7 (2011), pp. 960–986.

[20] J. Wahlström and L. Eriksson. “Nonlinear EGR and VGT Control with Integral Action for Diesel Engines”. *Oil & Gas Science and Technology - Rev. IFP* 66.4 (2011), pp. 573–586.

[21] J. Wahlström and L. Eriksson. “Output Selection and Its Implications for MPC of EGR and VGT in Diesel Engines”. und. *IEEE Transactions on Control Systems Technology* 21.3 (2013), pp. 932–940. DOI: 10.1109/TCST.2012.2191289.

[22] M. Jankovic and I. Kolmanovsky. “Delay Differential Equations: Recent Advances and New Directions”. Ed. by B. B. Springer US, 2009. Chap. Developments in control of time-delay systems for automotive powertrain applications, pp. 55–92.

[23] Y. Yildiz, A. Annaswamy, I. V. Kolmanovsky, and D. Yanakiev. “Adaptive Posicast Controller for Time-Delay Systems with Relative Degree n <= 2”. eng. *Automatica* 46.2 (2010), pp. 279–289. DOI: 10.1016/j.automatica.2009.11.008.

[24] F. Tschanz, A. Amstutz, C. H. Onder, and L. Guzzella. “Feedback Control of Particulate Matter and Nitrogen Oxide Emissions in Diesel Engines”. *Control Engineering Practice* 21.12 (2013), pp. 1809–1820. DOI: 10.1016/j.conengprac.2012.09.014.

[25] T. Poloni, B. Rohal-Ilkiv, and T. A. Johansen. “Mass Flow Estimation with Model Bias Correction for a Turbocharged Diesel Engine”. *Control Engineering Practice* 23.1 (2014), pp. 22–31. DOI: 10.1016/j.conengprac.2013.10.011.

[26] J. Zhao and J. Wang. “Effect of exhaust gas recirculation on biodiesel blend level estimation in diesel engines”. *Journal of Dynamic Systems, Measurement and Control-transactions of the Asme* 135.1 (2013), p. 011010. DOI: 10.1115/1.4006884.

[27] J. Zhao and J. Wang. “Adaptive Observer for Joint Estimation of Oxygen Fractions and Blend Level in Biodiesel Fueled Engines”. *IEEE Transactions on Control Systems Technology* 23.1 (2015), pp. 80–90. DOI: 10.1109/TCST.2014.2313003.

[28] J. B. Woodward and R. G. Latorre. “Modeling of diesel engine transient behavior in marine propulsion analysis.” *Transactions - Society of Naval Architects and Marine Engineers* 92 (1985), pp. 33–49.

[29] M. Blanke and J. A. Andersen. “On modelling large two stroke diesel engines: new results from identification.” *Proc. IFAC World Congress*. Budapest: Pergamon Press, 1984, pp. 2015–2020.

[30] E. Hendricks. “Compact, comprehensive model of large turbocharged, two-stroke diesel engines.” *SAE Technical Paper Series* (1986). DOI: 10.4271/861190.

[31] D. E. Winterbone and S. Jai-In. “The application of modern control theory to a turbocharged diesel engine powerplant”. *Proceedings of the Institution of Mechanical Engineers, Part I: Journal of Systems and Control Engineering* 205.19 (1991), pp. 69–83. DOI: 10.1243/PIME_PROC_1991_205_314_02.

[32] R. Banning, M. A. Johnson, and M. J. Grimble. “Advanced control design for marine diesel engine propulsion systems”. *Journal of Dynamic Systems Measurement and Control-transactions of the Asme* 119.2 (1997), pp. 167–174.

[33] A. Stefanopoulou and R. Smith. “Maneuverability and smoke emission constraints in marine diesel propulsion”. *Control Engineering Practice* 8.9 (2000), pp. 1023–1031. DOI: 10.1016/S0967-0661(00)00024-1.

[34] G. Theotokatos. “On the cycle mean value modelling of a large two-stroke marine diesel engine”. *Proceedings of the Institution of Mechanical Engineers Part M: Journal of Engineering for the Maritime Environment* 224.3 (2010), pp. 193–205.

[35] N. I. Xiros and G. Theotokatos. “Improved Transient Control of a Two-Stroke Marine Diesel Engine with Variable Geometry Turbine”. *Proceedings of the Asme Internal Combustion Engine Division Fall Technical Conference* (2011), pp. 85–94.

[36] C. Guan, G. Theotokatos, and P. Zhou. “Computational investigation of a large containership propulsion engine operation at slow steaming conditions”. *Applied Energy* 130 (2014), pp. 370–383.

[37] C. Guan, G. Theotokatos, and H. Chen. “Analysis of two stroke marine diesel engine operation including turbocharger cut-out by using a zero-dimensional model”. *Energies* 8.6 (2015), pp. 5738–5764.

[38] G. Theotokatos and V. Tzelepis. “A computational study on the performance and emission parameters mapping of a ship propulsion system”. *Proceedings of the Institution of Mechanical Engineers Part M: Journal of Engineering for the Maritime Environment* 229.1 (2015), pp. 58–76. DOI: 10.1177/147509021.

[39] MAN Diesel & Turbo. *The Dynamic Limiter Function*. Technical Paper. 2016.

[40] M. F. Pedersen, A. A. Andreasen, and S. Mayer. “Two-Stroke Engine Emission Reduction Technology: State-of-the-Art”. *CIMAC Congress* (2010).

[41] J. Kaltoft. “Tier III EGR for Large 2-Stroke MAN B&W Diesel Engines”. *Proceedings of the International Symposium on Marine Engineering*. 2011.

[42] MAN Diesel & Turbo. *Tier III Two-Stroke Technology*. Technical Paper. 2012.

[43] J. M. Hansen, C. Zander, N. Pedersen, M. Blanke, and M. Vejlgaard-Laursen. “Modelling for Control of Exhaust Gas Recirculation on Large Diesel Engines”. *IFAC-PapersOnLine, Elsevier Science* 46.33 (2013). IFAC Proceedings Volumes, pp. 380–385. DOI: 10.3182/20130918-4-JP-3022.00013.

[44] J. M. Hansen, M. Blanke, H. H. Niemann, and M. Vejlgaard-Laursen. “Exhaust Gas Recirculation Control for Large Diesel Engines - Achievable Performance with SISO Design”. *IFAC-PapersOnLine, Elsevier Science* 46.33 (2013). IFAC Proceedings Volumes, pp. 346–351. DOI: 10.3182/20130918-4-JP-3022.00011.

[45] G. Alegret, X. Llamas, M. Vejlgaard-Laursen, and L. Eriksson. “Modeling of a Large Marine Two-Stroke Diesel Engine with Cylinder Bypass Valve and EGR System”. *IFAC-PapersOnLine* 48.16 (2015). 10th IFAC Conference on Manoeuvring and Control of Marine Craft, MCMC 2015 Copenhagen, 24-26 August 2015, pp. 273 –278. DOI: 10.1016/j.ifacol.2015.10.292.

[46] X. Llamas and L. Eriksson. “Parameterizing Compact and Extensible Compressor Models Using Orthogonal Distance Minimization”. *Journal of Engineering for Gas Turbines and Power* 139.1 (2016), p. 012601. DOI: 10.1115/1.4034152.

[47] X. Llamas and L. Eriksson. “A Model of a Marine Two-Stroke Diesel Engine with EGR for Low Load Simulation”. *9th EUROSIM Congress on Modelling and Simulation*. Oulu, Finland, 2016.

[48] N. P. Kyrtatos. “From HERCULES A-B-C to HERCULES-2: cutting edge R&D in ship engines”. *Transportation Research Procedia* 14 (2016), pp. 1581–1590. DOI: 10.1016/j.trpro.2016.05.123.

[49] K. V. Nielsen, M. Blanke, L. Eriksson, and M. Vejlgaard-Laursen. “Control-Oriented Model of Molar Scavenge Oxygen Fraction for Exhaust Recirculation in Large Diesel Engines”. *Journal of Dynamic Systems, Measurement and Control - ASME* 139.2 (2017). DOI: 10.1115/1.4034750.

[50] K. V. Nielsen, M. Blanke, and L. Eriksson. “Adaptive Observer for Nonlinear Parameterised Hammerstein System with Sensor Delay - a Technology for Ship Emissions Reduction”. *Transactions on Control Systems Technology* (2016). Submitted.

[51] K. V. Nielsen, M. Blanke, L. Eriksson, and M. Vejlgaard-Laursen. “Adaptive Feedforward Control of Exhaust Recirculation in Large Diesel Engines”. *Control Engineering Practice* (2016). In review.

[52] K. V. Nielsen, M. Blanke, L. Eriksson, and M. Vejlgaard-Laursen. “Diesel Engine Control System to meet Strict Emission Requirements while Maintaining Full Ship Manoeuvring Capability”. *Applied Energy* (2016). Submitted.

[53] K. V. Nielsen, M. Blanke, and M. Vejlgaard-Laursen. “Nonlinear Adaptive Control of Exhaust Gas Recirculation for Large Diesel Engines”. *IFAC-PapersOnLine* 48.16 (2015). 10th IFAC Conference on Manoeuvring and Control of Marine Craft, MCMC 2015 Copenhagen, 24-26 August 2015, pp. 254 –260. DOI: 10.1016/j.ifacol.2015.10.289.

[54] HELCOM. *Workshop in Russia Advances NECA for Ships in Baltic and North Seas*. http://www.helcom.fi/news/Pages/Works in-Russia-advances-NECA-for-ships-in-Baltic-and-North-Seas.aspx. 2016.

[55] N. Watson and M. S. Janota. *Turbocharging the Internal Combustion Engine*. Macmillan, 1982.

[56] S. L. Dixon and C. A. Hall. *Fluid mechanics and thermodynamics of turbomachinery*. Elsevier, 2014, 537 pages.

[57] M. Blanke. “Requirements of Adaptive Techniques for Enhanced Control of Large Diesel Engines”. *Proc. IFAC Workshop on Adaptive Control and Signal Processing. Lund, Sweden*. IFAC, 1986.

[58] M. Blanke and P. B. Nielsen. “The Marine Engine Governor”. *Proceedings Second International Conference on Maritime Communications and Control*. London: Society of Marine Engineers, 1990, pp. 11–20.

[59] F. Baldi, K. Andersson, and G. Theotokatos. “Development of a combined mean value-zero dimensional model and application for a large marine four-stroke Diesel engine simulation”. *Applied Energy* 154 (2015), pp. 402–415. DOI: 10.1016/j.apenergy.2015.05.024.

[60] H. Wang, Y. Tian, J. Bosche, and A. El Hajjaji. “Modeling and Dynamical Feedback Control of a Vehicle Diesel Engine Speed and Air-Path”. *Journal of Dynamic Systems Measurement and Control-transactions of the Asme* 136.6 (2014), p. 061010. DOI: 10.1115/1.4027502.

[61] M. Huang, K. Zaseck, K. Butts, and I. Kolmanovsky. “Rate-Based Model Predictive Controller for Diesel Engine Air Path: Design and Experimental Evaluation”. *IEEE Transactions on Control Systems Technology* (2016). DOI: 10.1109/TCST.2016.2529503.

[62] G. Besançon. *Nonlinear observers and applications*. Springer Berlin Heidelberg, 2007.

[63] Ljung. “Asymptotic behavior of the extended Kalman filter as a parameter estimator for linear systems”. *IEEE Transac. on Automatic Control* 24.1 (1979), pp. 36–50.

[64] W. Zhou and M. Blanke. “Identification of a class of nonlinear state space models using RPE techniques”. *IEEE Transac. on Automatic Control* 34 (1989), pp. 312–316.

[65] J.-J. Slotine and W. Li. *Applied nonlinear control*. Prentice-Hall, 1991, 17+459 s.

[66] A. Annaswamy, F. Skantze, and A. Lohi. “Adaptive control of continuous time systems with convex/concave parametrization”. *Automatica* 34.1 (1998), pp. 33–49.

[67] H. Grip, T. Johansen, L. Imsland, and G.-O. Kaasa. “Parameter estimation and compensation in systems with nonlinearly parameterized perturbations”. *Automatica* 46.1 (2010), pp. 19–28.

[68] H. Grip, A. Saberi, and T. Johansen. “Estimation of states and parameters for linear systems with nonlinearly parameterized perturbations”. *Syst. and Control Letters* 60.9 (2011), pp. 771–777.

[69] X. Liu, R. Ortega, H. Su, and J. Chu. “On adaptive control of nonlinearly parameterized nonlinear systems: Towards a constructive procedure”. *Syst. and Control Letters* 60.1 (2011), pp. 36–43.

[70] V. Adetola, M. Guay, and D. Lehrer. “Adaptive estimation for a class of nonlinearly parameterized dynamical systems”. *IEEE Transac. on Automatic Control* 59.10 (2014), pp. 2818–2824.

[71] I. Tyukin, E. Steur, H. Nijmeijer, and C. van Leeuwen. “Adaptive observers and parameter estimation for a class of systems nonlinear in the parameters”. *Automatica* 49.8 (2013), pp. 2409–2423.

[72] I. Tyukin. “Adaptation algorithms in finite form for nonlinear dynamic objects”. *Automation and Remote Control* 64.6 (2003), pp. 951–974.

[73] E. Eskinat, S. Johnson, and W. Luyben. “Use of Hammerstein models in identification of nonlinear systems”. *AIChE Journal* 37.2 (1991), pp. 255–268.

[74] K. Narendra and P. Gallman. “An iterative method for the identification of nonlinear systems using a Hammerstein model”. *IEEE Transac. on Automatic Control* 11.3 (1966), pp. 546–550.

[75] P. Mattsson and T. Wigren. “Convergence analysis for recursive Hammerstein identification”. *Automatica* 71 (2016), pp. 179–186. DOI: 10.1016/j.automatica.2016.04.014.

[76] D. Laila and E. Gruenbacher. “Nonlinear output feedback and periodic disturbance attenuation for setpoint tracking of a combustion engine test bench”. *Automatica* 64 (2016), pp. 29–36. DOI: 10.1016/j.automatica.2015.10.054.

[77] P. Falugia, L. Giarre, and G. Zappa. “Approximation of the feasible parameter set in worst-case identification of Hammerstein models”. *Automatica* 41.6 (2005), pp. 1017–1024.

[78] E. Bai. “Frequency domain identification of Hammerstein models”. *IEEE Transac. on Automatic Control* 48.4 (2003), pp. 530–542.

[79] W.-X. Zhao and H.-F. Chen. “Adaptive tracking and recursive identification for Hammerstein systems”. *Automatica* 45.12 (2009), pp. 2773–2783.

[80] S. Sastry. *Nonlinear systems: analysis, stability and control*. Springer, 1999.

[81] H. K. Khalil. *Nonlinear systems*. Prentice Hall, 2002, 750 s.

[82] E. Alfieri, A. Amstutz, and L. Guzzella. “Gain-scheduled model-based feedback control of the air/fuel ratio in diesel engines”. *Control Engineering Practice* 17.12 (2009), pp. 1417–1425. DOI: 10.1016/j.conengprac.2008.12.008.

[83] D. Rupp and L. Guzzella. “Adaptive Internal Model Control with Application to Fueling Control”. *Control Engineering Practice* 18.8 (2010), pp. 873–881. DOI: 10.1016/j.conengprac.2010.03.011.

[84] Z. Qiu, J. Sun, M. Jankovic, and M. Santillo. “Nonlinear Internal Model Controller Design for Wastegate Control of a Turbocharged Gasoline Engine”. *Control Engineering Practice* 46 (2016), pp. 105–114. DOI: 10.1016/j.conengprac.2015.10.012.

[85] M. Imperato, O. Kaario, T. Sarjovaara, and M. Larmi. “Split fuel injection and Miller cycle in a large-bore engine”. *Applied Energy* 162 (2016), pp. 289–297. DOI: 10.1016/j.apenergy.2015.10.041.

[86] S. I. Raptotasios, N. F. Sakellaridis, R. G. Papagiannakis, and D. T. Hountalas. “Application of a multi-zone combustion model to investigate the NOx reduction potential of two-stroke marine diesel engines using EGR”. *Applied Energy* 157 (2015), pp. 814–823. DOI: 10.1016/j.apenergy.2014.12.041.

[87] M. Vejlgaard-Laursen and H. Olesen. “Controlling Tier III Technologies” (2016). 28th CIMAC World Congress on Combustion Engine.

[88] C. Walsh and A. Bows. “Size matters: Exploring the importance of vessel characteristics to inform estimates of shipping emissions”. *Applied Energy* 98 (2012), pp. 128–137. DOI: 10.1016/j.apenergy.2012.03.015.

Technical University of Denmark
Automation and Control (AUT)
Elektrovej Building 326
DK-2800, Kgs. Lyngby
Denmark
Phone: (+45) 45 25 35 76
Email: info@elektro.dtu.dk
www.elektro.dtu.dk